2005

CFD Modeling of Heat Recovery Steam Generator and its Components Using Fluent

Veera Venkata Sunil Kumar Vytla
University of Kentucky, vvvytl2@uky.edu

Abstract of Thesis

CFD Modeling of Heat Recovery Steam Generator and its Components Using Fluent

Combined Cycle power plants have recently become a serious alternative for standard coal- and oil-fired power plants because of their high thermal efficiency, environmentally friendly operation, and short time to construct. The combined cycle plant is an integration of the gas turbine and the steam turbine, combining many of the advantages of both thermodynamic cycles using a single fuel. By recovering the heat energy in the gas turbine exhaust and using it to generate steam, the combined cycle leverages the conversion of the fuel energy at a very high efficiency. The heat recovery steam generator forms the backbone of combined cycle plants, providing the link between the gas turbine and the steam turbine. The design of HRSG has historically largely been completed using thermodynamic principles related to the steam path, without much regard to the gas-side of the system. An effort has been made using resources at both UK and Vogt Power International to use computational fluid dynamics (CFD) analysis of the gas-side flow path of the HRSG as an integral tool in the design process. This thesis focuses on how CFD analysis can be used to assess the impact of the gas-side flow on the HRSG performance and identify design modifications to improve the performance. An effort is also made to explore the software capabilities to make the simulation an efficient and accurate.

KEYWORDS: Heat Recovery Steam Generator, Gas Turbine, Steam Turbine, Heat Exchangers, Distribution Grid, Duct Burner, Baffle

Veera Venkata Sunil Kumar Vytla

_____

02/18/2005

_____

CFD Modeling of Heat Recovery Steam Generator and its Components Using Fluent

By

Veera Venkata Sunil Kumar Vytla

Dr. George P. Huang
_____
Director of Thesis

Dr. Keith Kaufman
_____
Co-Director of Thesis

Dr. George P. Huang
_____
Director of Graduate Studies

02/18/2005
_____
Date

RULES FOR THE USE OF THESIS

Unpublished thesis submitted for the Master's degree and deposited in the University of Kentucky Library are as a rule open for inspection, but are to be used only with due regard to the rights of the authors. Bibliographical references may be noted, but quotations or summaries of parts may be published only with the permission of the author, and with the usual scholarly acknowledgements.

Extensive copying or publication of the thesis in whole or in part also requires the consent of the Dean of the Graduate School of the University of Kentucky.

Thesis

Veera Venkata Sunil Kumar Vytla

The Graduate School

University of Kentucky

2005

CFD Modeling of Heat Recovery Steam Generator and its Components Using Fluent

---

Thesis

A thesis submitted in partial fulfillment of the requirements for

degree of Masters of Science in Mechanical Engineering in

College of Engineering at the

University of Kentucky

By

Veera Venkata Sunil Kumar Vytla

Director: Dr. George P Huang, Professor of Mechanical Engineering

Co-Director: Dr. Keith Kaufman, Auxiliary faculty

Lexington, KY

2005

MASTER'S THESIS RELEASE

I authorize the University of Kentucky Libraries

to reproduce this thesis in

whole or in part for the purpose of research.

Signed: Veera Venkata Sunil Kumar Vytla

Date: 02/18/05

Dedication:

….To my beloved father

Acknowledgements

First, I would like to acknowledge the contribution of Dr. George P. Huang, my advisor, by whose influence and motivation, I have learned a great deal about computational fluid dynamics. Needless to say (though I still am saying it), this work could not have happened without his support, both financially and technically. He was always available to discuss the problems at hand with my project. Secondly, I would like to thank the support of my co-advisor, Dr. Keith Kaufman of Vogt Power International, for his valuable guidance throughout this study. His invaluable suggestions and ingenious ideas have taken the shape of this project. Also, thanks are expressed to funding institute. This research is supported by Vogt Power International, Louisville. This thesis would not have been complete without the reviews and comments of many people. I would also like to thank Dr. Raymond P. LeBeau being on my thesis committee and his help with my editing. I would also like to thank Dr. James E. Funk for being on my thesis committee. I would like to thank Jerry Grooms, System Administrator, CFD-ME cluster for his support throughout the research and his help in keeping the cluster operational.

I would like to thank Dr. K Narayana Rao, my mentor, for encouraging me to pursue my higher studies here at University of Kentucky. I would like to thank each one of my friends who made my stay at the University of Kentucky so wonderful.

Finally, I would like to thank my family. My mom has always been supportive of my education. I'm still not leaving college, Mom. Most of all, however, I would like to thank God from whom all of life's blessings flow.

Table of Contents

Chapter 8

List of Tables

List of Figures

List of Files

	Filename	size
1.	Vytla_thesis	18.3MB

Chapter 1
Introduction

1.1 Introduction to Combined-Cycle and HRSG

A significant amount of electricity is produced using simple-cycle and combined-cycle gas turbine power plants. The drawback in using a simple gas turbine cycle is that the exhaust temperatures are high. The maximum efficiency attainable from a simple gas turbine cycle is around 35%. The efficiency of the simple cycle system can be increased by recovering some of the heat energy carried away by the exhaust gas from the gas turbine and generating steam in a heat recovery steam generator (HRSG) system. If the steam generated is used for industrial purposes, the system is called co-generation; if used for running a steam turbine, the system is called combined-cycle power generation. The advantage of the combined-cycle is that the thermal efficiency of the cycle can reach a maximum value of 60% when operated at the optimum conditions. Due to their advantages, combined-cycle systems had been increasingly used in power plants. Combined-cycle systems have two thermodynamic cycles of operation, namely, the gas turbine cycle and the steam turbine cycle. These two thermodynamic cycles are connected by the HRSG, which extracts heat from the exhaust gas of the gas turbine and uses it to generate steam, which is used in turn to run the steam turbine. The HRSG

system is the main element that makes the concept of combined cycle possible. The layout of a combined cycle system is shown in figure 1-1.

The main components in a combined cycle power plants are the gas turbine, steam turbine and HRSG. The efficiency of the combined cycle power plant is influenced by the efficiency of the independent systems which form the combined cycle. In some cases the loss in efficiency in one system has a positive impact on the other system. The efficiency of the gas turbine system is reduced by increasing the gas turbine exhaust temperature, but this increases the steam generation capacity of the HRSG. The efficiency loss in the gas turbine has a negative affect on the over all performance of the system; it is advisable to operate the system at maximum gas turbine efficiency. The HRSG forms the heart of the combined cycle and its performance has a direct impact on the overall efficiency of the combined cycle system. The primary modes of heat transfer in the HRSGs are convection and conduction. The most common HRSG design has boiler tubes vertically oriented and the gas turbine exhaust passes through horizontally.

HRSGs are built as both single pressure units and multiple pressure systems. The most commonly used HRSGs are multiple pressure systems, as they offer improved efficiency and increased heat recovery. The configuration of the circuits within the HRSG is as follows: the high pressure (HP) circuits - re-heater, super-heater and evaporator (boiler) - are located in the hottest zone of the system, followed by intermediate pressure (IP) circuits and/or low pressure (LP) circuits. Generally, the evaporators are set up in a natural circulation, drum-type arrangement. Combined-cycle power plants may be equipped with supplementary, natural gas fired duct burners to increase the heat flow into the HRSG. Supplementary firing is appropriate in the HRSG

because there is enough oxygen available in the exhaust gas to support combustion, as only a part of oxygen contained in the air is used for combustion in the gas turbine. The supplementary firing results in increasing the efficiency of the system by increasing steam production. This results in increased mass flow through the economizers, which extracts more heat energy from the exhaust gas and thereby lowers the exhaust gas temperature. Atmospheric conditions and the steam requirements are the criteria based upon which the supplementary firing system is selected.

Combined-cycle systems are preferred over simple-cycle systems because of its environmentally friendly operation, which is achieved by reducing emissions as a result of combustion from the exhaust gases in the HRSG. HRSGs may include emission control systems to remove the nitrogen oxides and carbon-monoxide contents in the exhaust, depending upon the limitations at the site location.

1.2 Motivation

The performance of the HRSG affects the overall performance of the combined-cycle power plant. An accurate simulation of the performance of the HRSG is required to study its effect on the entire system. After an initial collaboration between the UKCFD group and Vogt Power International on the use of computational fluid dynamics (CFD) as a tool to analyze the flow in two HRSG designs, it is clear that CFD has the potential to become a useful tool to validate the performance of the HRSG, and to make some design changes to it. The successful utilization of CFD as a tool in the design of the HRSG can be done only when the CFD tools are appropriately applied and validated using approaches that accurately represent the flow and physics in the components of the

equipment being modeled. The CFD tool used for flow simulation of HRSG models is Fluent. Fluent offers a number of choices for modeling HRSG related model components. A careful evaluation of individual components would lead to a better success in overall predictions of HRSG performance.

1.3 Objectives

The design of the HRSG is done based upon the steam-side flow conditions without giving much consideration for the gas-side flow. In the design process, the gas side flow is assumed to be uniform throughout the HRSG system. This thesis concentrates on the evaluation of the existing design/s of the HRSG system by doing inner gas side flow analysis using Fluent, a CFD computational tool.

The first part of the thesis includes modeling the complete HRSG system, identifying the critical zones in the existing design, and making design changes to improve the gas-side flow in the critical zones (after the duct burner, flow in the inlet duct, flow entering the SCR and CO catalysts) without affecting the performance of the system. This includes a sub-model study of the some of the critical components like the burner, CO, and SCR catalysts in order to suggest design changes to improve the gas-side flow. An explanation about how the suggested changes in design help in overcoming the existing problems is also included. The second part involves making the suggested design changes in the full model and comparing the flow conditions with the original design.

Heat exchangers are the most important components in the HRSG. During this work, an effort is made to explore the modeling techniques available in Fluent for modeling heat exchangers that represent the actual case. This part involves exploring and

testing the heat exchanger module capabilities in Fluent and comparing these results with CARDS predictions.

1.4 Thesis Outline

The remaining portion of the thesis is explained in subsequent chapters. Chapter 2 concentrates on a literature review and existing modeling methods used to study the performance of HRSG. Chapter 3 discusses the main components of the HRSG and the function performed by these components. Chapter 4 discusses the computational procedure involved in modeling the flow and boundary conditions applied for different components of the HRSG. Test cases for both designs used in this thesis are detailed in Chapter 5. The flow modeling results for the Beatrice HRSG are discussed in Chapter 6. The flow modeling results for the Current Creek HRSG are discussed in Chapter 7. This chapter also includes the results of burner sub-model study, followed by concluding remarks in Chapter 8.

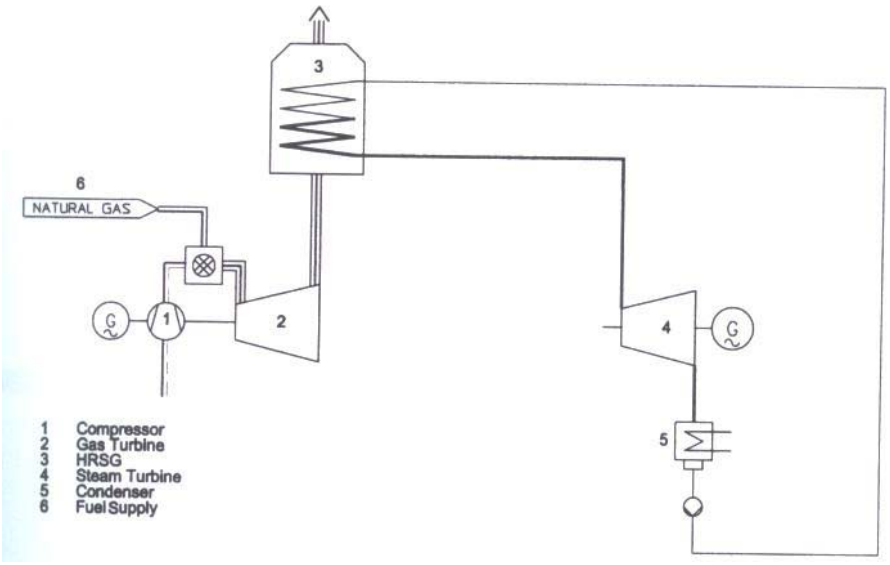

Figure 1-1: Combined cycle layout

Chapter 2

Literature Review

2.1 Review on HRSG Optimization and Modeling

The increasing demand for energy at the present time can be met by combined-cycle power plants with low fuel consumption. The factor that favors the use of combined-cycle power plants is its ability to use low carbon content fuels and its low impact on the environment. It is proven theoretically that the efficiency of the combined cycle can reach a value as high as 60%; this efficiency is reached only when all the components in the combined cycle are operating at the optimum conditions. Researchers are currently trying to achieve this level of efficiency. The hierarchical strategy implied for optimization of the whole combined-cycle power plant is as follows: optimization of the gas turbine cycle, optimization of the operating parameters of the HRSG, and detailed optimization of the single heat exchanger sections in the HRSG. One of the suggested ways to reach the theoretically maximum efficiency is by increasing the turbine inlet temperature [1]. This requires a highly advanced cooling system to cool down the blades of the gas turbine. With existing technology levels, focus can be fixed on the HRSG, and its operating parameters to improve the efficiency of the combined-cycle plants. Optimization of the operating parameters of HRSG is the first step in the optimum design

of the whole plant as stated in [2]. Different approaches used in deciding the optimum design and operating parameters of the HRSG are discussed in [2-4, 6, 7]. Reddy, Ramkiran, Ashok Kumar and Nag [3] suggested a second law analysis of the waste heat recovery steam generator. This method is basically used to optimize and design various thermal units by minimizing the entropy generation in the unit. The operating parameters are non-dimensionalized, and an equation for the entropy generation number is derived using these parameters. The entropy generation number helps to study the effect of the dimensionless operating parameters. Valdes and Jose suggested the application of influence coefficients for the optimization of HRSG. The influence co-efficients are mathematically obtained using Newton-Raphson. This method gives a better understanding of the influence of design parameters on the cycle performance. Thermodynamic optimization technique is applied and used by Casarosa and Franco [2]. Unlike the second law analysis of the HRSG the objective function in this method deals with minimizing the exergy losses, considering only the irreversibility due to temperature difference between hot and cold streams. Even though this method does not apply any constraint on the cost of the HRSG and on the surface area, it still gives a rough idea about the selection of operating parameters for the HRSG. Another method called thermo-economic optimization - which deals with two different objective functions for minimizing the exergy losses along with minimizing the cost of the HRSG is discussed in [2].

Studies prove that the performance of the HRSG affects the overall performance of the combined-cycle. It is necessary to be able to simulate the performance of HRSG to study the effects of various design and operating parameters of the HRSG on the

performance of the entire cycle. Mathematical models are developed to simulate and study the performance of the HRSG. Ongrio, Ugursal, Taweel and Walker developed a numerical method to predict the performance of HRSG [9], considering the changes in the design as mush as possible and keeping the computational complexity manageable. The proposed method calculates the velocity and temperature fields by discretization and the solution of conservation equations (continuity, momentum and energy) derived for a HRSG of particular geometry and duty. Dumont and Heyen suggested a mathematical model for modeling and designing a once-through heat recovery steam generator [8]. In a conventional boiler, each tube plays a well-defined role like water preheating, vaporization and superheating. Empirical equations are readily available to predict the average heat transfer in each region which is not the case in a once through boiler. This increases the mathematical complexity as well as the number of equations to be solved for modeling these boilers. For the flow in the water side, as the separation of different zones in a once-through boiler is not clear the first step in the solution process involves the estimation of flow pattern in the tubes. Once the patterns are estimated, the appropriate heat transfer equations are selected. For the flow in the gas-side, equations used for a conventional boiler can be used. Care is taken to consider the effects of fins and fouling on the value of the heat transfer co-efficient. Knudsen, Morrison, Behnia and Furbo, used a computational fluid dynamics (CFD) model to analyze the flow structure in a vertical mantle heat exchanger [10]. The flow structure and heat transfer in the inner tank of the glass model tank is simulated using the CFD code Fluent 6.0 to solve the flow and energy equations. In this case only half of the tank is modeled, as the conditions in the other half are symmetrical. This reduces the problem size and saves computational

time without any loss of accuracy. The numerical results produced with the CFD simulation are in agreement with the experimental results for the same case. This demonstrates the capability of the CFD model to simulate flows with heat transfer.

The results from various models proved helpful in predicting the performance of the HRSG with the change in design and operating parameters. The ever increasing technology in the field of HRSG resulted in the use of supplementary firing in the HRSG, as a potential option to improve the efficiency of the system. This necessitates having a numerical flow model with the capability to simulate combustion and flow in the HRSG model, as well as the flexibility to simulate these for different designs with acceptable accuracy.

Chapter 3

HRSG Components

HRSG systems are designed to achieve high thermal efficiencies and reduce the emissions in the combined cycle. This can be achieved by proper design of each component involved in the HRSG system. The components of HRSG system that contribute to the above objectives are: the inlet duct, distribution grid, duct burners, heat exchangers, SCR & CO catalyst modules, AIG, breaching, and exhaust stack. The surface geometries of Beatrice HRSG and Current Creek HRSG showing the components of the HRSG are shown in Figures 3-1, and 3-2, respectively.

3.1 Inlet Duct

It is desirable to design the HRSG so that the pressure loss on the exhaust side, or back pressure, remains as low as possible. The ideal design of the HRSG inlet duct results in increase of static pressure within the system. The inlet duct connects to the gas turbine exhaust flange and directs the exhaust gases onto the first heating surface. The flow entering the heating surface should be uniform for optimal thermal performance. The walls of the inlet duct are lined with three layers of insulating materials to avoid heat

loss and prevent damage to duct materials from the impact of high velocity exhaust gases. The design of the inlet duct should maintain the high velocity flow in the center of the passage area, but not allow high velocities to impact the duct walls.

3.2 Duct Burner

The exhaust gas from the gas turbine consists of substantial amounts of excess air, as the main combustion process in the gas turbine has to be diluted to reduce the temperatures that could be attained in the combustion process because of limitations on the metallurgical properties of materials used in the gas turbine. This excess air can be used for supplementary firing of fuel in the HRSG systems, increasing the heat recovery and steam generation rates in the HRSG system. Gas fired duct burners are provided in the HRSG system to provide supplementary firing in the system. Most of the duct burners have horizontal natural gas elements or runners that span the whole width of the gas path.

For the ideal operation of the duct burners it is desirable to increase the flow velocity entering the burners. The ideal velocity profile entering the burner plane element depends upon the design of the burner. The straightness and uniformity are also equally important, along with magnitude of the flow. In general, for ideal operation of the burner, the velocity profile should be ±25% of average velocity, with velocity vectors normal to the burner plane. Areas of high velocity in the flow cause the flame to impinge upon the burner surfaces and on the side walls. Distribution grids and/or flow straightening vanes are used in expanding ducts to achieve the desired velocity profile. Sometimes it is desirable to use baffles between the burners to increase the flow velocity to the desired value, as it is always advisable to have very high flow velocities for better combustion.

The shape of the baffles is decided based upon the past experience of the designer with similar situations.

The duct burner array configuration for Beatrice HRSG consists of two duct burners. Each duct burner has sixty-three nozzles evenly distributed through out the length with a nozzle diameter of 0.1''. The duct burner configuration is shown in figure 3-3.

The duct burner array configuration for the Current Creek HRSG consists of six duct burners provided with a total of fourteen wing baffles as shown in figure 3-4. As the burner array is located after the first heat exchanger box, the flow entering the burner plane needs to be accelerated; this flow acceleration is achieved by the placing of wing baffles, which also directs the flow into the burner planes. Each duct burner has a total of 300 nozzles, 150 above the horizontal plane and 150 below the horizontal plane, with the nozzles oriented $\pm 30^0$ from the horizontal plane. The actual model includes unfired nozzles, six on each end of the burner duct, which are modeled as walls.

3.3 Distribution Grid

The distribution grid is generally located upstream to the burners. The purpose of the distribution grid is to achieve the desired velocity profile entering the burners. The application of distribution grid is seen only in the Beatrice HRSG. As this HRSG is designed to operate with the side exhaust of gas turbine, the velocity profile entering the HRSG is not uniform. It is desirable to have even flow distribution entering the duct burners as well as the first heating surface. The distribution grid plays an important role in the performance of the burner.

3.4 Heat Exchangers

The most general type of heat exchangers used in HRSG are the tube type heat exchangers with/without fins. There are three different types of heat exchangers installed into a HRSG system: pre-heaters, evaporators, and super-heaters. Pre-heaters are used to raise the temperature of the water to the saturation temperature at that pressure. Evaporators serve the function of converting the saturated water to steam by adding the latent heat. Super-heaters are used to raise the temperature of the saturated steam. Tube type heat exchangers are used in all the three heat exchangers. The number of rows of tubes and the number of tubes per row are selected based upon the heat exchanger duty. Evaporators are generally designed for natural circulation. Forced circulation can be used in pre-heaters and super-heaters. The tubes are provided with fins (solid, serrated) to increase the surface area of the heat exchanger. It is not possible to model the heat exchangers with the exact geometry because of limitations on the mesh size. The assumptions and simplifications made while modeling heat exchangers are discussed in chapter 4.

3.5 Selective Catalytic Reduction (SCR) System and AIG

The emission of NO_x is controlled by the use of SCR catalyst. The reduction in NO_x products is achieved by injecting ammonia into the exhaust allowing the NO_x in the exhaust gas to react with ammonia. The reactions involved in an SCR are as follows:

$$4NO + 4NH_3 + O_2 \rightarrow 4N_2 \uparrow + 6H_2O \quad \text{.....3.2}$$

$$2NO_2 + 4NH_3 + O_2 \rightarrow 3N_2 \uparrow + 6H_2O \quad \text{..... 3.3}$$

The reaction of the NO_x with ammonia is the key in controlling the emission. In an SCR system the reaction takes place in the SCR catalyst bed mounted in the exhaust gas flow path. The most common materials used for these are titanium oxide, vanadium pentoxide, precious metals, and zeolites (aluminosilicates). The ideal operating range of the transition metal catalysts (titanium, vanadium) is generally 450 ^{o}F to 850 ^{o}F, while the zeolites operate at much higher temperatures ranging between 850 ^{o}F to 1050 ^{o}F. The most common structural configuration is block type catalyst manufactured in parallel plate or honeycomb configurations. Ammonia is injected into the system through a grid injection arrangement, which is also an integral part of the SCR named the Ammonia Injection Grid (AIG). It is located upstream of the SCR catalyst module. The purpose of the AIG is to inject ammonia uniformly into the exhaust gas entering the SCR system. For the uniform mixing of injected ammonia into the exhaust gas, the flow distribution of the exhaust gas at the AIG location should be within ±15% of the average velocity.

3.6 Breaching and Exhaust Stack

The gas flow from the heat exchangers is directed into the exhaust stack through the breaching. The breaching is the perforated plate which typically has four columns of holes at an angle ranging from 90^{o} to 120^{o}. The purpose of the breaching is to direct the flow into the exhaust stack and thereby allow the smooth exhaust of the gas without any re-circulating regions forming in the exhaust stack. The gases are emitted to atmosphere via the HRSG stack.

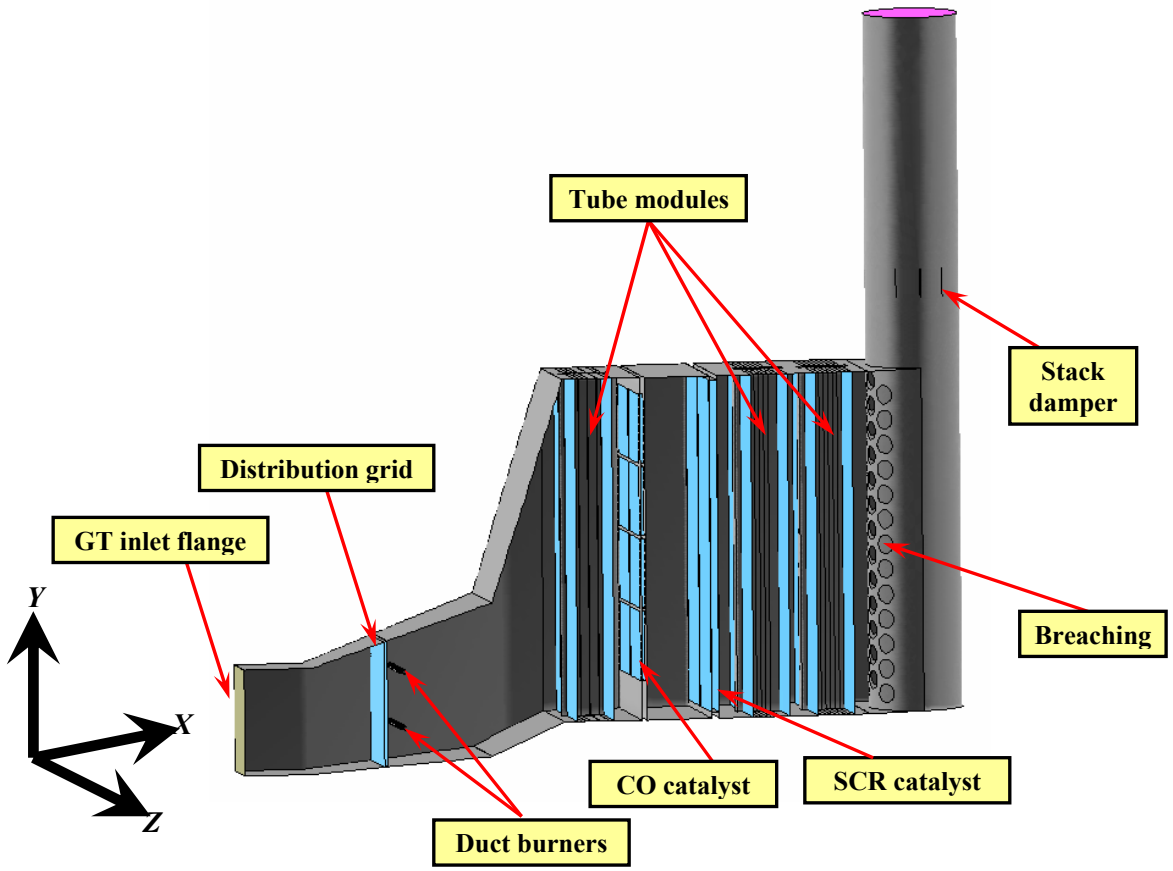

Figure 3-1: Figure showing components of HRSG (Beatrice HRSG)

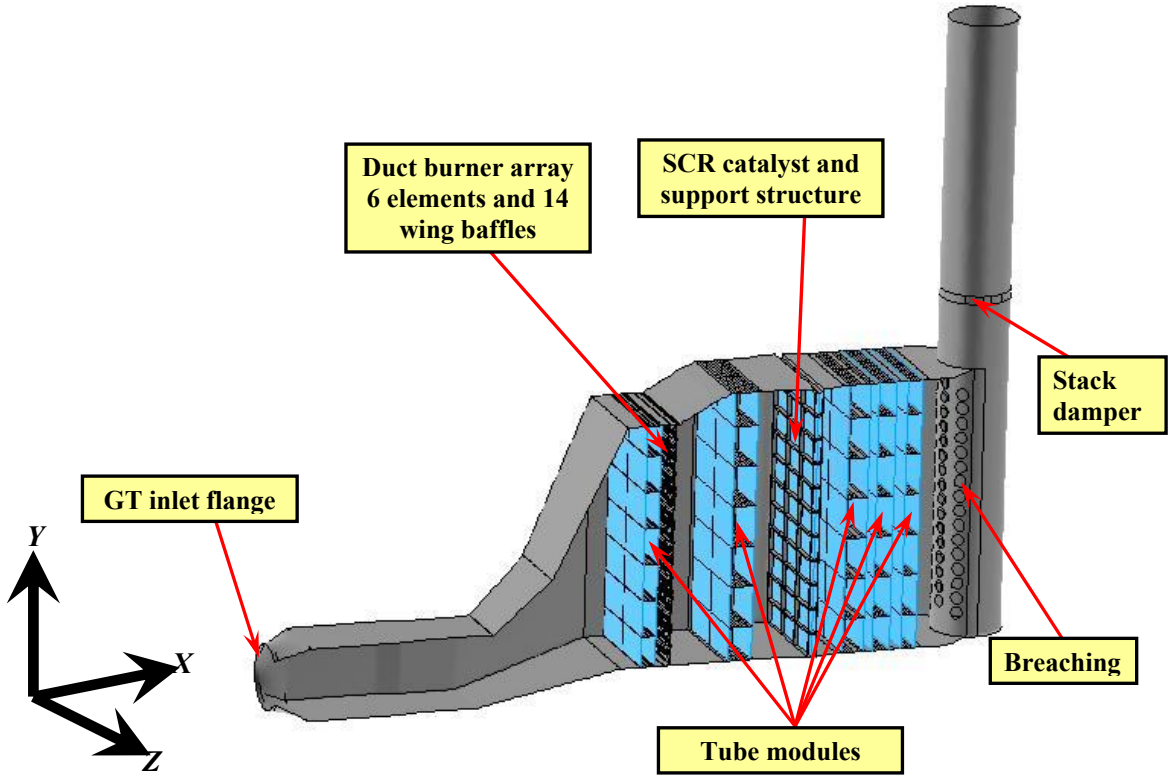

Figure 3-2: Figure showing components of HRSG (Current Creek HRSG)

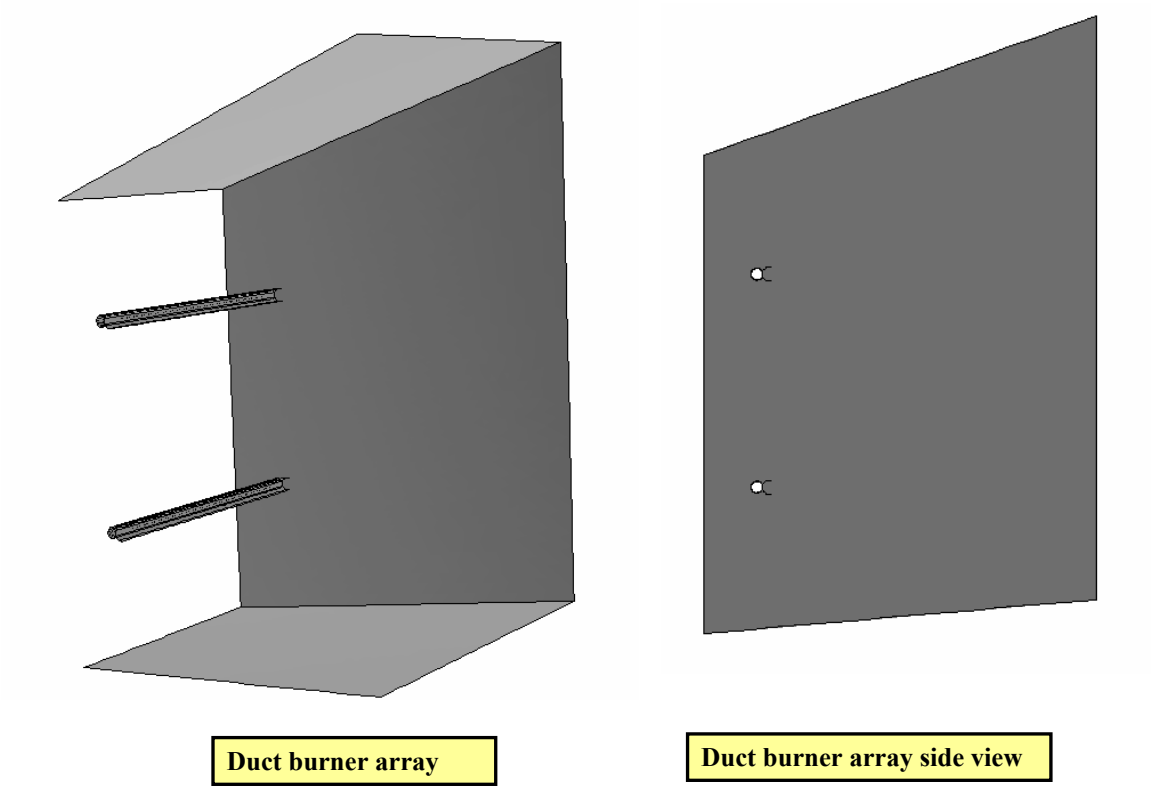

Figure 3-3: Duct burner array arrangement, Beatrice HRSG

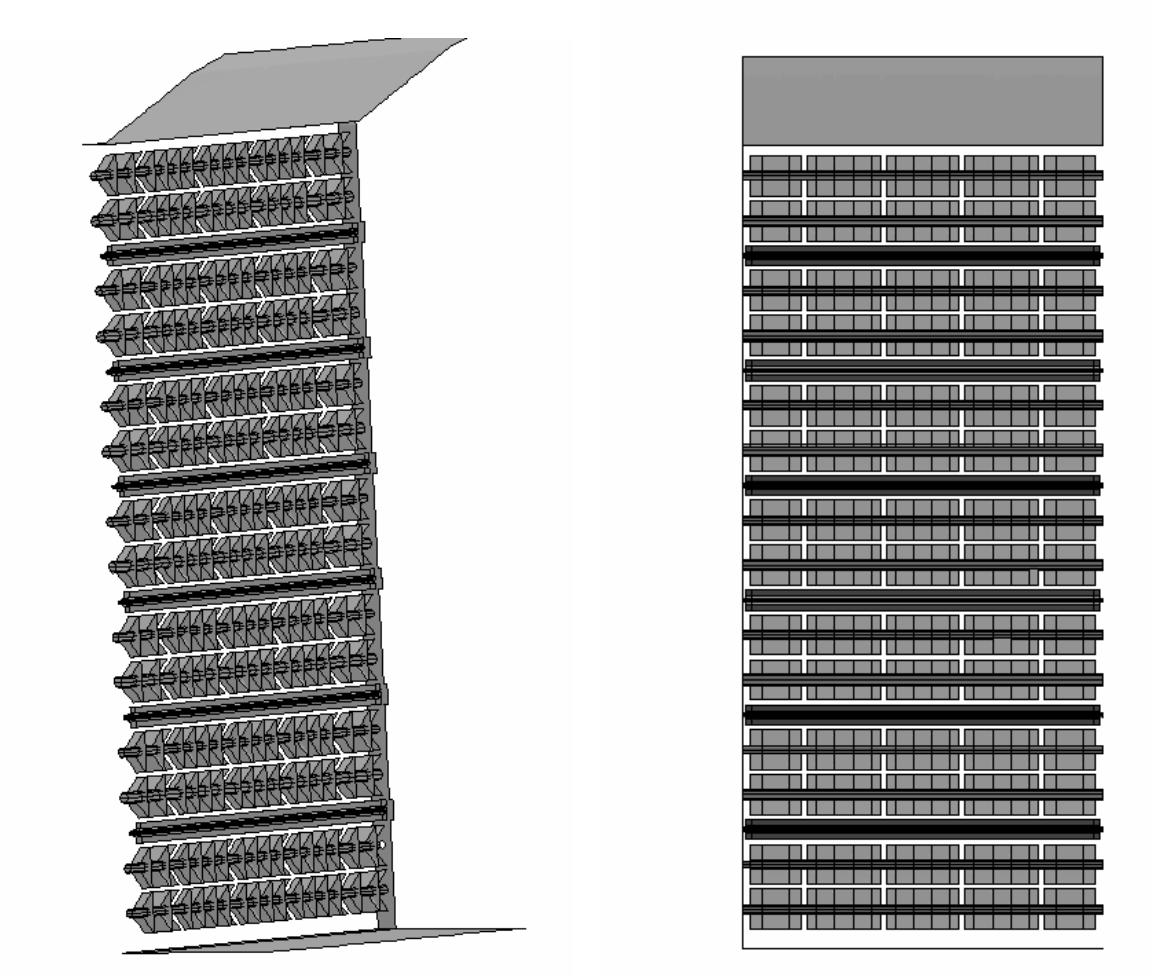

Figure 3-4: Duct burner array arrangement, Current Creek HSRG

Chapter 4

Computational Procedure

The step by step procedure involved in a CFD solution process is given as follows:

1. Dimensions of the model are read from the design drawings
2. Generation of geometry
3. Mesh generation
4. CFD simulation and refinement/ adaptation of grid
5. Post processing and analysis of results

The diagrammatic representation of the steps involved is shown in figure 4-1.

The commercial CFD solver, Fluent 6, is used as a processor to complete the flow modeling of the models discussed in this thesis. The preprocessor, GAMBIT, which comes as a package along with Fluent, is used for generating and meshing the geometry. The mesh generated is used to simulate the case in the CFD solver. The results are visualized and the data is presented using the post processing capabilities of Fluent.

4.1 Preprocessing

The solution of any CFD process begins with the generation of the mesh. The preprocessor GAMBIT is used to create the geometry and generate the mesh. The steps involved in CFD preprocessing are: generation of geometry, meshing of lower entities, meshing of higher entities and defining the boundary conditions.

4.1.1 Generation of Geometry

The geometry can be generated either starting from scratch or by working over imported geometry from other software like CAD/IDEAS. The geometry for the HRSG models discussed in this thesis is generated from scratch using the top-to-bottom design approach. The top-to-bottom design approach involves creating primitives – volumes of standard shapes such as bricks and cylinders - rotating and translating the primitives as needed, and performing the Boolean operations on the primitives, such as combining, subtracting, and splitting.

Technical drawings of the models are used to generate the three-dimensional model [5]. The dimensions are read from the design drawings and vendor technical drawings for components like duct burners, SCR catalyst and CO catalyst. Using these details the geometry is generated to represent the actual equipment as closely as possible. The geometry includes the "inner gas path" from the inlet of the HRSG through the exhaust [5]. This may include the inlet duct, duct burner elements, volume representation of the distribution grid, heat exchanger modules, the SCR & CO catalyst modules, exhaust duct breaching and the stack, depending upon the system being modeled. The geometry of the models discussed in this thesis is shown in figure 4-2 and figure 4-3. The

geometry includes only the exhaust gas path with some assumptions and simplifications made for some of the HRSG components like the heat exchangers, duct burners and SCR & CO catalyst sections. The simplifications applied on some of the components are discussed in chapter three.

4.1.2 Meshing of Lower Entities

Based on the complexity of the geometry being handled, the geometry has to be divided into smaller regions in order to apply constraints and control the quality of the resulting mesh. Any volume generated is a combination of faces. Faces are formed as a combination of closed edges, and an edge is formed by joining two vertices either by a straight line or following a contour as necessary. The lower entities in a volume are the faces and edges which are used to generate this volume. The first stage in meshing the volume begins with meshing the edges. Once the meshing of all the edges is complete, face mesh can be generated based upon the existing edge mesh elements. If a structured mesh is generated for the given volume, the quality of the mesh volume can be controlled by both the edge and face mesh. In case of unstructured meshing it is advisable to use some additional features of GAMBIT like the size function to restrict the size and quality of the mesh. In the HRSG model, the region around the duct burner should have a fine mesh compared to the other regions. So care is to be taken while splitting the volume into sub-volumes, which gives some flexibility in controlling the mesh quality. This also allows the user to use two different meshing schemes Cooper, and TetHyb/T-grid scheme on both the sides of a common face forming two volumes representing two different zones in the model effectively.

4.1.3 Meshing of Higher Entities

Based on the constraints applied while meshing the lower entities (e.g. mesh on the edges of a face), the final mesh of the volume is generated. The accuracy of the result of any CFD code depends on the quality of the mesh, so care is to be taken while generating the mesh. Dividing the model into small zones or sub-volumes helps in controlling the mesh quality. In addition to mesh quality, the other important thing to consider while meshing the model is the mesh size of the full model. The size of the mesh generated should be computationally manageable, as time required to get a converged solution for a CFD problem depends directly on the size of the mesh. A compromise is to be made while selecting the mesh size for a particular problem. While trying to keep the mesh resolution fine in some of the critical flow regions - for example, near the duct burners to be able to capture the complicated mechanism of combustion along with the flow - care is to be taken to keep the mesh size computationally manageable.

The computational mesh for the models is generated using 3-D hexa-hederal, tetrahedral and hex-wedge mesh types, which provides better representation of the geometry and at the same time limits the overall mesh size. The meshing schemes used to generate the mesh are hex/wedge with Cooper or Tet/hybrid with T-grid. Hex/wedge with the Cooper scheme allows the user to use the meshed faces on both ends of volume to generate the mesh for the entire volume. This type of meshing helps to control the quality of the mesh effectively. The Cooper scheme can be applied for regular geometries and for volumes which have similar mesh elements on both the faces. For volumes with much more complex shapes and with different mesh elements on each face, the Tet/Hybrid T-grid scheme is used. The mesh is generated using the Cooper scheme whenever possible,

and the Tet/Hybrid scheme for some complex sections. The maximum skewness in the mesh is less than 0.8. The computational mesh generated for the Beatrice HRSG consists of 637,627 elements. For the Current Creek HRSG, considering the complexity of the model two different mesh sizes are used to make sure that the results do not vary largely. The number of elements in a coarse mesh is 2,770,000 and 3,845,000 for fine mesh. The results for the fine mesh are discussed in this thesis.

4.1.4 Defining the Boundary Conditions

Once the mesh generation is completed for the entire HRSG system, appropriate boundary conditions need to be applied for the surfaces. This step includes defining the walls and specifying the zones for the distribution grid, heat exchangers, SCR & CO catalysts, and exhaust stack, along with the HRSG inlet and exhaust conditions. This completes the preprocessing stage and the problem is ready to be solved in a CFD solver.

4.2 Processing

A 3D steady-state, incompressible solution for Navier-Stokes equations with species transport with/without chemical reactions was performed using Fluent. Fluent solves the Reynolds-averaged form of Navier-Stokes equations, considering the conservation of mass, momentum, energy and species transport with/without the chemical reactions for fired/unfired cases. A standard two equation turbulence model (k-ε) with wall functions is applied to model the turbulent flow. Pressure velocity coupling of momentum and continuity equations is obtained using the SIMPLE algorithm. An eddy dissipation model with two-step reaction chemistry model is applied to model gas

combustion for duct fired conditions. The boundary conditions applied for the models are discussed below.

4.3 Boundary Conditions

Appropriate boundary conditions need to be applied at the HRSG inlet (GT exhaust profile), duct burner nozzles (fired case), volumetric regions representing heating surface modules, SCR and CO catalyst modules, the stack exit, and the HRSG duct and casing liner walls.

4.3.1 GT Exhaust Velocity Profile/HRSG Inlet Velocity Profile

The inlet velocity distribution of the HRSG system is specified using the velocity profile from the exhaust of the gas turbine with for which it is designed to operate. Beatrice HRSG is designed to operate with left hand exhaust of gas turbine "GE Frame MS7001EA". The Current Creek HRSG is designed with axial exhaust of "GE7FA" gas turbine [5].

The diagrammatic representation of the gas turbine and HRSG location for Beatrice HRSG are shown in figure 4-4a. The HRSG is located on the left-hand side of the gas turbine using a left-hand exhaust from the exhaust plenum. The velocity profile measured at the expansion joint outlet flange is shown in figure 4-4b. The velocity distribution shown is given for equally spaced points and the values shown are normalized velocities at ISO conditions. The distribution given can be applied to the HRSG inlet by developing a user defined function (UDF) that allows the user to specify the inlet profiles for velocity, temperature and any turbulence parameter at the inlet. The

inlet velocity profile applied using the UDF is shown in figure 4.5. The mass flow rate and temperature of the exhaust gas at the inlet of HRSG depends upon the load conditions of the gas turbine.

The inlet velocity distribution for Current Creek model consists of a normalized axial velocity profile at the expansion outlet flange. The distribution is given as a function of the radius and normalized by the average velocity at the exhaust area. Swirl angle is provided as a function of the GT load to allow determination of tangential velocities. The turbine outlet conditions for Current Creek model are shown in figure 4-6. This velocity profile is applied to the model using a UDF. The applied inlet velocity contours and the inlet temperature profiles are shown in figure 4-7. Inlet boundary conditions based upon the gas turbine exhaust for both the HRSG models are shown in tables 4-1 and 4-2.

4.3.2 Duct Burner

Boundary conditions for duct burner nozzles consist of the natural gas mass flow rate and fuel composition specified for the fired conditions. The mass flow rate of fuel is calculated using the design data, heat input and the lower heating value for each case. The geometrical area of fuel nozzles per burner element is modeled to correctly represent the velocity and direction of the actual fuel injection into the system. For unfired conditions, fuel mass flow rate at the nozzles is set to zero. The burner element manifold pipe and flame stabilizer baffle walls are modeled as solid walls. Conduction heat transfer is allowed across the flame stabilizer baffles and modeled using conjugate heat transfer.

The burner configuration for the Current Creek model includes unfired wing baffles, which are located between the burner elements to increase the exhaust gas velocity at the burner face. There are a total of six burner elements and fourteen wing baffle elements, two baffle elements located one above and one below the burner element, and one additional wing baffle each on top and bottom to further reduce the flow area. Each duct burner has a total of 300 nozzles, 150 above the horizontal plane and 150 below the horizontal plane, with the nozzles oriented $\pm 30^0$ from the horizontal plane. Instead the duct burners are modeled as having 150 nozzles with 75 above the horizontal and 75 below the horizontal. However, the total fuel nozzle area and orientation are maintained the same as that in the actual case to keep the inlet velocity and orientation close to the actual case. The wing baffle located above the burner element also serves as a supporting baffle, giving some support for the burner element. The wing baffle and pipe supports are modeled as solid walls with conduction. The burner element configuration with the wing baffle arrangement for the Current Creek HRSG is shown in figure 4-8.

The burner configuration for the Beatrice model includes two duct burner elements, located in the inlet duct upstream to the first heating surface. Each duct burner has sixty-three nozzles evenly distributed throughout the length, each with a nozzle diameter of 0.1''. The modeled burner has forty-two elements and the nozzle diameter is adjusted to match the total burner inlet area of all the burner elements being modeled with that of the actual area. The nozzle areas modeled are circular in shape. Baffles are not included in the design of the burner elements for this model. The burner element includes the flame stabilizers which are defined as walls. The actual model includes small pores in the flame stabilizers, but these pores are modeled as walls in the simulation. The

duct burners are designed and supplied by John Zinc Burner. The configuration of the burner element is shown in figure 4-9.

4.3.3 Distribution Grid

The distribution grid is located between the inlet of the HRSG and the duct burners. The purpose of the distribution grid is to smooth out the variations in the flow field along the cross section caused because of the inlet velocity profile. The performance of the duct burners depends upon the flow velocity deviation from the average velocity. Smaller the deviation better the performance. The distribution grid is applicable only for the Beatrice model as the flow is not uniform at the entrance of the HRSG and these should be smoothed out before the flow reaches the duct burners to have a better performance of the burner. The distribution grid is represented in the model as a volume of porous media with high inertial resistance in the non flow directions and the resistance in the flow direction set to match the pressure drop from the performance sheet.

In the case of Current Creek model the burner array is located between the heat exchanger modules the heat exchanger module located upstream of the burner array acts similar way as a distribution grid making the flow entering the duct burner array uniform.

4.3.4 Heat Exchanger Modules

The general type of heat exchangers used in HRSG are tube-type heat exchangers with/without fins. It is not practically possible to represent the heat exchanger module exactly the same way with all of the tube modules, as this would result in creating a very large and complicated computational mesh. Instead, the tube bundle modules are

modeled as appropriately sized porous volume regions in the HRSG, with gas side pressure drop characteristics and heat transfer. Exact modeling of individual tubes with fins is not necessary to realistically represent the large-scale flow characteristics of the exhaust gas through the HRSG. Using this approach the only data lost are the small scale velocity changes around the tubes, which can be represented by the pressure drop characteristics of the porous media and the heat transfer model. The tube bundle modules are divided into separate zones as shown in figures 3-10 and 3-11**.** This allows the user to specify the heat duty and pressure drop characteristics separately for each of the module sections. The values for heat duty and pressure drop are set using the Vogt Power Internationals (VPI) thermal performance program CARDS.

4.3.5 SCR & CO Catalyst System

One of the advantages that make the use of the combined-cycle systems favorable are their eco-friendly operation (low emissions). The emissions resulting from a combined cycle is small compared to the simple gas turbine cycle. The major emissions resulting from the combustion mechanism are the NO_x and CO products. Two emission control devices, SCR and CO catalyst systems, will be installed on each combined-cycle system to check these emissions. The Selective Catalyst Reduction (SCR) system is used to reduce the emission of NO_x. The SCR system injects ammonia using the Ammonia Injection Grid (AIG) upstream of a catalyst bed to react with and reduce the emissions of NO_x from the gas turbine and duct burners. An oxidation catalyst will be installed that will reduce CO emissions by oxidizing them completely to carbon dioxide (CO_2).

SCR and CO catalyst regions are modeled in the similar way as the distribution grid. The dimensions of baffles and internal support structures are read from the drawings provided by the VPI and the vendors. The baffles and supporting walls are modeled as walls with no slip boundary condition. The inertial resistance coefficient for the region was specified to achieve the pressure drop specified by the vendor. Pollutant emission control reactions in these catalysts are not simulated for both the designs; a detailed sub-model study can be performed to study the performance and effectiveness of these emission control devices.

The computational mesh for the HRSG models does not include the AIG because of the size limitations. The flow distribution at the location of the AIG is studied, as the flow entering the AIG should be uniform to facilitate uniform mixing of the injected ammonia in the exhaust gas.

4.3.6 HRSG Duct and Casing Walls

The HRSG casing walls consist of linear panels, a layer of fiber blanket insulation, and the exterior steel casing [5]. These three layers of insulation are represented in the model as wall. The composite thermal conductivity can be calculated from the individual conductivity values of each of the above materials and can be applied to the wall. For all of the designs of HRSG discussed in this thesis the heat lost from the walls and casing is assumed to be negligible. The wall is treated as a perfectly insulated wall with no heat loss by applying the boundary condition, adiabatically insulated, with no slip boundary condition, and the gas velocity is set to be zero on the wall.

4.3.7 Breaching and Stack Exit

The gas flow from the heat exchanger is directed into the exhaust stack through breaching. There are two boundary conditions applied at this region: interior and wall. The interior boundary condition is applied to represent the holes in the plate and the remaining plate is modeled as wall. The walls of the exhaust stack are modeled as insulated walls allowing no heat loss from the system. The flow outlet at the exhaust stack is taken as a standard pressure outlet boundary condition. Atmospheric pressure is applied at the exit of the HRSG [5].

Case	Flue gas density	Flow	Duct burner heat input	Avg. exhaust velocity	Gas temp.
	(lb/ft^3)	(lb/hr)	(MMBtu/hr)	(FPM)	(^0F)
Fired case	0.025422	2,064,000	16	9,405	1028
Unfired case	0.025976	2,064,000	0	9,405	1028

Table 4-1: Gas turbine exhaust conditions (Beatrice HRSG)

Case	Flue gas density	Flow	Duct burner heat input	Avg. exhaust velocity	Gas temp.
	(lb/ft^3)	(lb/hr)	(MMBtu/hr)	(FPM)	(^0F)
Fired case	0.024469	2,939,700	450.7	11,822	1118
Unfired case	0.024469	2,939,700	0	11,822	1118

Table 4-2: Gas turbine exhaust conditions (Current Creek HRSG) [5]

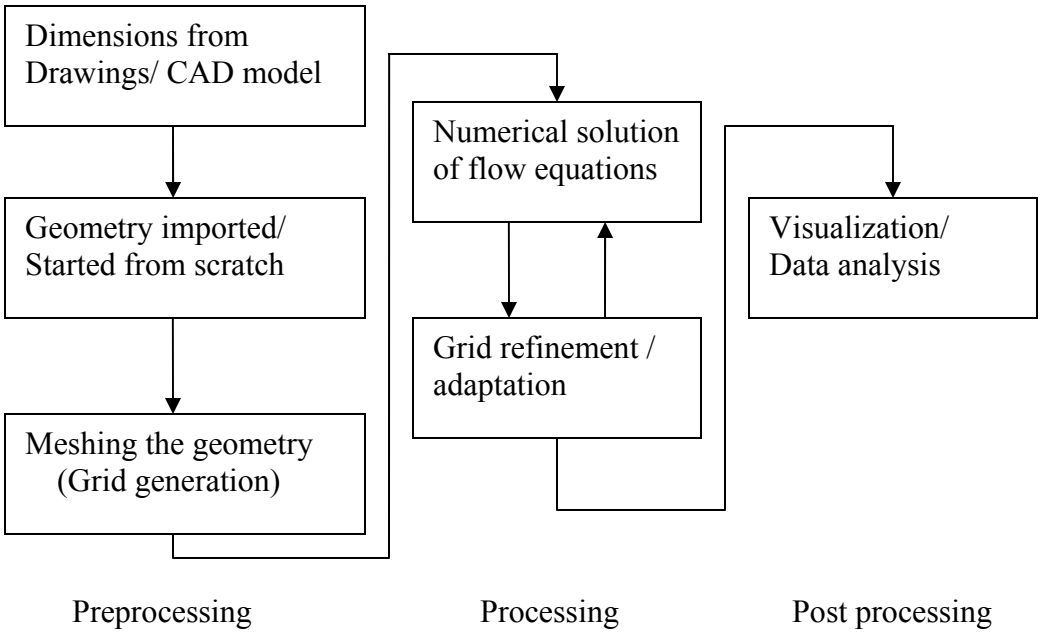

Figure 4-1: Step by step procedure of CFD solution

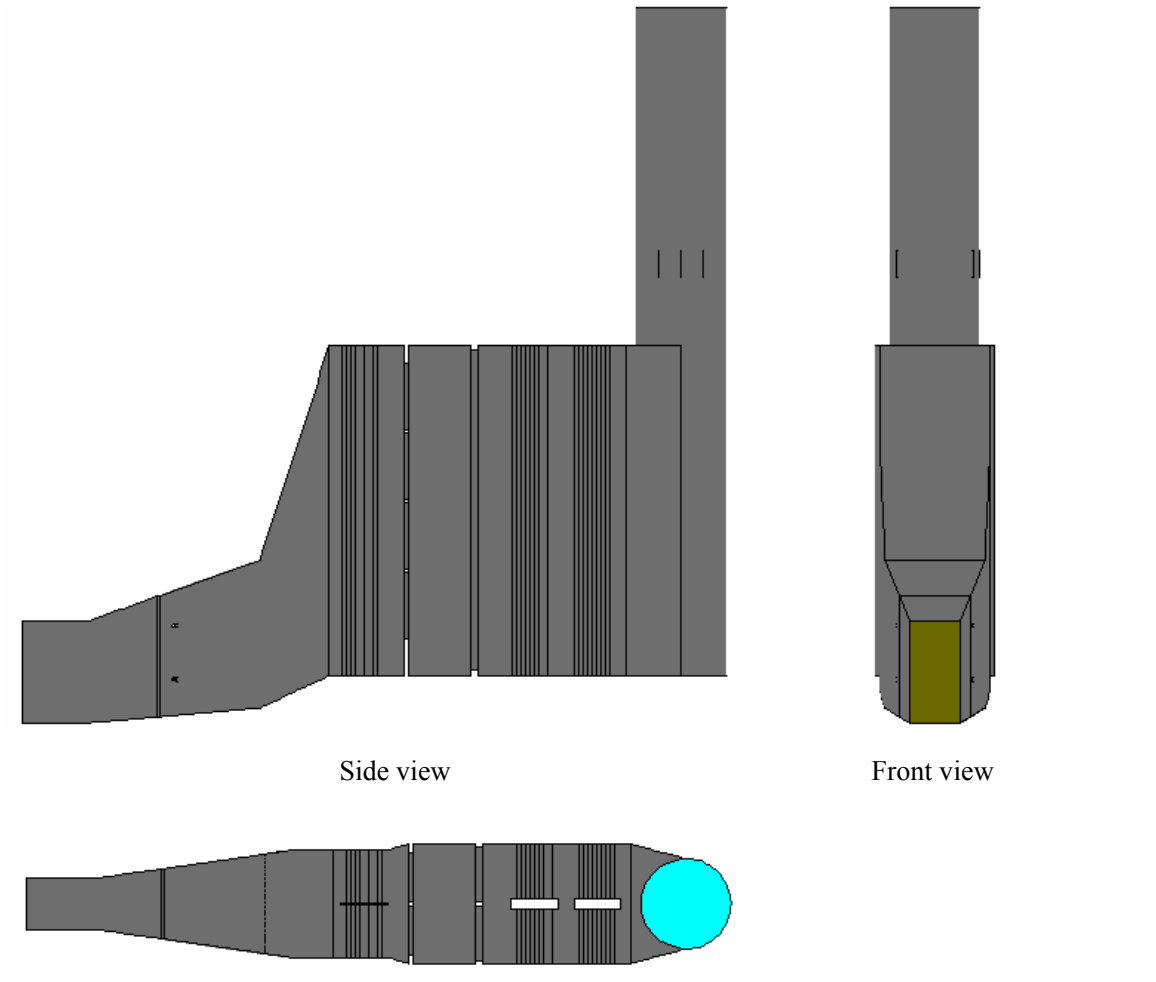

Side view

Front view

Plan view

Figure 4-2: Geometry of Beatrice HRSG, surface details

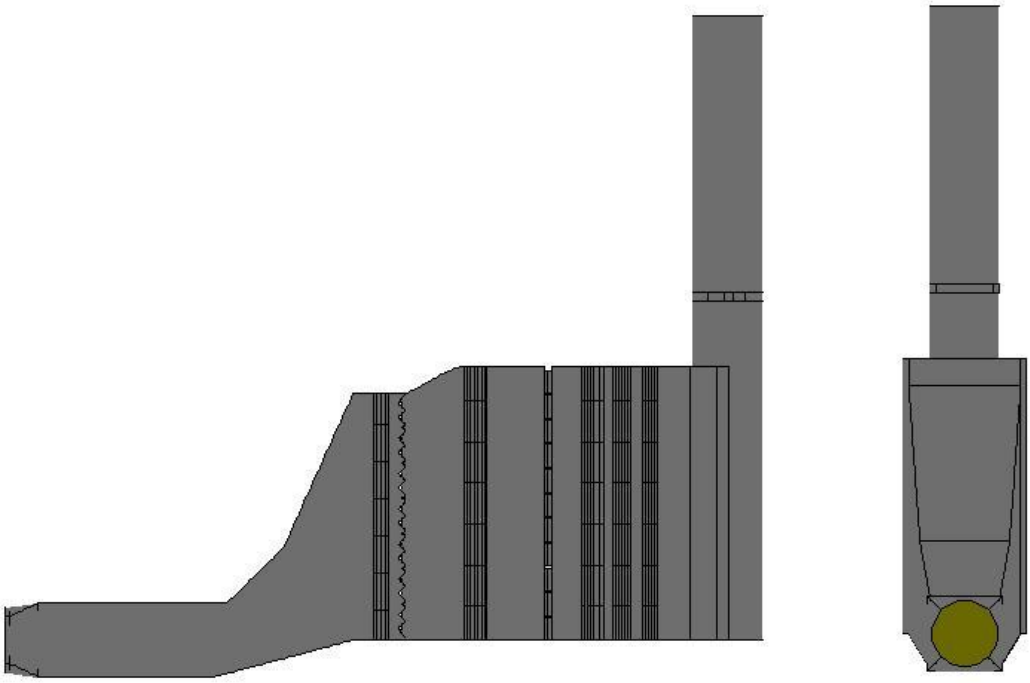

Side view

Front view

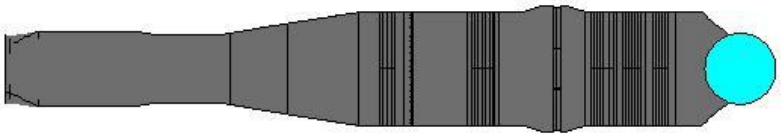

Plan view

Figure 4-3: Geometry of Current Creek HRSG, surface details

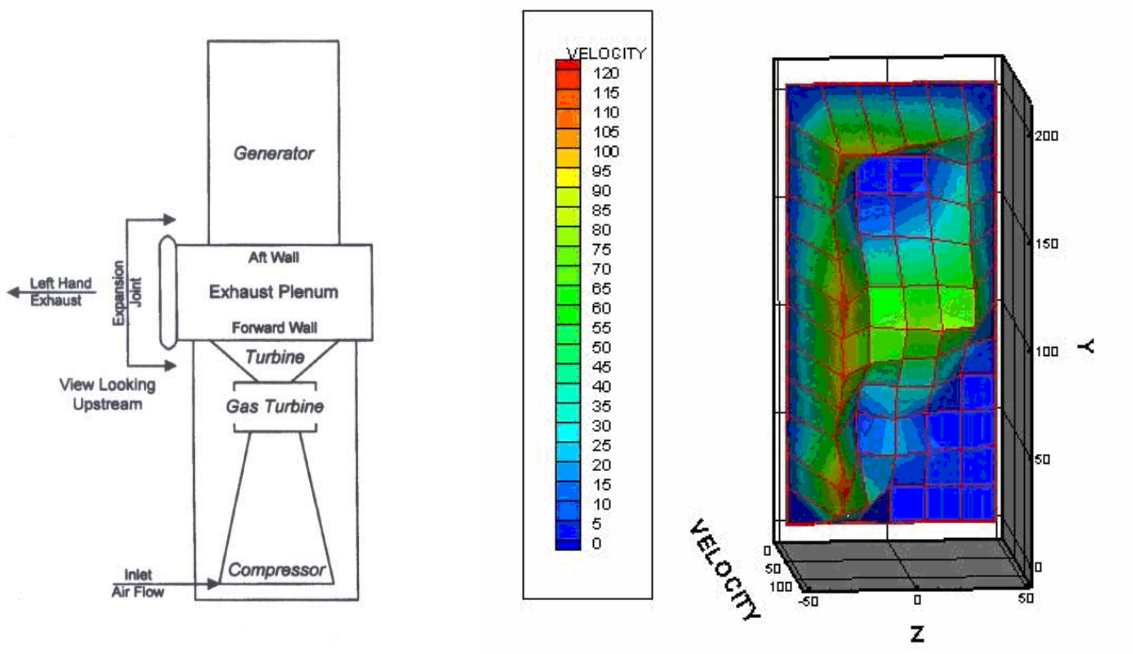

GT - HRSG GT exhaust velocity profile (GE Data)

Figure 4-4: Turbine outlet conditions for Beatrice HRSG

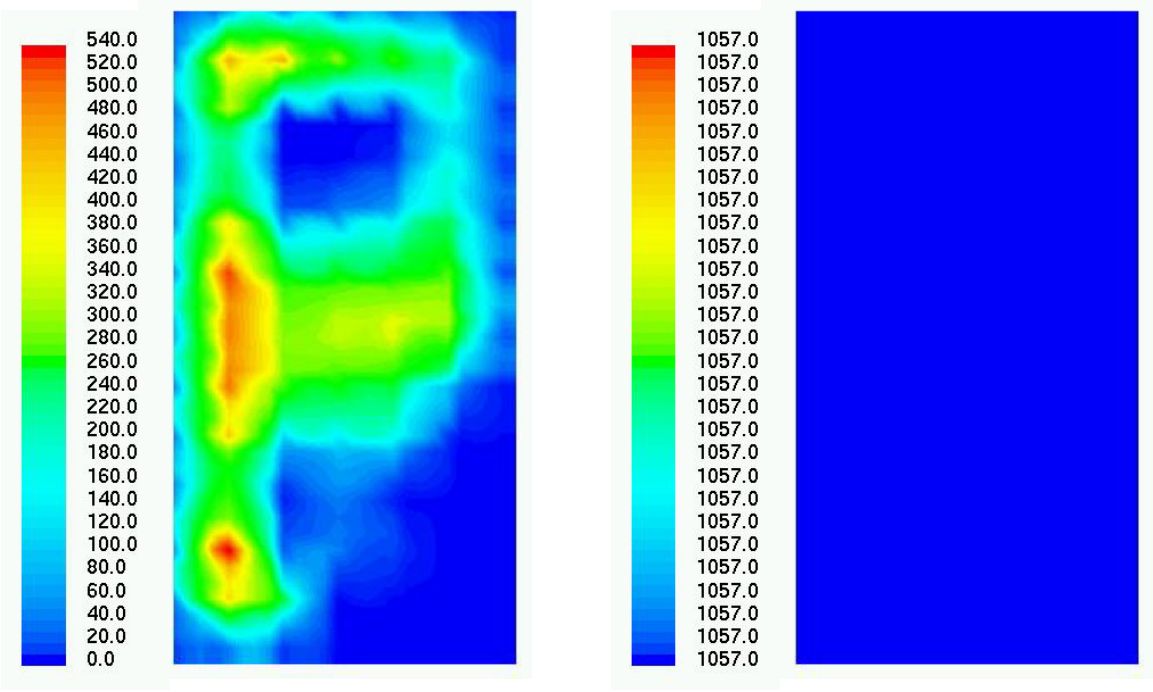

Inlet X-velocity contour (ft/s) Temperature contour (^{o}f)

Figure 4-5: Beatrice HRSG inlet conditions

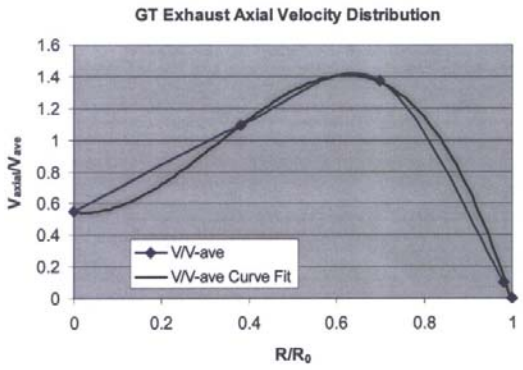

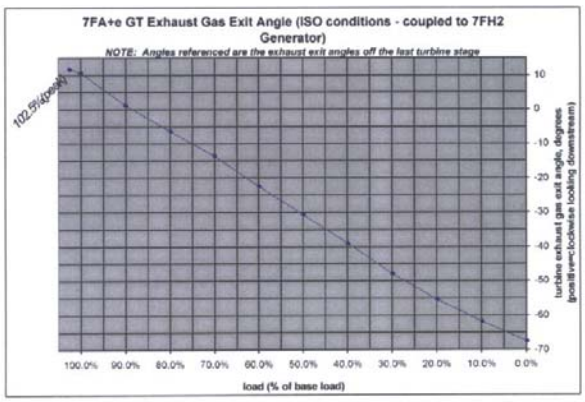

GT exhaust velocity profile (GE Data) GT exhaust velocity profile (GE Data)

Figure 4-6: Turbine outlet conditions for Current Creek HRSG [5]

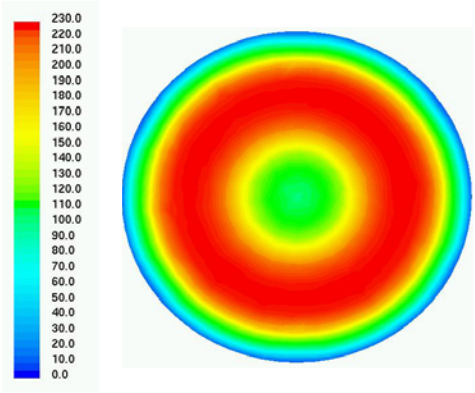

X-velocity contour (ft/s)

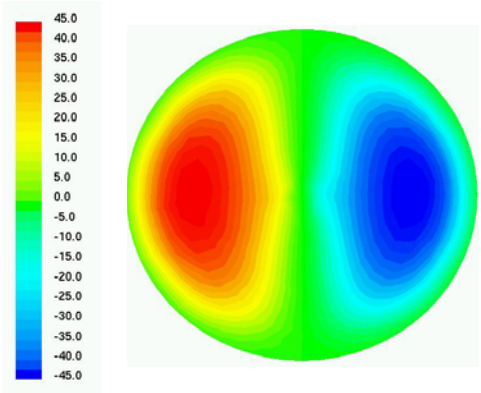

Y-velocity contour (ft/s)

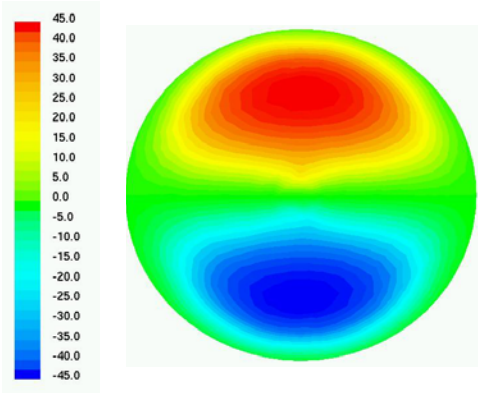

Z-velocity contour (ft/s)

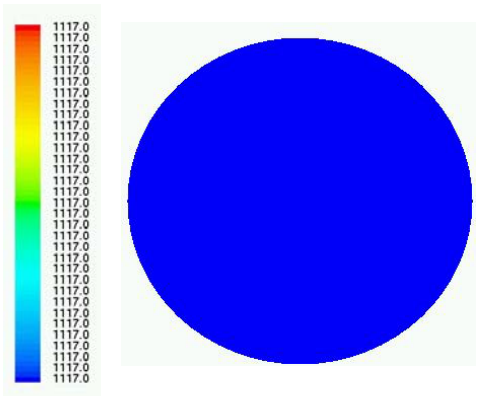

Temperature contour (f)

Figure 4-7: Current Creek HRSG inlet conditions

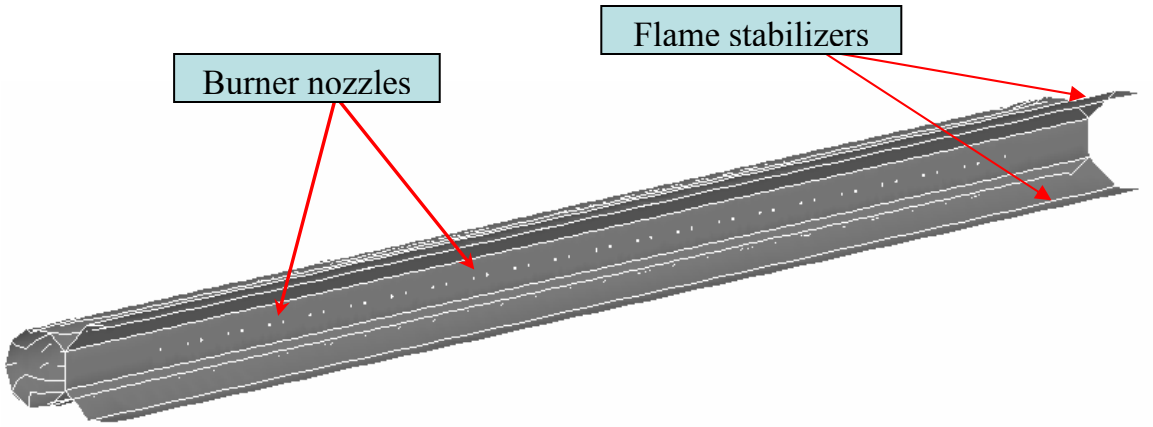

Figure 4-8: Burner configuration, Beatrice HRSG

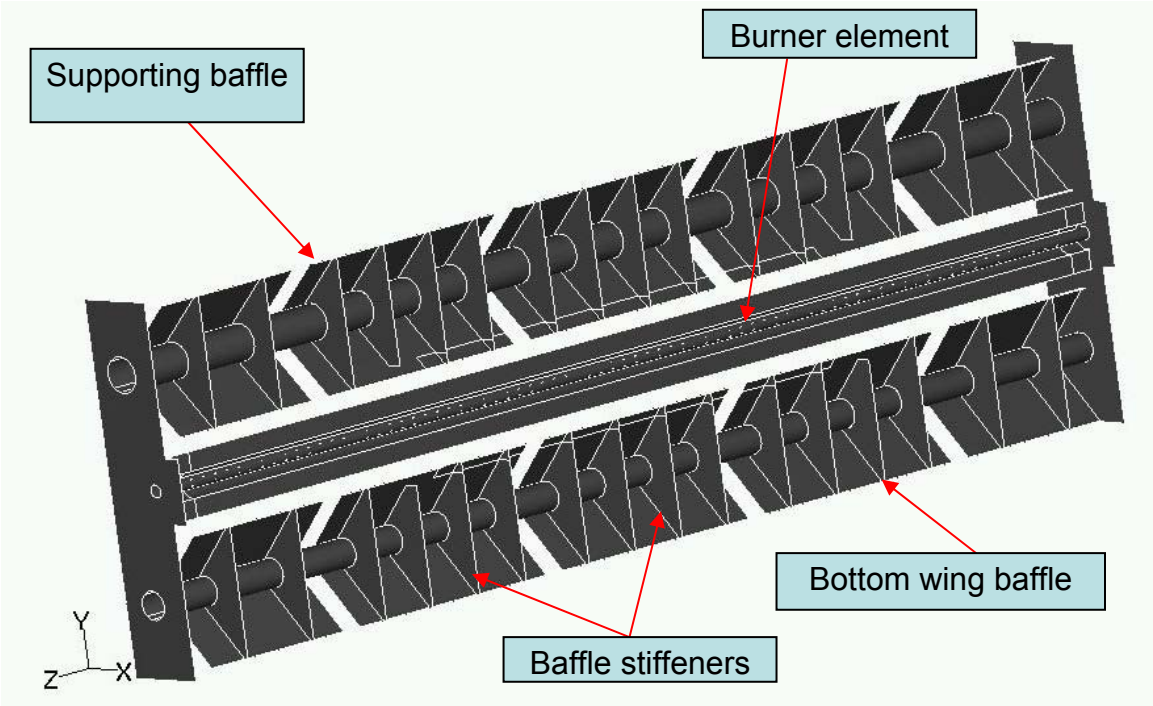

Figure 4-9: Burner configuration, Current Creek HRSG

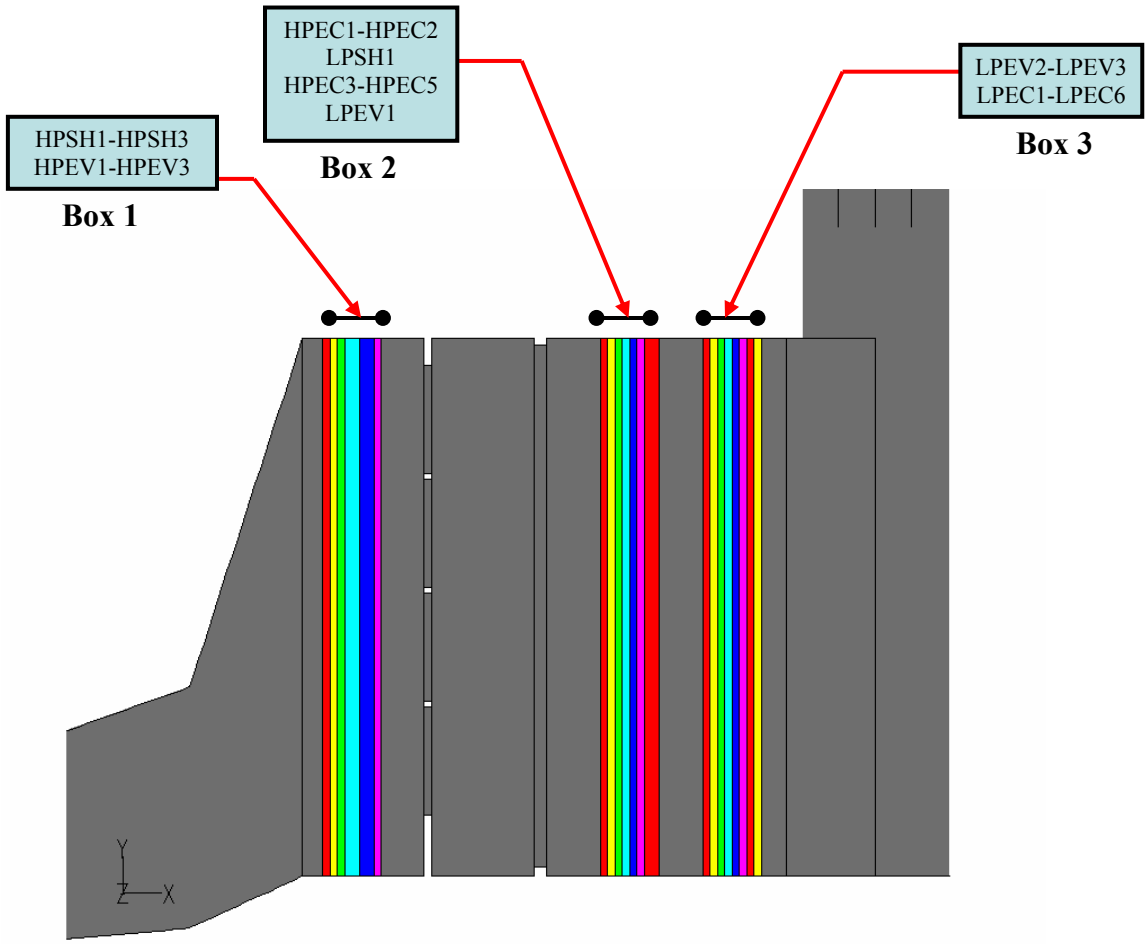

Figure 4-10: Heat exchanger sections Beatrice HRSG

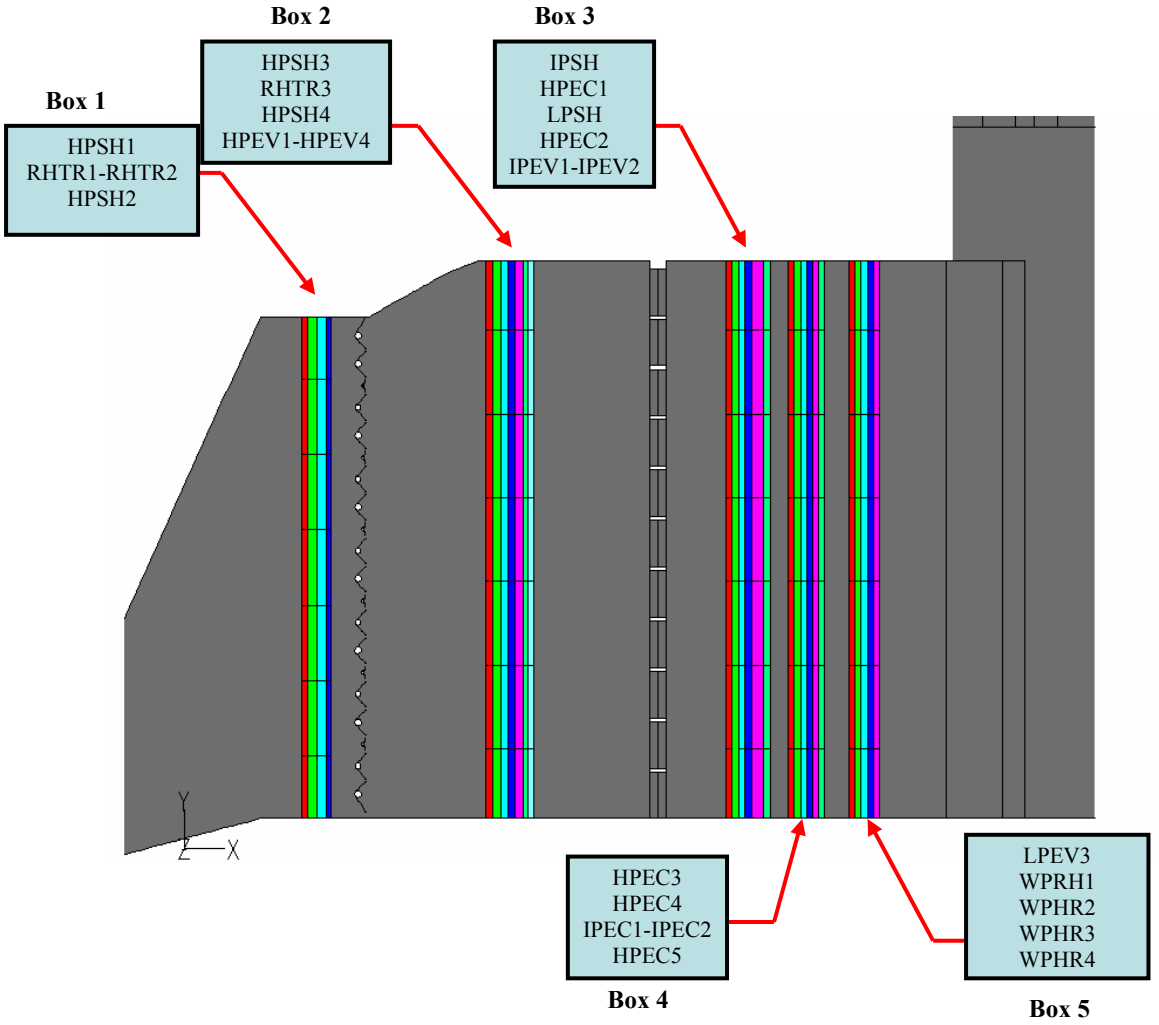

Figure 4-11: Heat exchanger sections, Current Creek HRSG

Chapter 5

Analyzed Cases

5.1 Beatrice HRSG

The following performance conditions were analyzed for the Beatrice HRSG design based on the thermal performance prediction from CARDS (in-house thermal performance code for VPI).

1. Fired case (100% GT Load, $T_{amb} = 97^0$ F)

2. Unfired case (100% GT Load, $T_{amb} = 97^0$ F)

The turbine exhaust conditions are read from the table 3.1. Gas turbine exhaust velocity profile as shown in fig 3.4 is applied as the inlet velocity profile for the HRSG by defining a UDF at inlet. The inlet velocities are scaled to achieve the desired mass flow rate as given by the turbine exhaust conditions.

The inlet exhaust gas temperature is set constant and the value is read from the table 3.1. The species composition is read from the exhaust gas conditions and applied at the inlet of HRSG.

5.1.1 Fired Case

This case uses a supplementary firing of methane. The mass flow rate of fuel is calculated using the value of heat energy added to the exhaust gas and the given lower heating value of the fuel. The flow rate of fuel is distributed evenly between the two burner elements shown in fig 4.4. The performance conditions for this case are presented in table 5.1.

5.1.2 Unfired Case

This case does not use supplementary firing. This can be attained by setting the flow rate of fuel at the burner inlet to zero, or by simply defining the burner inlet to be walls. The performance conditions for this case are presented in table 5.2.

5.2 Current Creek HRSG

The following performance conditions were analyzed for the Current Creek HRSG design based on the thermal performance prediction from CARDS (in house thermal performance code for VPI).

1. Fired case
2. Unfired case

The turbine exhaust conditions are read from the table 3.2. Inlet velocity profile as shown in figure 3.7 is applied at the HRSG inlet with the inlet velocities scaled to achieve the desired mass flow rate as given in the turbine exhaust conditions. The inlet exhaust gas temperature is set constant and the value is read from the table 3.2. The species composition is read from the exhaust gas conditions and applied at the inlet of HRSG.

5.2.1 Fired Case

This case modeling consists of six burner elements with a natural gas fuel inlet with fuel rates read from the performance table 5.6. Fuel properties are defined for the natural gas as specified in the specified fuel gas data sheet. The performance conditions for this case are presented in table 5.4. (fired case)

5.2.2 Unfired Case

This case is set in a similar way to the unfired Beatrice case, with the burner being set as wall. The performance conditions for this case are presented in table 5.3 (unfired case)

	Steam/Water side				Gas side		
Section	**Flow**	**Temperature**		**Duty**	**Temperature**		**Pressure drop**
		In	Out		In	Out	
	(lbs/hr)	(^{o}F)		(MMBtu/hr)	(^{o}F)		(inch WC)
HPSH1	276536	919	997	13.25	1056	1033	0.38
HPSH2	275832	786	926	25.27	1033	988	0.34
HPSH3	275832	597	787	51.37	988	897	0.32
HPEV1	179877	586	597	103.11	897	712	0.69
HPEV2	83753	586	597	48.01	712	624	0.99
HPEV3	12202	586	597	6.99	624	611	0.48
HPEC1	278618	569	585	6.15	611	600	0.32
HPEC2	278618	535	569	12.13	600	578	0.47
LPSH1	55554	352	555	6.15	578	566	0.17
HPEC3	278618	511	535	8.23	566	551	0.27
HPEC4	278618	454	511	18.13	551	517	0.43
HPEC5	278618	357	454	29.11	517	463	0.41
LPEV1	46407	345	354	43.15	463	382	0.74
LPEV2	4519	345	354	4.20	382	374	0.24
LPEV3	4629	345	354	4.30	374	366	0.33
LPEC1	381780	330	343	5.02	366	356	0.21
LPEC2	381780	306	330	9.41	356	338	0.34
LPEC3	381780	277	306	11.54	338	316	0.33
LPEC4	381780	240	277	14.18	316	289	0.32
LPEC5	381780	195	240	17.43	289	256	0.30
LPEC6	381780	140	195	20.97	256	216	0.28

Exhaust Gas Flow	2,064,000	lbs/hr
Exhaust Gas Temp.	1028	^{o}F
Gas Constituents	CO_2	5.77%
	H_20	5.82%
	N_2	72.99%
	O_2	14.13%

Table 5-1: Performance conditions, Beatrice fired case (100 % GT load t_{amb} 97^{o}F)

	Steam/Water Side				Gas side		
Section	**Flow**	**Temperature**		**Duty**	**Temperature**		**Pressure drop**
		IN	Out		In	Out	
	(lbs/hr)	(^{o}F)		(MMBtu/hr)	(^{o}F)		(inch WC)
HPSH1	263881	911	979	11.00	1028	1008	0.37
HPSH2	263881	781	913	22.64	1008	969	0.33
HPSH3	263881	589	782	48.22	969	883	0.31
HPEV1	171937	582	590	100.23	883	702	0.68
HPEV2	80225	582	590	46.77	702	616	0.98
HPEV3	11719	582	590	6.83	616	604	0.47
HPEC1	266547	567	581	5.36	604	594	0.32
HPEC2	266547	535	567	10.95	594	574	0.47
LPSH1	56926	352	551	6.18	574	562	0.17
HPEC3	266547	511	535	7.44	562	548	0.27
HPEC4	266547	456	511	16.99	548	517	0.43
HPEC5	266547	356	456	28.55	517	463	0.41
LPEV1	47563	347	354	43.37	463	382	0.74
LPEV2	4626	347	354	4.22	382	374	0.24
LPEV3	4737	347	354	4.32	374	366	0.33
LPEC1	368719	333	345	4.52	366	357	0.21
LPEC2	368719	311	333	8.66	357	341	0.34
LPEC3	368719	282	311	10.91	341	320	0.33
LPEC4	368719	245	282	13.77	320	294	0.32
LPEC5	368719	198	245	17.40	294	260	0.30
LPEC6	368719	140	198	21.51	260	219	0.28

Exhaust gas flow	2,064,000	lbs/hr
Exhaust gas temp.	1028	^{o}F
Gas constituents	CO_2	5.77%
	H_20	5.82%
	N_2	72.99%
	O_2	14.13%

Table 5-2: Performance conditions, Beatrice unfired case (100% GT load t_{amb} 97^{o}F)

	Steam/Water Side				Gas side		
Section	**Flow**	**Temperature**		**Duty**	**Temperature**		**Pressure drop**
		IN	OUT		IN	OUT	
	(lbs/hr)	(^{o}F)		(MMBtu/hr)	(^{o}F)		(inch WC)
HPSH1	703822	1024	1054	13.92	1114	1097	0.19
RHTR1	344978	959	1063	19.49	1097	1074	0.46
RHTR2	385419	959	1042	17.33	1074	1053	0.45
HPSH2	703822	1004	1024	9.04	1053	1042	0.28
HPSH3	700440	860	1014	74.51	1540	1456	0.12
RHTR3	727816	733	967	93.02	1456	1350	0.17
HPSH4	700440	644	860	173.72	1350	1149	0.27
HPEV1	277193	565	645	155.29	1149	965	0.25
HPEV2	253854	565	645	142.21	965	792	0.42
HPEV3	118480	565	645	66.37	792	710	0.38
HPEV4	50913	565	645	28.52	710	675	0.36
IPSH	37860	471	588	3.2	675	671	0.05
HPEC1	700440	496	565	58.61	671	597	0.33
LPSH	17037	315	570	2.24	597	594	0.03
HPEC2	700440	423	496	56.96	594	522	0.31
IPEV1	28511	417	472	23.16	522	493	0.35
IPEV2	9349	417	472	7.59	493	483	0.28
HPEC3	700440	396	423	19.8	483	458	0.19
HPEC4	700440	366	396	21.78	458	430	0.15
IPEC1*	37860	316	416	3.98	430	423	0.08
HPEC5	700440	321	366	33.16	425	382	0.25
LPEV1	28922	280	315	25.99	382	349	0.24
LPEV2	13357	280	315	12	349	333	0.23
LPEV3	5740	280	315	5.16	333	326	0.23
WPHR1	761302	247	280	25.02	326	294	0.21
WPHR2	761302	215	247	24.8	294	262	0.21
WPHR3	761302	183	215	24.51	262	230	0.20
WPHR4	761302	152	183	23.94	230	198	0.19

Exhaust Gas Flow	2939700	Lbs/hr
Exhaust Gas Temp.	1118	F
Gas Constituents	CO_2	5.77%
	H_20	5.82%
	N_2	72.99%
	O_2	14.13%

Table 5-3: Performance Conditions, Current Creek Fired Case

	Steam/Water Side				Gas Side		
Section	**Flow**	**Temperature**		**Duty**	**Temperature**		**Pressure Drop**
		IN	OUT		IN	OUT	
	(lbs/hr)	(^{o}F)		(MMBtu/hr)	(^{o}F)		(inch WC)
HPSH1	360862	972	1051	16480000	1113	1093	0.19
RHTR1	194992	839	1062	22960000	1093	1066	0.46
RHTR2	217454	839	1033	22250000	1066	1039	0.45
HPSH2	360862	859	972	24080000	1039	1009	0.27
HPSH3	360856	779	860	18450000	1009	987	0.08
RHTR3	412446	726	839	24650000	987	956	0.12
HPSH4	360856	558	779	65680000	956	875	0.20
HPEV1	137193	547	559	88240000	875	765	0.20
HPEV2	131635	547	559	84670000	765	657	0.35
HPEV3	63975	547	559	41150000	657	605	0.33
HPEV4	28052	547	559	18040000	605	581	0.32
IPSH	58783	419	487	2770000	581	578	0.05
HPEC1	360856	499	546	20840000	578	551	0.30
LPSH	51215	292	450	4180000	551	545	0.03
HPEC2	360856	417	499	33170000	545	502	0.29
IPEV1	44359	383	421	37610000	502	453	0.34
IPEV2	14425	383	421	12230000	453	437	0.26
HPEC3	360856	399	417	7290000	437	428	0.18
HPEC4	360856	368	399	11710000	428	413	0.14
IPEC1*	58784	293	382	5410000	413	408	0.08
HPEC5	360856	295	368	27210000	405	370	0.24
LPEV1	32085	289	293	29380000	370	331	0.23
LPEV2	14668	289	293	13430000	331	313	0.22
LPEV3	6247	289	293	5720000	313	305	0.22
WPHR1	470862	269	289	9890000	305	292	0.21
WPHR2	470862	238	269	14460000	292	273	0.21
WPHR3	470862	194	238	21110000	273	245	0.20
WPHR4	470862	130	194	30110000	245	205	0.19

Exhaust Gas Flow	2939700	lbs/hr
Exhaust Gas Inlet Temp.	1118	^{o}F
Gas Composition (by weight)	CO_2	5.77%
	H_20	5.82%
	N_2	72.99%
	O_2	14.13%

Table 5-4: Performance Conditions, Current Creek Unfired Case

Chapter 6

Results and Analysis (Beatrice HRSG)

The cases with the inlet conditions discussed in chapter 5 for Beatrice HRSG are discussed in this chapter. The following test cases were analyzed using the computational flow model, fired case, unfired case and modified fired case. The test conditions selected represent extreme cases. Other available cases are either at high gas flow rates or the part-load conditions of GT. The fired cases are selected based on conditions requiring the highest burner input combined with the lowest GT mass flow, thus making these cases ideal to check the performance of the design. The predicted results were analyzed to understand the flow and evaluate the design in the following areas of interest [5]:

- Flow distribution within the inlet duct
- Flow distribution into the burner elements
- Burner performance
- Flow distribution and gas temperature distribution at the heating surface
- Flow distribution into the emission control equipment

Layout of figures:

This chapter discusses the simulation results for the Beatrice HRSG. Simulations are carried out for three different cases: a fired case, an unfired case, and a modified design fired case. Figures relating to the fired case are shown from figures 6-1 through 6-14. Figures 6-1 and 6-2 show the details of stream traces within the model colored by velocity magnitude. Figure 6-3 shows the axial velocity components along the width of the HRSG. Figure 6-4 shows the temperature distribution along the width of the HRSG. Figure 6-5 shows gas flow and temperature distribution entering HPSH1 (Box 1). Figure 6-6 shows the contours of gas flow and temperature distribution leaving HPEV3 (Box 1). Figure 6-7 shows the contours of gas flow and temperature distribution entering the CO catalyst. Figure 6-8 shows the contours of gas flow and temperature distribution entering the SCR catalyst. Figures 6-9 and 6-10 show the contours of gas flow and temperature distribution entering and leaving heat exchanger box 2, respectively. Figures 6-11 and 6-12 show the contours of gas flow and temperature distribution entering and leaving heat exchanger box 3, respectively. Figure 6-13 show the static pressure contour along the width of HRSG. Figure 6-14 shows the comparison of gas side pressure drop in each of the heat exchanger sections and the average gas temperature entering the different heat exchanger with that of CARDS.

Figures related to the unfired case are shown in figures 6-15 through 6-25. Figure 6-15 shows the temperature distribution along the width of the HRSG. Figure 6-16 shows gas flow and temperature distribution entering the first heat exchanger surface i.e. heat exchanger box 1. Figure 6-17 shows gas flow and temperature distribution leaving heat exchanger box 1. Figure 6-18 shows gas flow and temperature distribution entering the

CO catalyst. Figure 6-19 show gas flow and temperature distribution entering the SCR catalyst. Figures 6-20 and 6-21 shows contours of gas flow and temperature distribution entering and leaving heat exchanger box 2, respectively. Figures 6-22 and 6-23 shows contours of gas flow and temperature distribution entering and leaving heat exchanger box 3, respectively. Figure 6-24 shows the static pressure contour along the width of HRSG. Figure 6-25 shows the comparison of gas side pressure drop in each of the heat exchanger sections and the average gas temperature entering the different heat exchanger with that of CARDS.

Figures related to the modified design, fired case are shown from figure 6-26 through figure 6-38. Figures 6-26 and 6-27 show the details of stream traces within the model colored by velocity magnitude. Figure 6-28 shows the axial velocity components along the width of the HRSG. Figure 6-29 shows the temperature distribution along the width of the HRSG. Figure 6-30 show contours of gas flow and temperature distribution entering the first heat exchanger surface i.e. heat exchanger box 1. Figure 6-31 show contours of gas flow and temperature distribution leaving heat exchanger box1. Figure 6-32 show contours of gas flow and temperature distribution entering the CO catalyst. Figure 6-33 show contours of gas flow and temperature distribution entering the SCR catalyst. Figures 6-34 and 6-35 shows contours of gas flow and temperature distribution entering and leaving heat exchanger box 2, respectively. Figure 6-36 shows gas flow and temperature distribution entering heat exchanger box 3. Figure 6-37 shows the static pressure contour along the width of HRSG. Figure 6-38 shows the comparison of gas side pressure drop in each of the heat exchanger sections and the average gas temperature entering the different heat exchanger with that of CARDS.

Figures related to the heat exchanger modeling approaches are shown in figures 6-39 to 6-41. Figure 6-39 shows the direction in which macros are numbered in a heat exchanger model. Figure 6-40 shows the gas temperature range comparison between the fixed heat rejection method and the fixed coolant inlet temperature method. Figure 6-41 shows the comparison of core friction coefficient values for different core friction exponent values.

6.1 Inlet Conditions and Inlet Duct

The gas velocity distribution in the inlet duct is important, as the inlet duct directs the gas flow from the GT exhaust to the heat exchanger surfaces in the HRSG. A uniform distribution of flow into heat exchangers is desired for a stable thermal performance. The regions of back flow in the inlet duct are to be limited. Especially in case of an HRSG system designed to operate on a side exhaust GT, the inlet flow velocity is biased to one side, which results in large recirculation area in the inlet duct.

For the Beatrice design, the gas velocity profile at the exhaust of the gas turbine and the velocity profile entering the inlet of HRSG are shown in figure 3-5 and figure 3-6, respectively. This HRSG is designed to operate with the side exhaust GT. It is necessary to add some flow control devices like the distribution grid in the inlet duct to provide an even distribution of gas within the duct burners located in the inlet duct and the heat exchangers located downstream of the duct burners.

Results for the fired case, unfired case, and modified fired case are presented in this chapter. Figures 6-1 and 6-2 show the steam traces in the model for fired case. It is observed that there is a large amount of recirculation in the inlet duct near the top burner

region. Considering the design constraint's the modification suggested is to change the design of distribution grid and replace the existing distribution grid with one in which the gas side pressure drop is increased to twice the initial value. Figures 6-26 and 6-27 show the stream traces for the modified fired case. It is observed that by the use of the distribution grid with more pressure drop, the recirculation strength in the inlet duct near the top burner is reduced, but not completely eliminated. The variations of static pressure for the three cases fired case, unfired case and modified design, fired case is shown in figures 6-13, 6-24 and 6-37, respectively. As expected the pressure recovery is seen in the expansion parts of the inlet duct.

6.2 Conditions at the Duct Burner

The flow distribution in the inlet duct is discussed in section 6.1. The design of HRSG includes duct burners to facilitate supplementary firing based upon the steam requirements and the atmospheric conditions. The maximum duty for which these burners are designed is 16 MMBTU/hr. The flow velocity entering the burner should meet some requirements like even gas velocity distribution and velocity components normal to the burner plane for the ideal performance of the burner. It is observed that the original design of the distribution grid is inadequate to serve these flow requirements for the burner from the stream line plots. It is also evident that the modified distribution grid is also not sufficient enough to meet the flow requirements of the burner. In addition to the increased pressure drop, it is suggested to fire only the bottom burner instead of using both burners. The temperature contour along the boiler width showing the impact of

adding fuel using two burners and using only the bottom burner is shown in figures 6-4 and 6-29.

6.3 Flow Distribution into the First Heat Exchanger Surface

Gas flow and temperature distribution into the heat exchangers are the primary design criteria, since a uniform distribution of mass and heat flux into the tube banks results in stable performance of the system. The gas flow distribution into the first heat exchanger also influences the distribution into the heat exchangers downstream [5].

The gas velocity distribution at the first heat exchanger surface is shown in figures 6-5, 6-16 and 6-30 for the three cases modeled (the fired case, unfired case and modified fired case, respectively). The velocity distribution for the unfired case shows that the velocity distribution is uniform except for the high peak located near the bottom floor of the model. This is the effect of the side-biased inlet velocity profile of the HRSG. It is observed that around 78% of the velocities are with in +/-20% of the average velocity for the fired case and around 81% of the velocities are with in +/-20% of the average velocity for the modified fired case. As the duty of the burner is small, the temperature variation at the first heat exchanger surface because of this heat addition is not very high. The temperature distribution at the first heat exchanger surface is shown in figures 6-5, 6-16 and 6-30. High temperature peaks at the first heat exchanger surface in the modified fired case is seen at the bottom wall because of firing the only the bottom duct burner. The temperature profile is uniform along the width of the boiler with range varying between +/-75^{o}F of the average value.

6.4 CO & SCR System

The velocity distribution entering the CO catalyst, at the location of Ammonia Injection Grid (AIG), and entering the SCR are discussed in this section. The gas distribution into the catalysts is shown in the Figures 6-7, 6-8, 6-18, 6-19, 6-32, and 6-33 for the three cases modeled (the fired case, unfired case and modified fired case). The gas flow distribution at different locations for the three cases modeled is summarized in table 6-1. It is observed that at the CO plane, the percentage of area falling within the required +/-15% of the average velocity is around 60%. This can be attributed to the wall effects at this plane. This is verified by observing the velocity profile at a location upstream of the CO catalyst. The velocity profile showed that the velocity distribution is uniform and is within the limits set by VPI for good performance of the CO catalyst.

6.5 Flow Distribution through Downstream Heat Exchangers

The flow distribution into the first heat exchanger surface (Box 1) is discussed in Section 6.3. The gas velocity distribution along the boiler width for the fired case is shown in figure 6-3. This figure shows that the velocity is relatively low and uniform downstream of the burner duct. Interior velocities downstream of box 1 range from 8ft/s to 16ft/s with low velocities near the walls. Figures 6-9 to 6-12 show the axial velocity distribution entering and leaving each of the heat exchanger module boxes. It is observed that the flow distribution is uniform and symmetric with the expected variations in temperature distribution. The gas velocity distribution for the modified fired case is shown in figure 6-28. This figure shows that the velocity is relatively low and uniform downstream of the burner duct. Interior velocities downstream of box 1 are within the

same range as for the fired case, with small velocities near the walls. Figures 6-34 to 6-37 show the axial velocity distribution entering and leaving each of the heat exchanger module boxes for modified fired case. It is observed that the flow distribution is uniform and symmetric, with the expected variations in temperatures seen.

The comparison of the predicted gas side pressure drop in each of the heat exchanger sections and the average gas temperature entering each of the heat exchangers with the CARDS predictions is shown in figures 6-14, 6-25, 6-38 for the three cases modeled. It is observed that the temperature prediction is in agreement with the CARDS prediction. The prediction of the gas side pressure drop in Fluent is high compared to CARDS which means that the pressure drop parameters in the model need to be adjusted to meet the designed value.

6.6 Heat Exchanger Modeling

The inputs needed for modeling the heat exchanger are the heat rejection and the pressure drop parameters. Heat transfer in the heat exchanger is modeled in Fluent using the heat exchanger module. The heat exchanger module within Fluent allows the user to specify heat transfer in the heat exchanger in two different ways: fixed heat rejection, and fixed inlet temperature. Flow through a heat exchanger also involves loss of pressure. Gas side pressure drop in a heat exchanger can also be modeled in two different ways: by specifying the inertial resistance parameters in the porous media or by using the heat exchanger module, which uses the heat exchanger geometry information to calculate the resistance parameters for a pressure drop.

6.6.1 Modeling Heat Transfer

As discussed heat transfer in a heat exchanger can be modeled using the heat exchanger module within Fluent. The heat exchanger module allows the user to specify the coolant flow direction, number of passes in the heat exchanger and even the pass to pass direction of the coolant in the heat exchanger there by allowing the user to represent the heat exchanger as close as possible to the actual case. The fluid zone representing the heat exchanger core is split into macros. Macros are constructed based on the specified number of passes, the number of macro rows per pass, the number of macro columns per pass, and the corresponding coolant inlet and pass-to-pass directions. Macros are numbered from *0* to *n-1* in the direction of coolant flow, where n is the number of macros. Numbering of the macros is shown in figure 6-39. The next step in the setting of the heat exchanger module involves the selection of heat exchanger models either the simple effectiveness model or the NTU model. The simple effectiveness model can be used to model heat transfer from the coolant to the gas, whereas the NTU model can be used for heat transfer from the coolant to the gas or vice-versa. The next step after selecting the heat exchanger model is specifying the coolant properties and conditions. The heat transfer in the heat exchanger module can be specified in two methods: fixed heat rejection, and fixed coolant inlet temperature.

6.6.1.1 Fixed Heat Rejection

The fixed heat rejection method is used in cases with known heat exchange in the heat exchanger to predict the temperature contours. The total heat rejection is divided among the number of macros defined earlier while setting the coolant settings for the heat

exchanger. It is observed that the heat balance is in agreement with CARDS. Even though the average value of gas temperature at different sections of heat exchangers is in good agreement with the CARDS predictions, the range of the gas temperature predicted is high in some situations. The procedure for the case set up using this approach is given in A-1.

6.6.1.2 Fixed Coolant Inlet Temperature

In order to bring the range of the gas side temperature close to the actual value, a second approach called the fixed coolant inlet temperature is used. This method allows the user to specify the coolant inlet temperature and adjust the heat exchanger effectiveness (NTU) to attain the duty of the heat exchanger. The procedure for the case set up using this approach is given in A-2. The case is set, and the solution is allowed to progress till it converges. Once the solution is converged the duty of heat exchanger is verified and compared with the CARDS value. The procedure involved in checking the heat exchanger duty is shown in A-4. Based upon the duty of the heat exchanger the heat exchanger effectiveness i.e. NTU value is adjusted to get the actual duty of heat exchanger. It is not possible to exactly match the duty of heat exchanger using this method, but we can achieve a value close to the actual value. The results for Beatrice HRSG using this approach, with the NTU value and the resulting heat exchanger duty is shown in table 6-2 for both fired and unfired cases.

It is observed that this method of defining the heat exchanger duty compared to the previous method of fixed heat rejection resulted in better prediction of gas temperature range. The gas temperature range comparison between the above two

methods is shown in figure 6-40. The disadvantage in using this method compared to the other method is that it takes more time to get the results, as the effectiveness needs to be adjusted to attain the designed duty of heat exchanger. It can also be seen from table 6-2 that the same value of NTU results in large error in heat duty for fired case than the unfired case. The results discussed for the Beatrice model use fixed heat rejection, as it is the most convenient way to get the results quickly with reasonable accuracy and because we are concentrating on the flow distribution with little consideration given to the gas temperature distribution.

6.6.2 Modeling Pressure Drop

The pressure drop in the heat exchanger core is modeled using the porous media model in the Fluent. The gas side pressure drop in the heat exchanger core can be modeled using the heat exchanger module, which uses the geometry of the heat exchanger to generate the resistance parameters for pressure drop in the porous media, or by directly specifying the pressure drop parameters as input in the porous media.

6.6.2.1 Setting Porous Media Pressure Drop Parameters

In this method the pressure drop parameters of the heat exchanger core are set directly by adjusting the porous media resistance parameters. The procedure involves setting the inertial resistance parameter value in the two non-flow directions at a high value and setting a value for the flow direction in such a way that the desired pressure drop in the heat exchanger section is attained. The values of inertial resistance applied in the Beatrice model to get the designed pressure drop are given in table 6-3. It is observed

that the pressure drop obtained in the heat exchanger is directly proportional to the inertial resistance factor in the flow direction, keeping the resistance factor in the two non-flow directions constant at a high value. The procedure for setting the porous media resistance parameters is detailed in appendix A-3.

6.6.2.2 Using the Heat Exchanger Module

The pressure loss in the heat exchanger module can be set using the heat exchanger module, which requires the input parameters like the heat exchanger geometry and some pressure drop parameters discussed in this section. The pressure drop parameters and effectiveness define the heat exchanger core model. You can enable this model to calculate porous media parameters by entering the command `(set! auto-set-porous? #t)` into the Fluent console window. The porous media inputs are automatically set based on your inputs to the heat exchanger model [11].

The pressure loss in the heat exchanger can be expressed as: $\Delta p = \frac{1}{2} f \rho_m U_{A\min}^2$, [11]

Where

Δp is the gas side pressure drop

f *is the* gas side pressure loss co-efficient

ρ_m is the mean gas density

$U_{A_{\min}}$ is the gas velocity at the minimum flow area

The pressure loss coefficient is computed using the heat exchanger geometry parameters given by the equation $f = \left(K_c + 1 - \sigma^2\right) - \left(1 - \sigma^2 - K_e\right)\frac{\upsilon_e}{\upsilon_i} + 2\left(\frac{\upsilon_e}{\upsilon_i} - 1\right) + f_c \frac{A}{A_c}\frac{\upsilon_m}{\upsilon_i}$, [11]

Where,

σ is the minimum flow to face area ratio

K_c *is the* entrance loss coefficient

K_e is the exit loss coefficient

A is the gas-side surface area

A_c is the minimum cross-sectional flow area

f_c is the core friction factor

υ_e is the specific volume at the exit

υ_i is the specific volume at the inlet

υ_m is the mean specific volume $\equiv \frac{1}{2}(\upsilon_e + \upsilon_i)$

The geometry and the flow resistance parameters, which are the inputs in the heat exchanger module, are used to set up large resistances in the two non-streamwise directions, effectively forcing the gas flow in the core to be unidirectional. The procedure for setting the pressure drop parameters is in similar ways as the fixed inlet parameters. In this approach the pressure drop parameters are applied based upon the geometry of the heat exchanger. The inputs for the pressure drop parameters are tabulated in table 6-4. The procedure for the case set up using this approach is similar to the procedure shown in A-2. The case is set, and the solution is allowed to progress till it converges. Once the solution is converged the pressure drop in each of the heat exchanger is verified and compared with the desired value. In this attempt the core friction exponent is fixed and the core friction coefficient is adjusted to get the designed pressure drop. The disadvantage of using this method compared to the other method is that it takes more time to get the results. The results are analyzed to try and calibrate the value of core

friction coefficient which yields the designed pressure drop in the heat exchanger depending upon the geometry of the heat exchanger, instead of iteratively setting the pressure drop parameters either using the porous media resistance parameters or using the heat exchanger model. Different sets of values for core friction coefficient are plotted for different values of core friction exponent as shown in figure 6-41. It can be observed that for core friction exponents of -0.4 and -0.5 the value of core friction coefficient is following the same pattern. An effort is made to generalize the value of "a" using the geometrical parameters of heat exchanger, unfortunately no particular pattern is observed to come to a final conclusion on selecting the value of core friction co-efficient based upon the geometry of heat exchanger.

In order to effectively use this method to setup the resistance parameters, parameters need to be calibrated. To make use of this feature directly in the modeling additional work need to be carried using the data from CARDS for different heat exchanger configurations.

Velocity Evaluations	***Fired case***	***Unfired case***	***Modified fired case***
Avg. gas velocity entering HPSH1 (ft/s)	24.02	23.13	24.03
%HPSH1 area within 20% V_{avg}	78%	78%	81%
Max. axial velocity at HPSH1 (% of V_{avg})	33(137%)	31.5(136%)	32(133%)
Avg. gas velocity entering CO (ft/s)	22.7	22.1	22.9
%CO area within 15% V_{avg}	62%	61%	62%
Avg. gas velocity entering SCR (ft/s)	16.7	16.16	16.7
%SCR area within 15% V_{avg}	86%	86%	86%
Avg. gas velocity entering HPEC1 (ft/s)	16.0	16.0	16.0
Avg. gas velocity entering LPEV2 (ft/s)	13.32	12.89	13.3

Table 6-1: Summary of Velocity evaluations at key locations, Beatrice model

Heat Exchanger	*Fired case*			*Unfired case*		
	NTU	*Duty (w)*		*NTU*	*Duty (w)*	
		Fluent	*CARDS*		*Fluent*	*CARDS*
Heat exchanger box 1						
HPSH1	1.0	3880100	3883575	1.0	3737970	3789914
HPSH2	1.05	7448820	7400775	1.05	7462480	7283126
HPSH3	0.44	15075700	15056547	0.44	15573600	14946992
HPEVAP1	1.15	30489800	30221541	1.15	33474500	30211829
HPEVAP2	0.93	12892600	14071731	0.93	13411400	14067335
HPEVAP3	0.93	1357570	2048769	0.93	1228700	2050323
Heat exchanger box 2						
HPEC1	0.6	1286910	1802565	0.6	1638620	1753510
HPEC2	0.74	2999890	3555303	0.74	3187060	3482524
LPSH	2.1	1852090	1802565	2.1	1657160	1787167
HPEC3	0.64	2251210	2412213	0.64	2499520	2366079
HPEC4	0.67	4471900	5313903	0.67	4622350	5242561
HPEC5	0.75	8016900	8532141	0.75	8139520	8470776
LPEVAP1	1.2	11628600	12647265	1.2	11317300	12592404
Heat exchanger box 3						
LPEVAP2	0.25	1374770	1231020	0.25	1108710	1226340
LPEVAP3	0.35	1084130	1260330	0.35	1149230	1256192
WPHR1	0.35	1367470	1471362	0.35	1533100	1455239
WPHR2	0.5	2569980	2758071	0.5	2597480	2733185
WPHR3	0.53	3151006	3382374	0.53	3125340	3362451
WPHR4	0.55	4009630	4156158	0.55	3940210	4145485
WPHR5	0.58	5047680	5108733	0.58	4975540	5112556
WPHR6	0.57	6120760	6146307	0.57	6068770	6171510
	Error		**4.3%**	Error	Lessthan **1%**	

Table 6-2: NTU Values used to calibrate the heat exchanger model along with the specified duty for each heat exchanger, Beatrice model (SI units)

Heat Exchanger	***R [m^{-1}]***	***$BP_{desired}$ [inch WC]***	
		Fired case	***Unfired case***
HEAT EXCHANGER BOX 1			
HPSH1	40	0.38	0.37
HPSH2	35	0.34	0.33
HPSH3	40	0.32	0.31
HPEVAP1	55	0.69	0.68
HPEVAP2	80	0.99	0.98
HPEVAP3	80	0.48	0.47
HEAT EXCHANGER BOX 2			
HPEC1	55	0.32	0.32
HPEC2	85	0.47	0.47
LPSH	35	0.17	0.17
HPEC3	50	0.27	0.27
HPEC4	90	0.43	0.43
HPEC5	80	0.41	0.41
LPEVAP1	80	0.74	0.74
HEAT EXCHANGER BOX 3			
LPEVAP2	52	0.24	0.24
LPEVAP3	74	0.33	0.33
WPHR1	48	0.21	0.21
WPHR2	80	0.34	0.34
WPHR3	80	0.33	0.33
WPHR4	75	0.32	0.32
WPHR5	75	0.30	0.30
WPHR6	75	0.28	0.28
Distribution Grid	4	0.60	0.60
CO	45	0.69	0.69
SCR	135	1.55	1.55

Table 6-3: Values used to calibrate the heat exchanger model along with the specified pressure drop each case, Beatrice model

Heat exchanger	*σ*	*A (in^2)*	*A_c(in^2)*	*a*	*ΔP Cards*	*ΔP Fluent*
Heat exchanger box 1						
HPSH1	0.52	3544834	73914.7	0.1289	0.37	0.38
HPSH2	0.4879	3944278	69226.1	0.0881	0.33	0.33
HPSH3	0.49	3944278	69226.1	0.0939	0.31	0.32
HPEVAP1	0.49	7633622	69226.1	0.1330	0.68	0.69
HPEVAP2	0.49	11450430	69226.1	0.1422	0.98	0.99
HPEVAP3	0.49	5725217	69226.1	0.1451	0.47	0.48
Heat exchanger box 2						
HPEC1	0.491	3816811	70216.1	0.1684	0.32	0.32
HPEC2	0.491	5725217	70216.1	0.1581	0.47	0.47
LPSH	0.491	2421793	74394.8	0.1759	0.17	0.17
HPEC3	0.491	3816811	70216.1	0.1525	0.27	0.27
HPEC4	0.491	5725217	70216.1	0.1613	0.43	0.43
HPEC5	0.491	5725217	70216.1	0.1689	0.41	0.41
LPEVAP1	0.491	11450430	70216.1	0.1750	0.74	0.74
Heat exchanger box 3						
LPEVAP2	0.491	3816811	70216.1	0.2000	0.24	0.24
LPEVAP3	0.4914	5725217	70216.1	0.1604	0.33	0.31
WPHR1	0.4914	3816811	70216.1	0.1770	0.21	0.21
WPHR2	0.4914	5725217	70216.1	0.1850	0.34	0.34
WPHR3	0.4914	5725217	70216.1	0.1885	0.33	0.33
WPHR4	0.4914	5725217	70216.1	0.1932	0.32	0.31
WPHR5	0.4914	5725217	70216.1	0.1992	0.3	0.3
WPHR6	0.4914	5725217	70216.1	0.2074	0.28	0.28

Table 6-4: Input to heat exchanger model to get the designed pressure drop in each of the heat exchanger for b = -0.2 and K_c, K_e = 0, Beatrice model

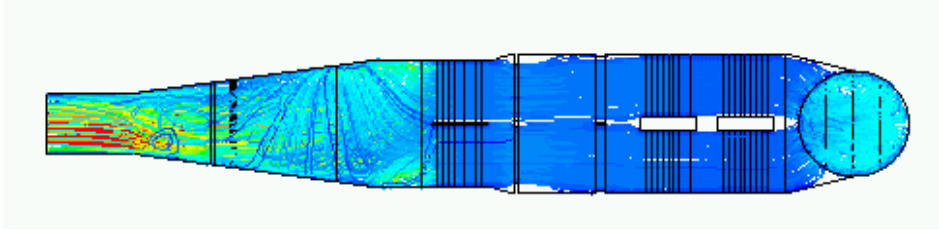

Plan view

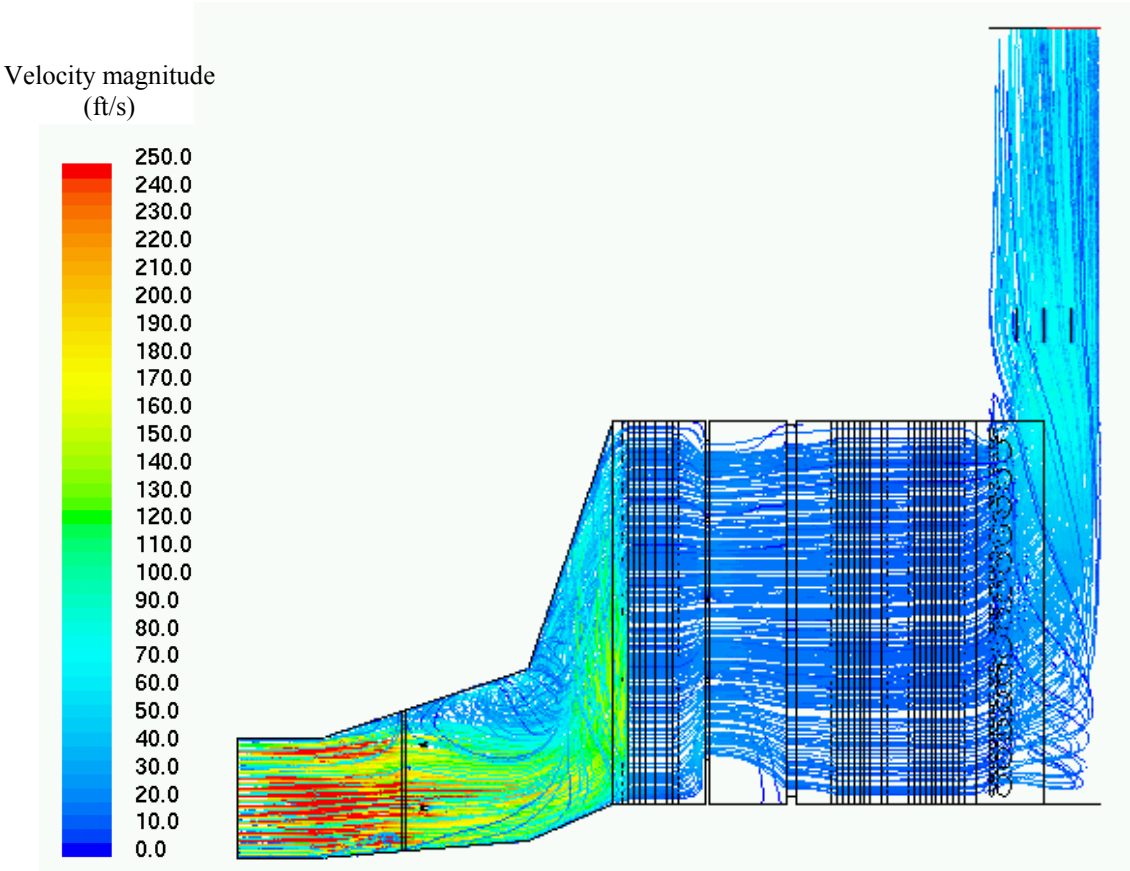

Side view

Figure 6-1: Stream traces colored by velocity magnitude, fired case

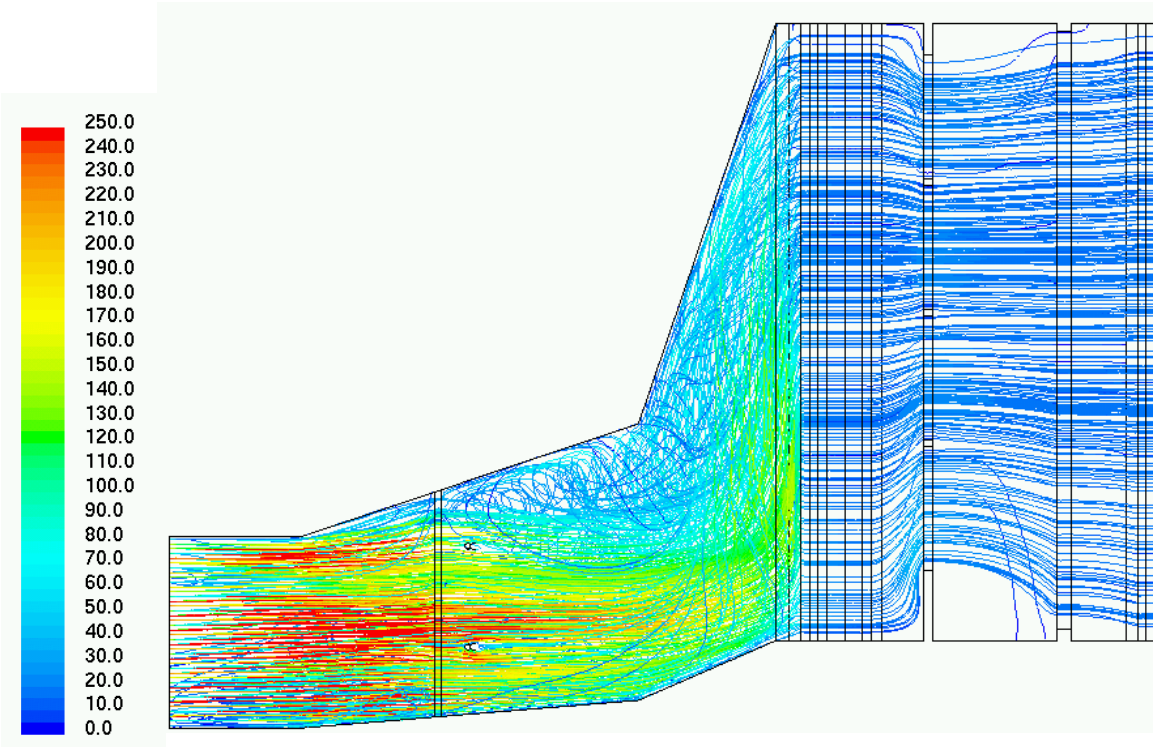

Figure 6-2: Details of stream traces colored by gas velocity magnitude (ft/s) in the inlet duct, fired case

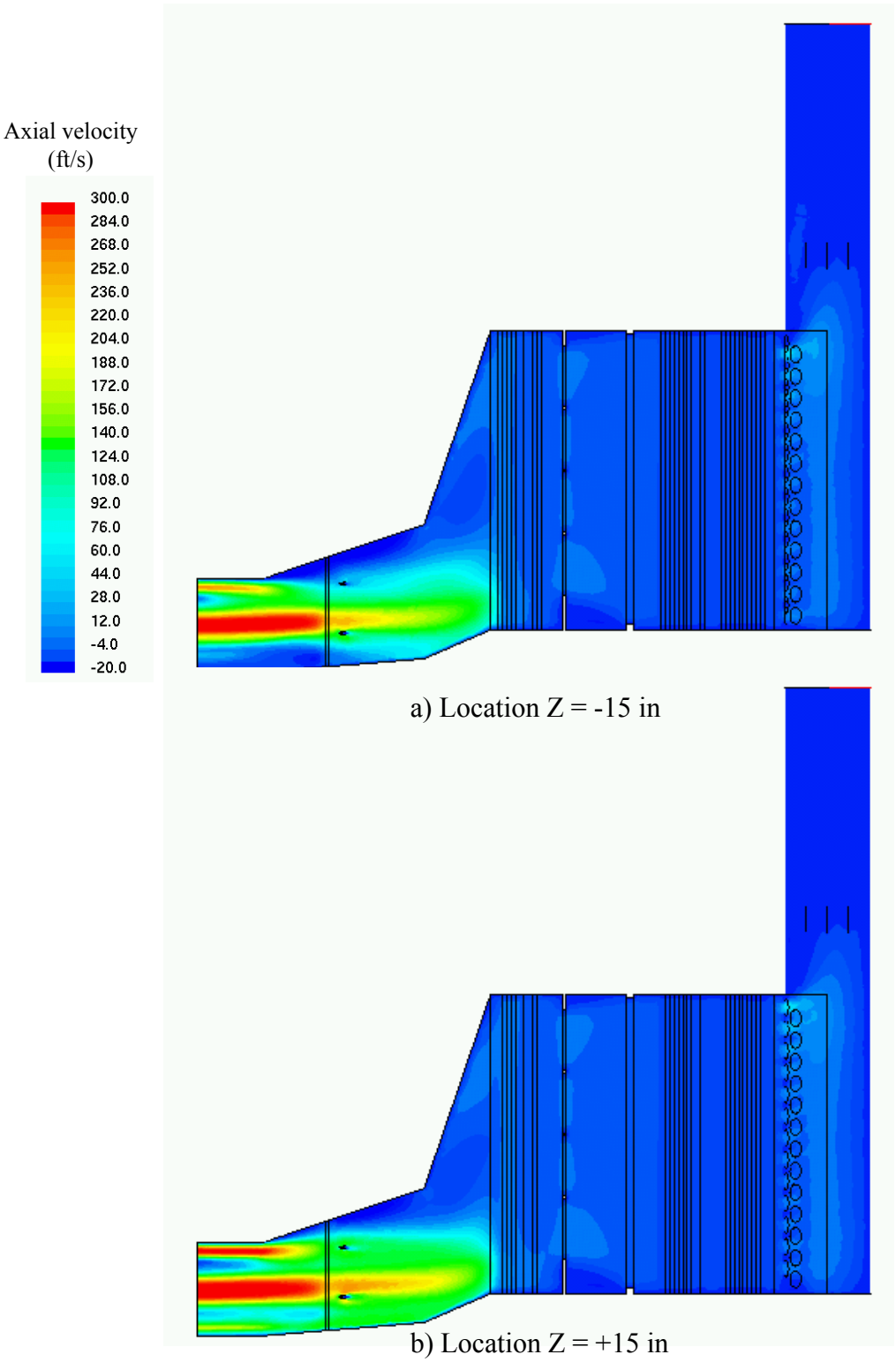

Figure 6-3: Contours of gas axial velocity (ft/s) along the boiler width at locations z= +/- 15 in., fired case

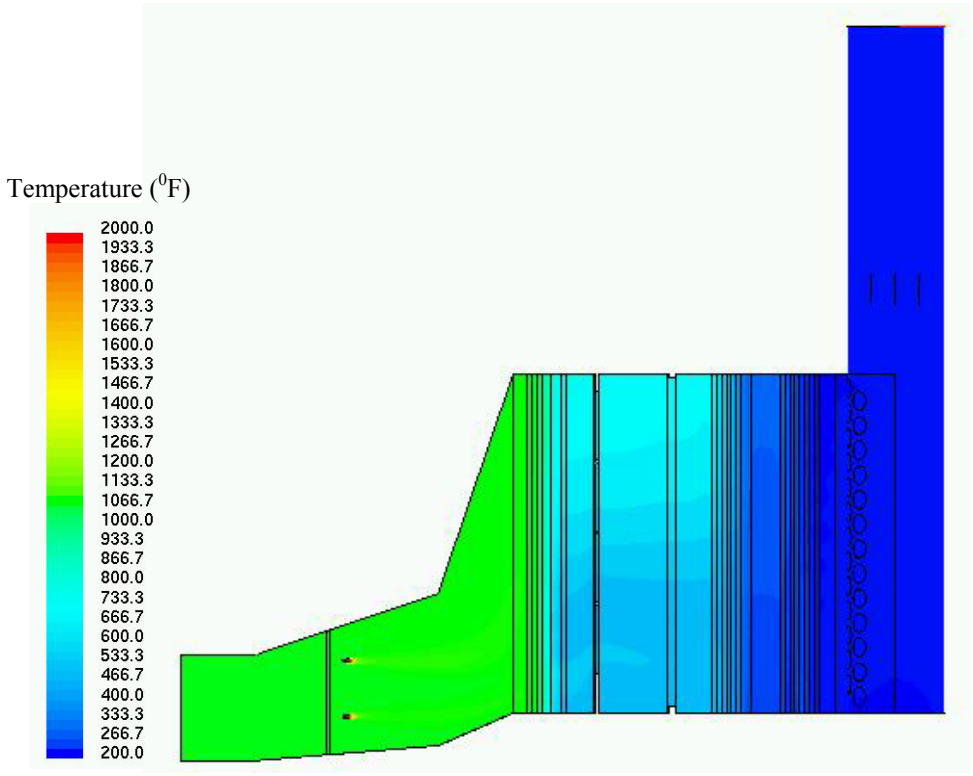

a) Location Z = 15in

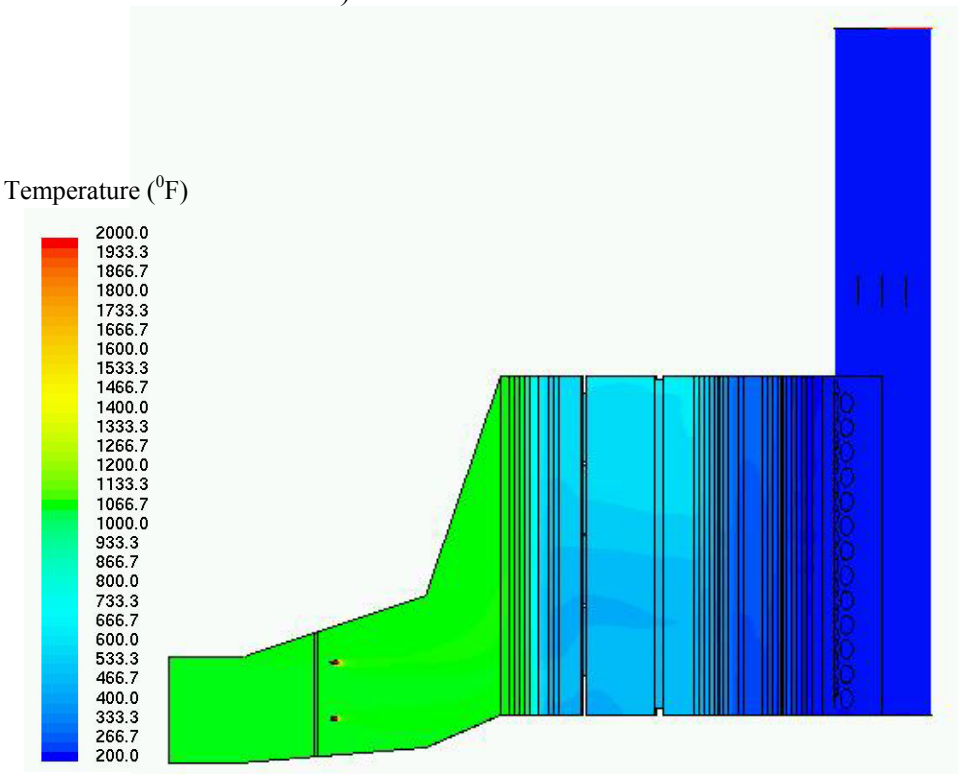

b) Location Z = -15in

Figure 6-4: Contours of gas temperature (^{o}F) along the boiler width at locations z= +/- 15 in., fired case

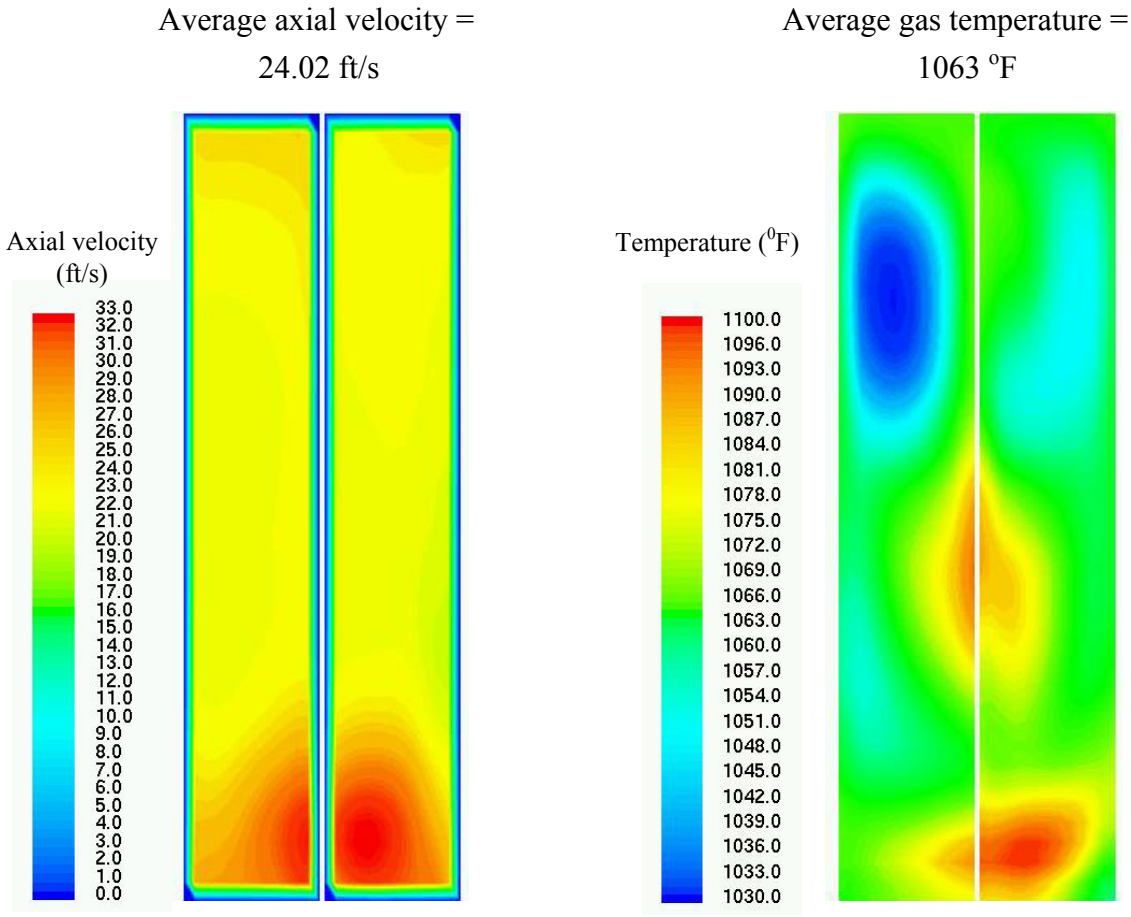

Figure 6-5: Contours of gas axial velocity component (ft/s) and gas temperature entering HPSH1 (Box 1), fired case

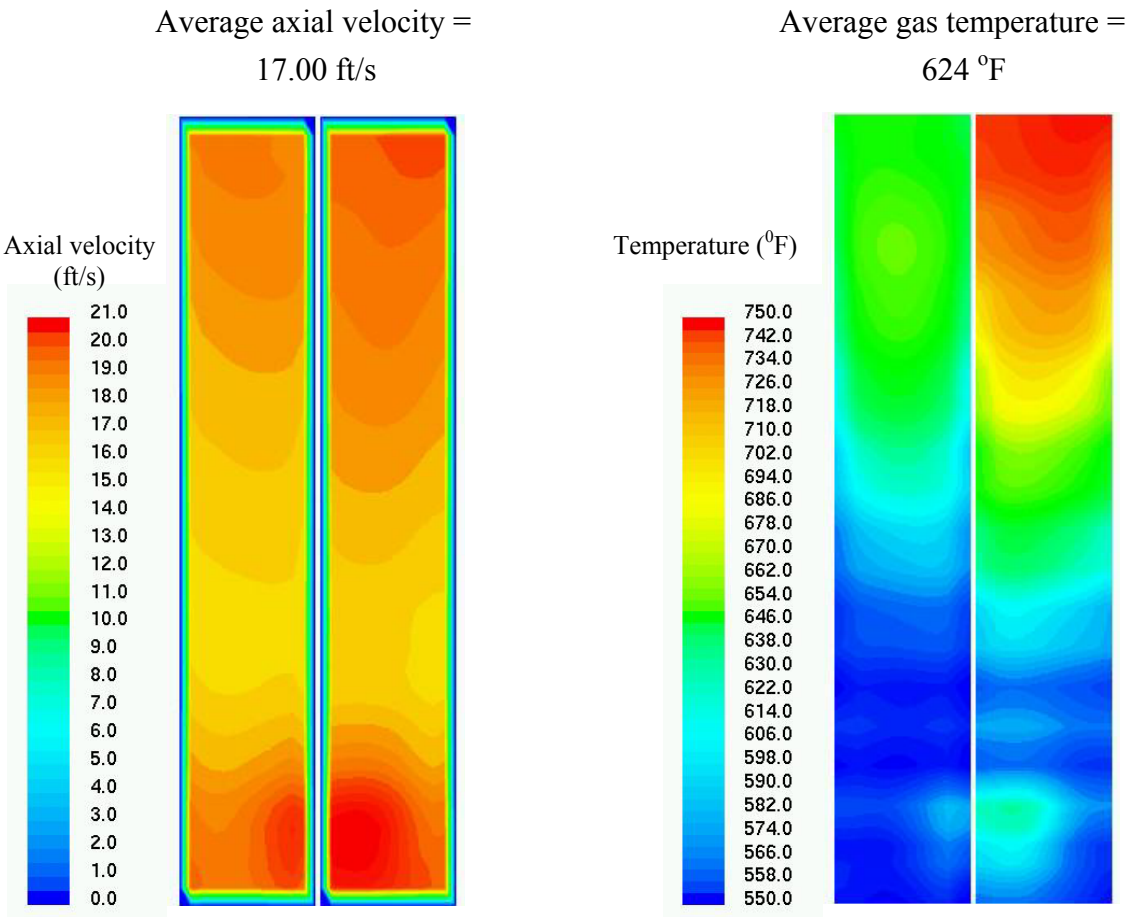

Figure 6-6: Contours of gas axial velocity component (ft/s) and gas temperature leaving HPEV3 (Box 1), fired case

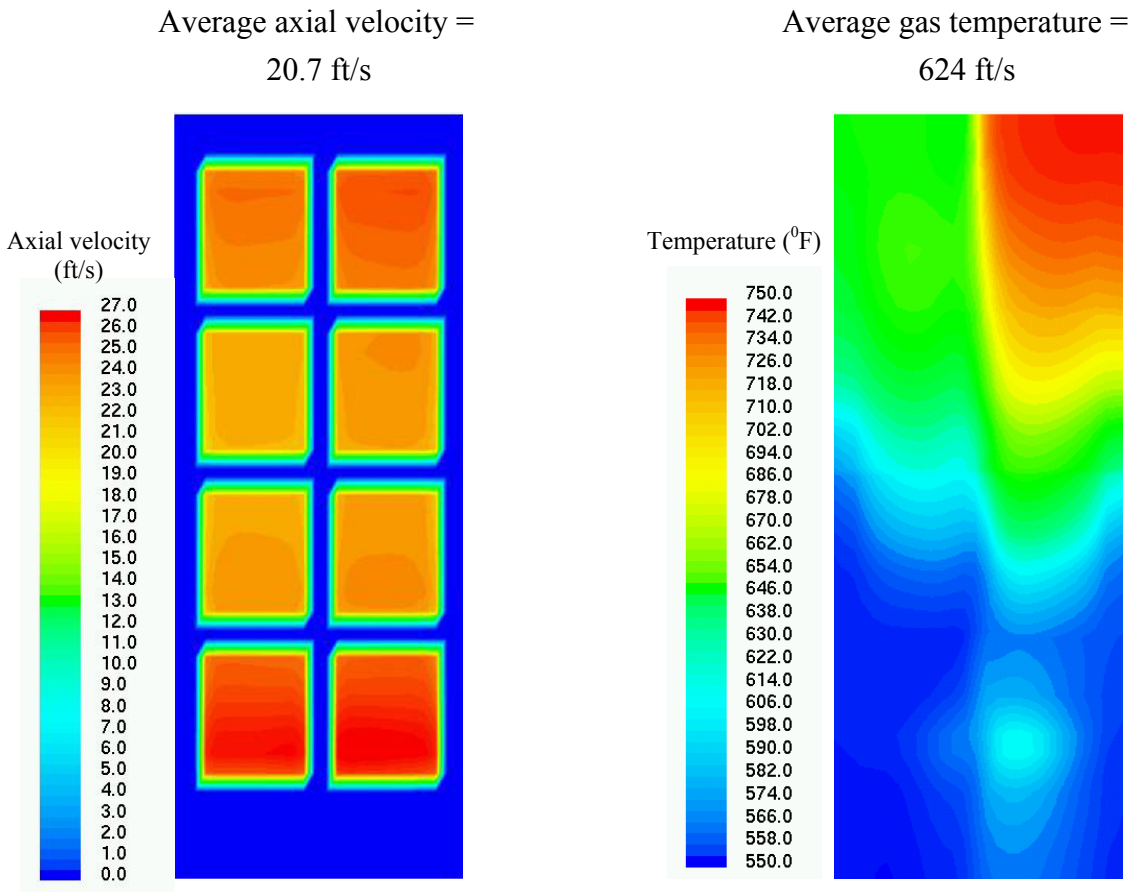

Figure 6-7: Contours of gas axial velocity component (ft/s) and gas temperature (^{o}F) entering CO catalyst, fired case

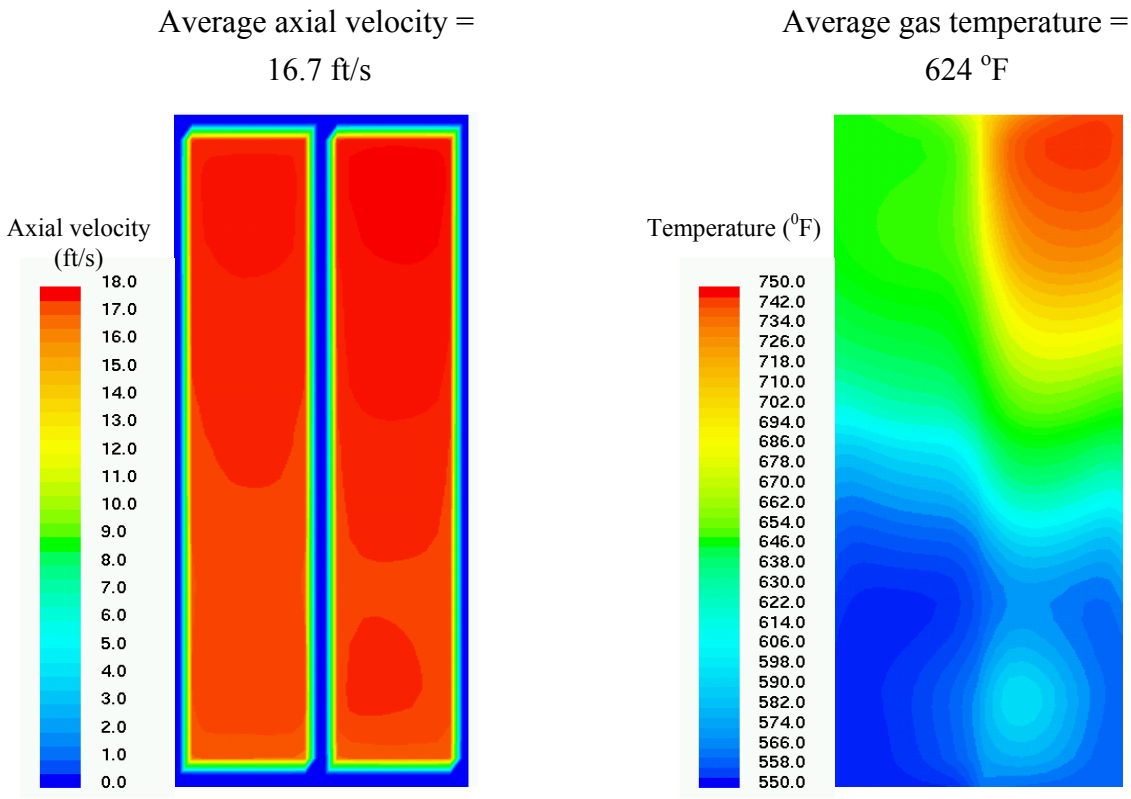

a) Entering SCR catalyst

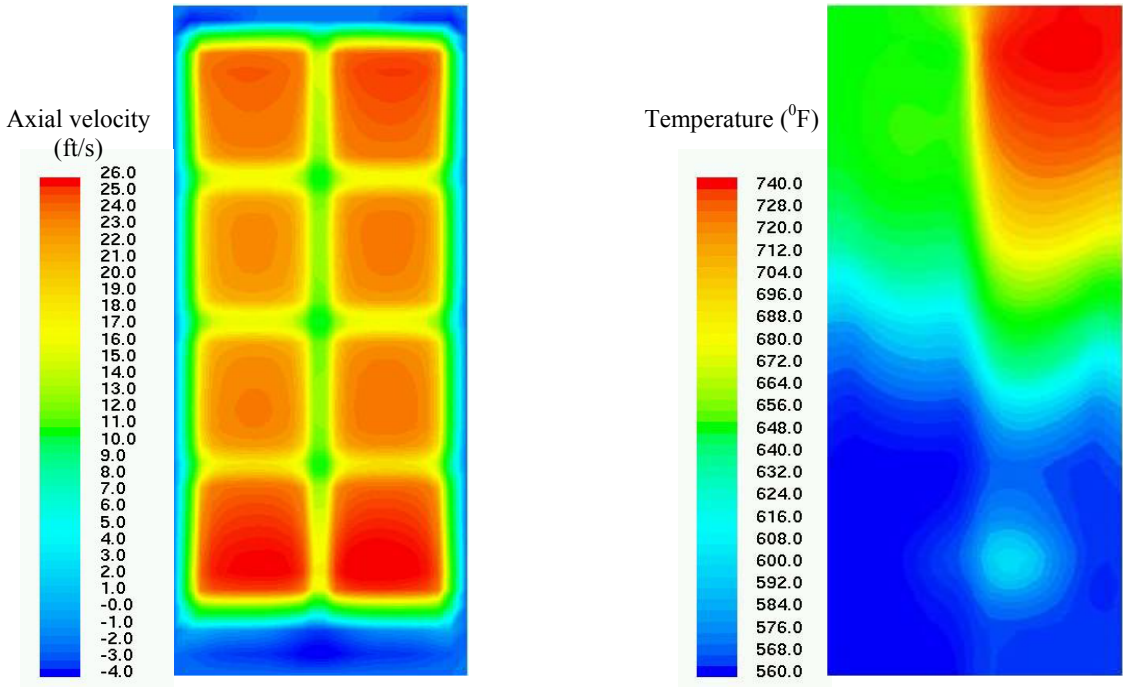

b) at AIG location

Figure 6-8: Contours of gas axial velocity component (ft/s) and gas temperature (°F) entering SCR Catalyst, fired case

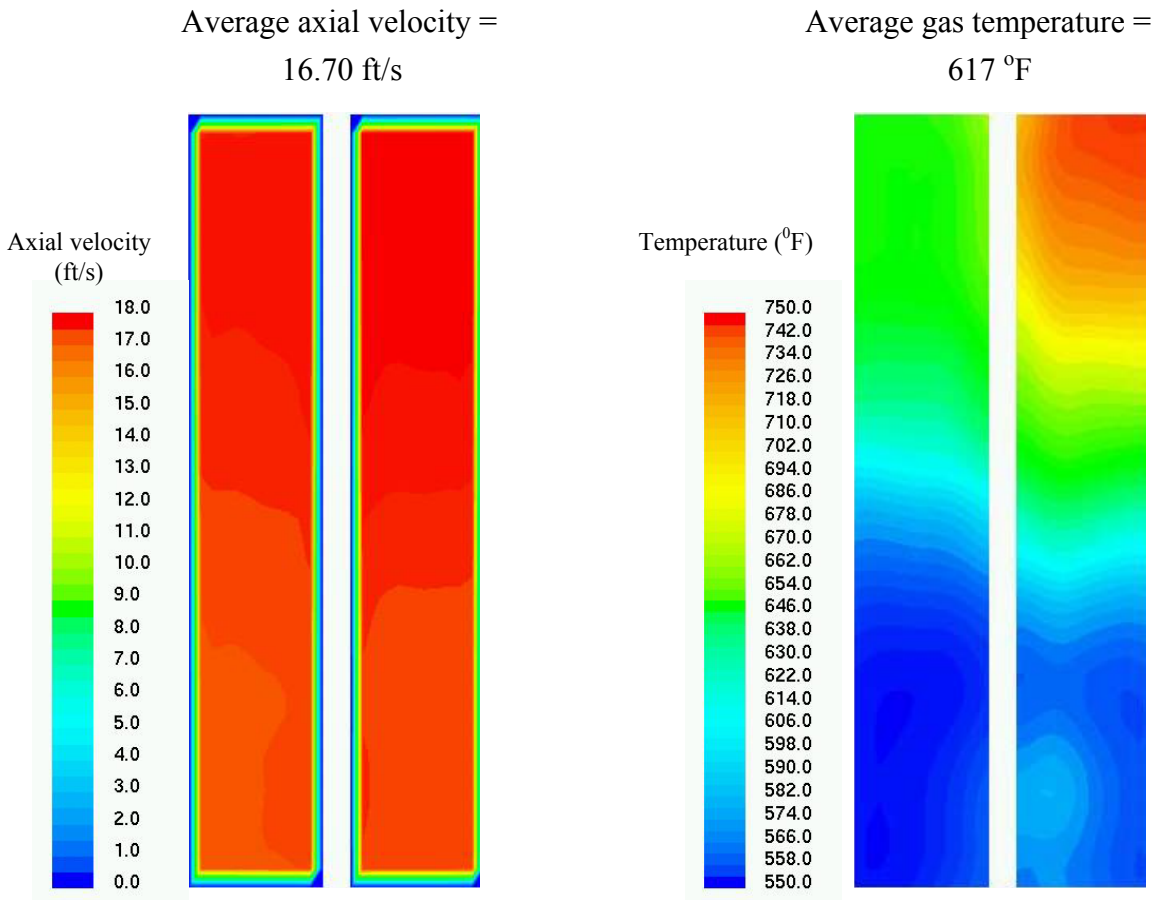

Figure 6-9: Contours of gas axial velocity component (ft/s) and gas temperature (°F) entering HPEC1 (Box2), fired case

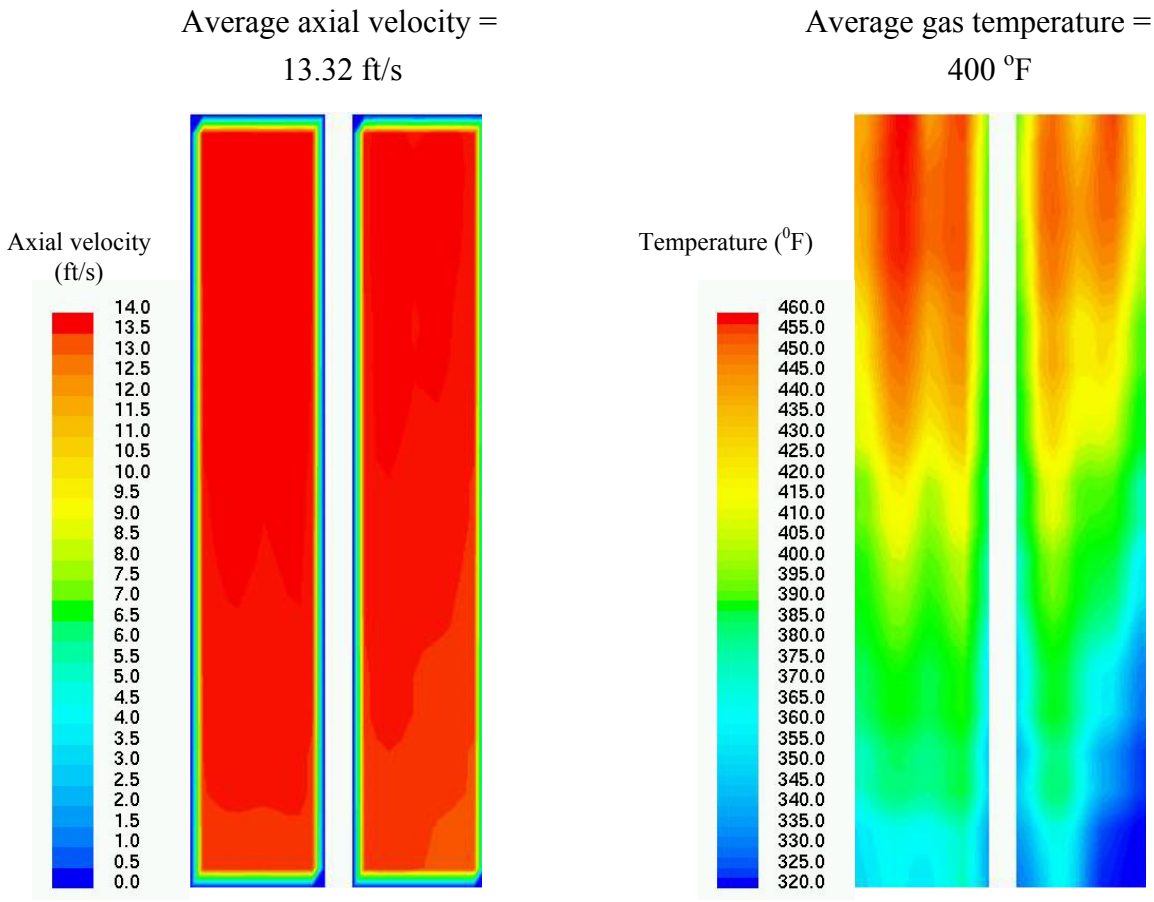

Figure 6-10: Contours of gas axial velocity component (ft/s) and gas temperature (°F) leaving LPEV1 (Box 2), fired case

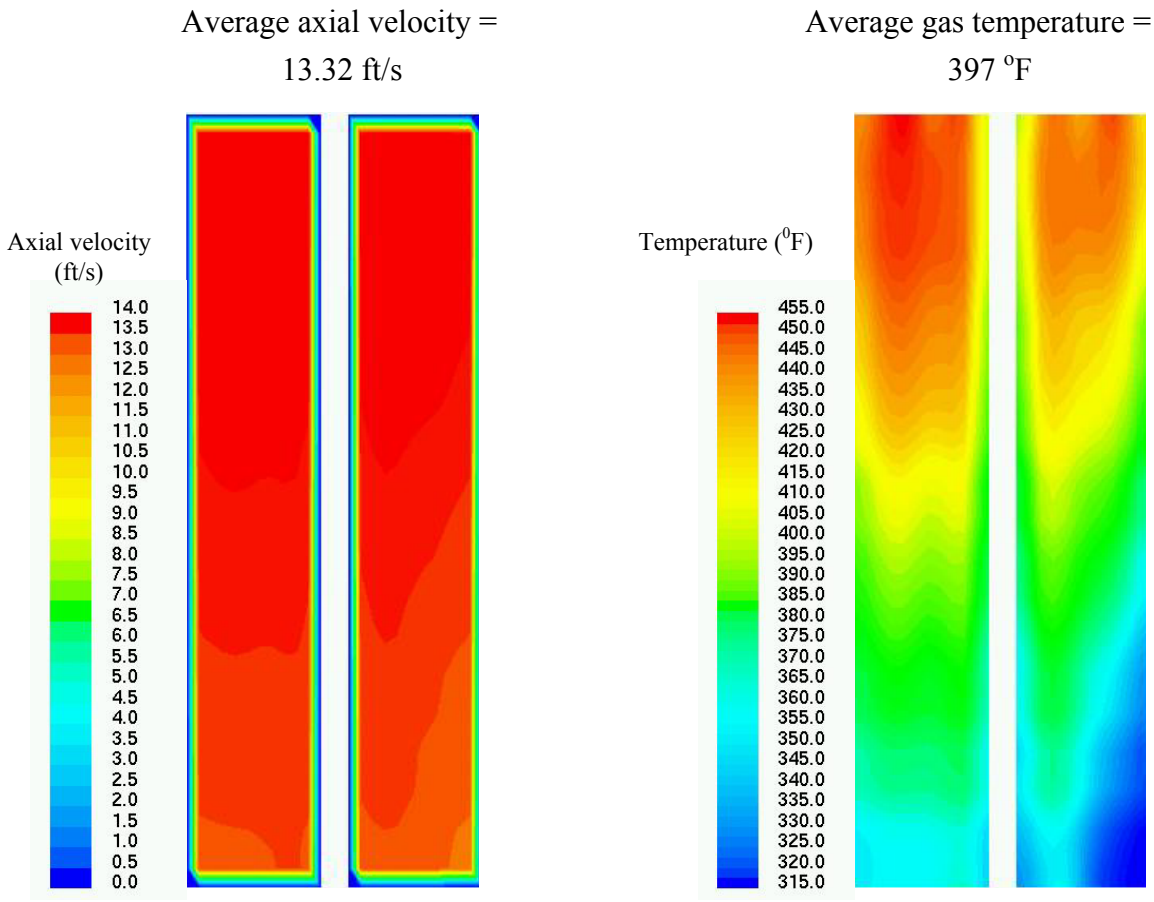

Figure 6-11: Contours of gas axial velocity component (ft/s) and gas temperature (°F) entering LPEV2 (Box 3), fired case

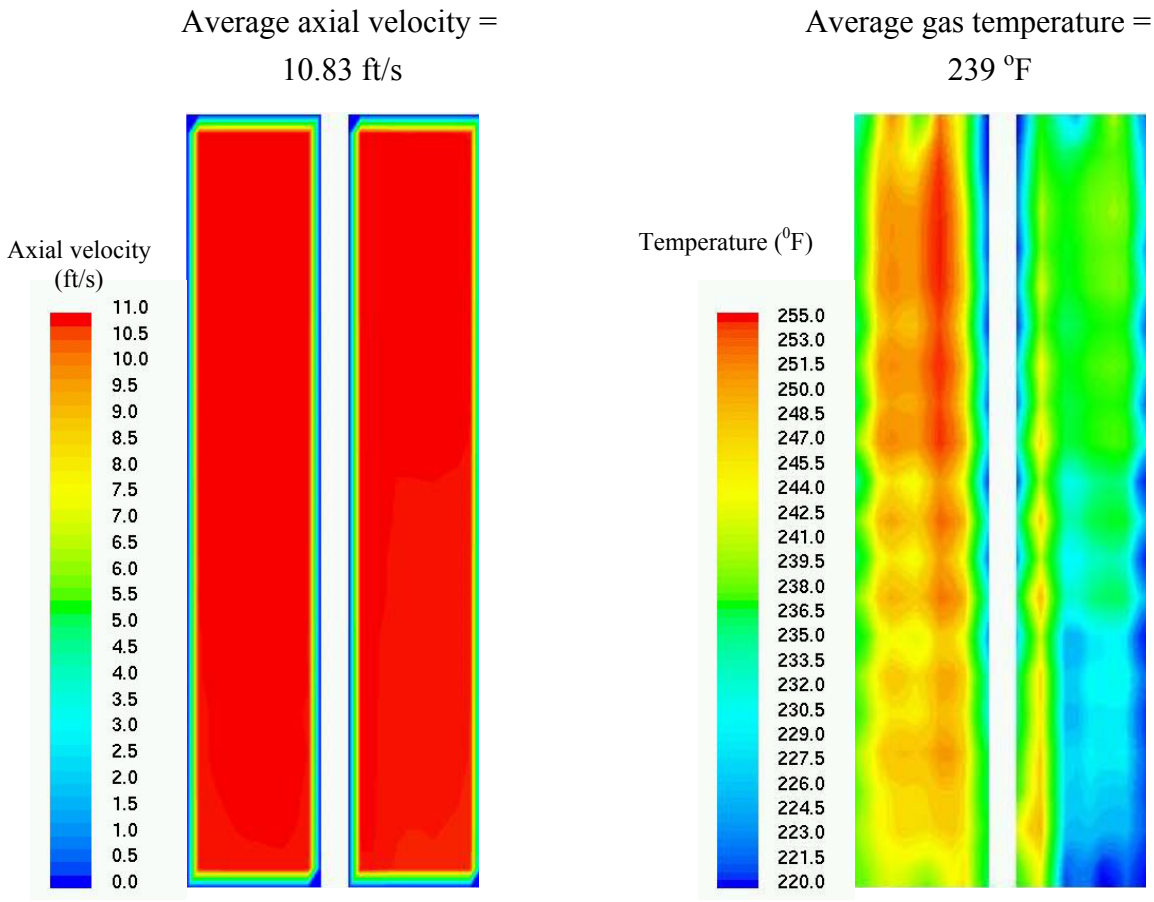

Figure 6-12: Contours of gas axial velocity component (ft/s) and gas temperature (°F) leaving WPHR6 (Box 3), fired case

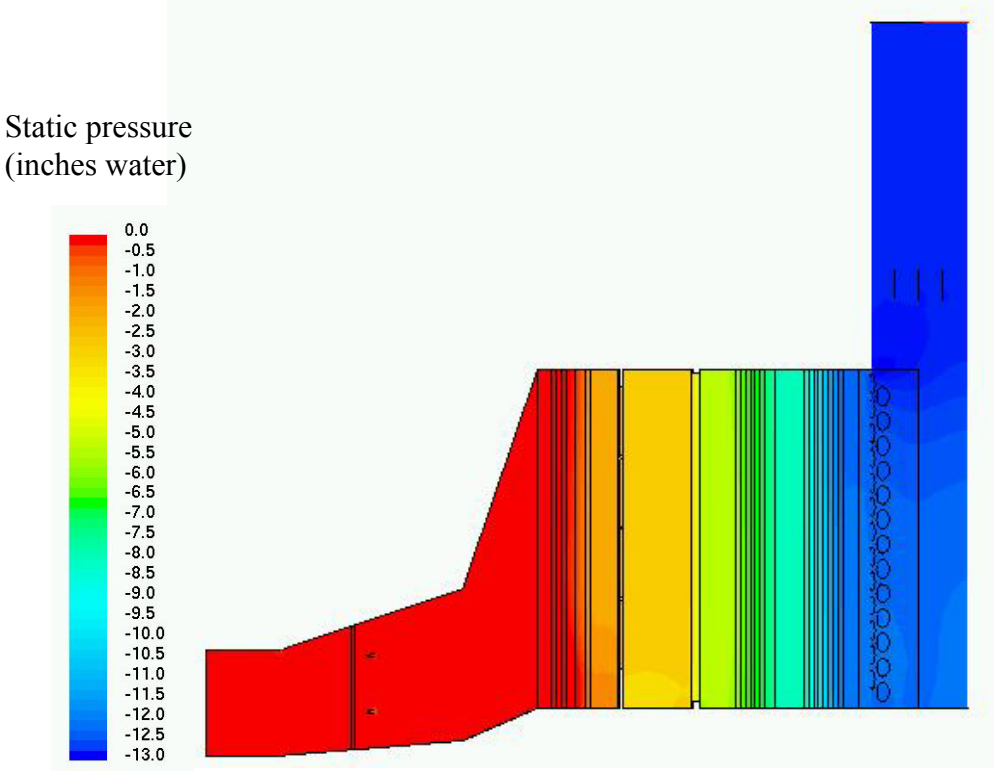

Figure 6-13: Static pressure contour along mid section of model (inch WC), fired case

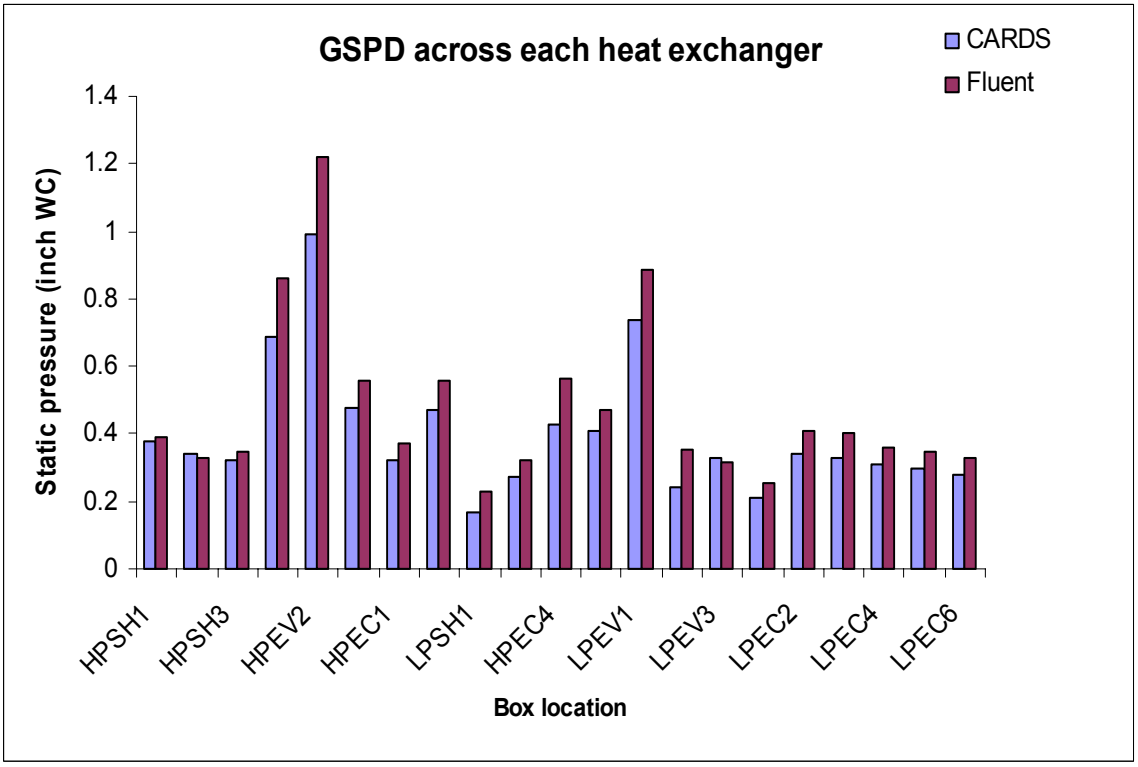

a) Comparison of module GSPD (Fluent Vs CARDS)

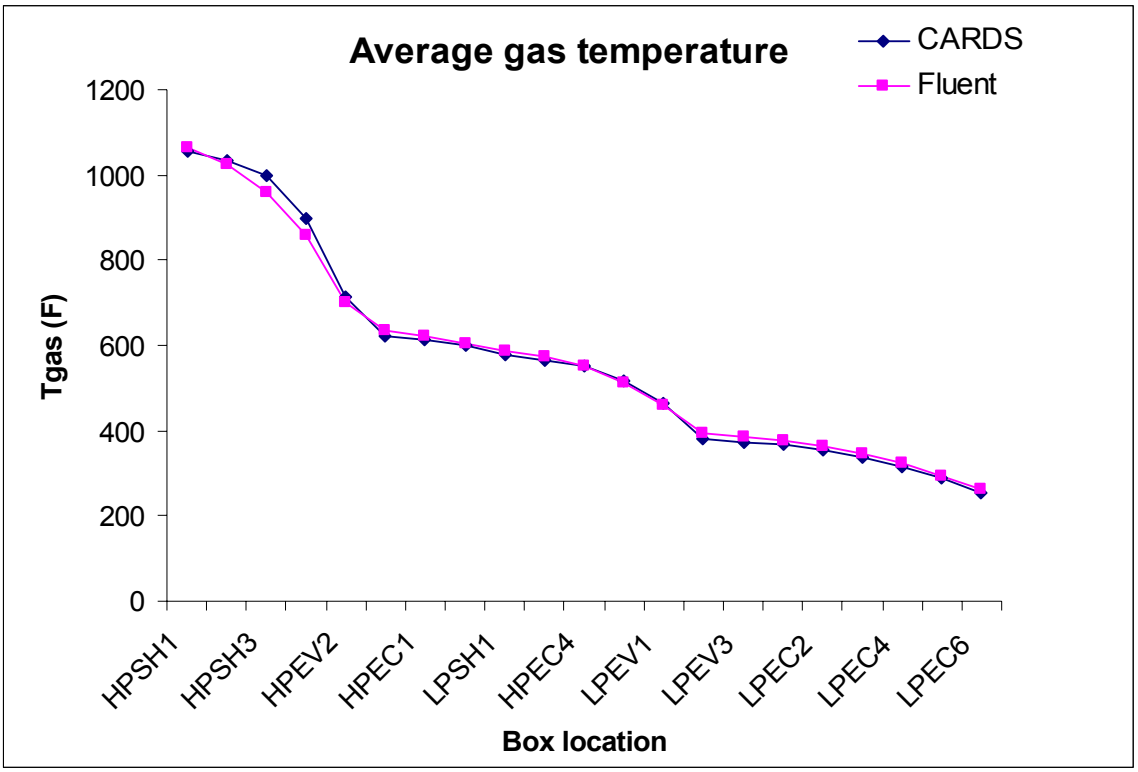

b) Comparison of average gas temperature (Fluent Vs CARDS)

Figure 6-14: Pressure drop and average gas temperature comparison charts, fired case

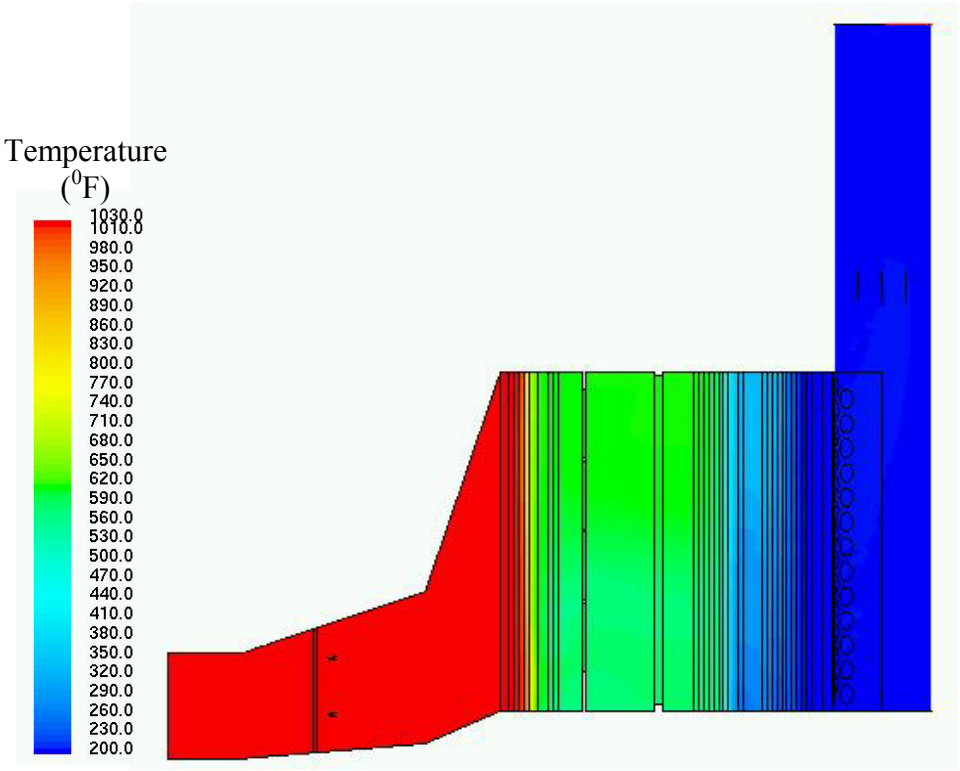

a) Location Z = 15in

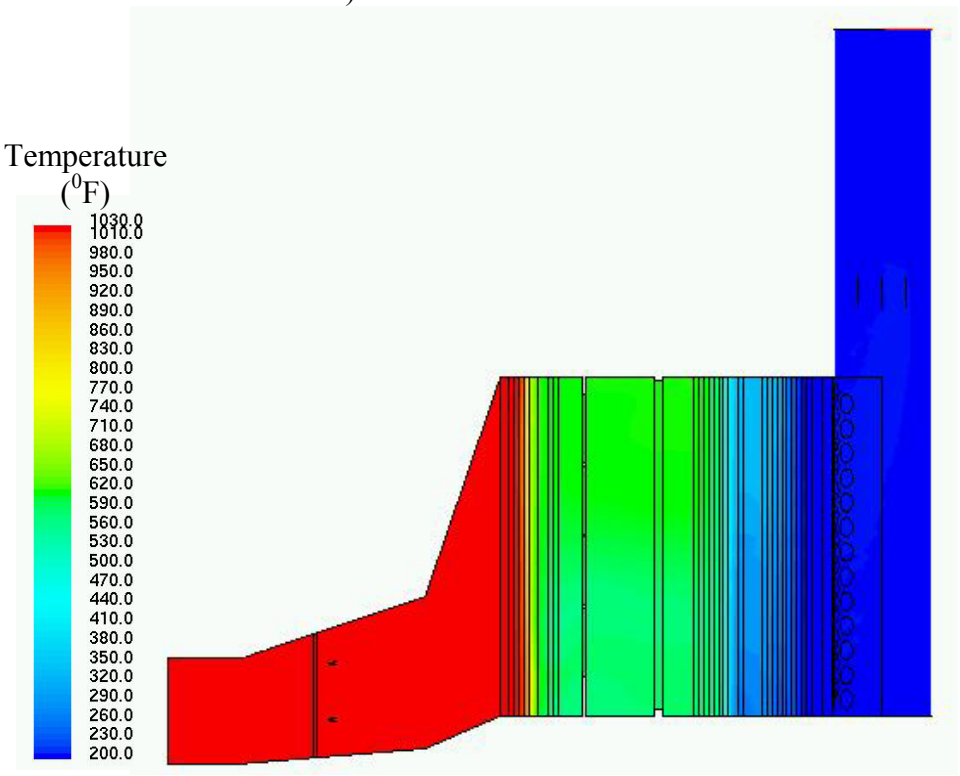

b) Location Z = -15in

Figure 6-15: Contours of gas temperature (^{o}F) along the boiler width at locations z= +/- 15 in., unfired case

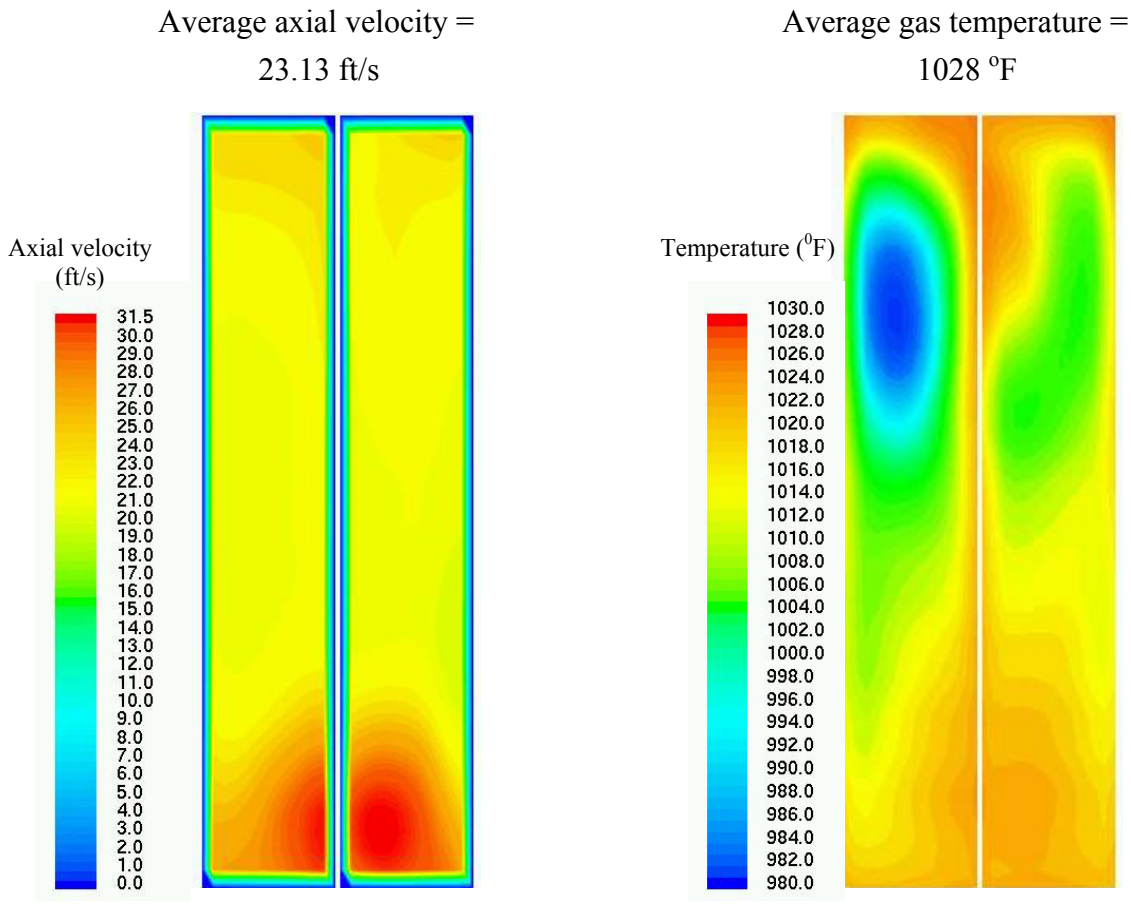

Figure 6-16: Contours of gas axial velocity component (ft/s) and gas temperature (°F) entering HPSH1 (Box 1), unfired case

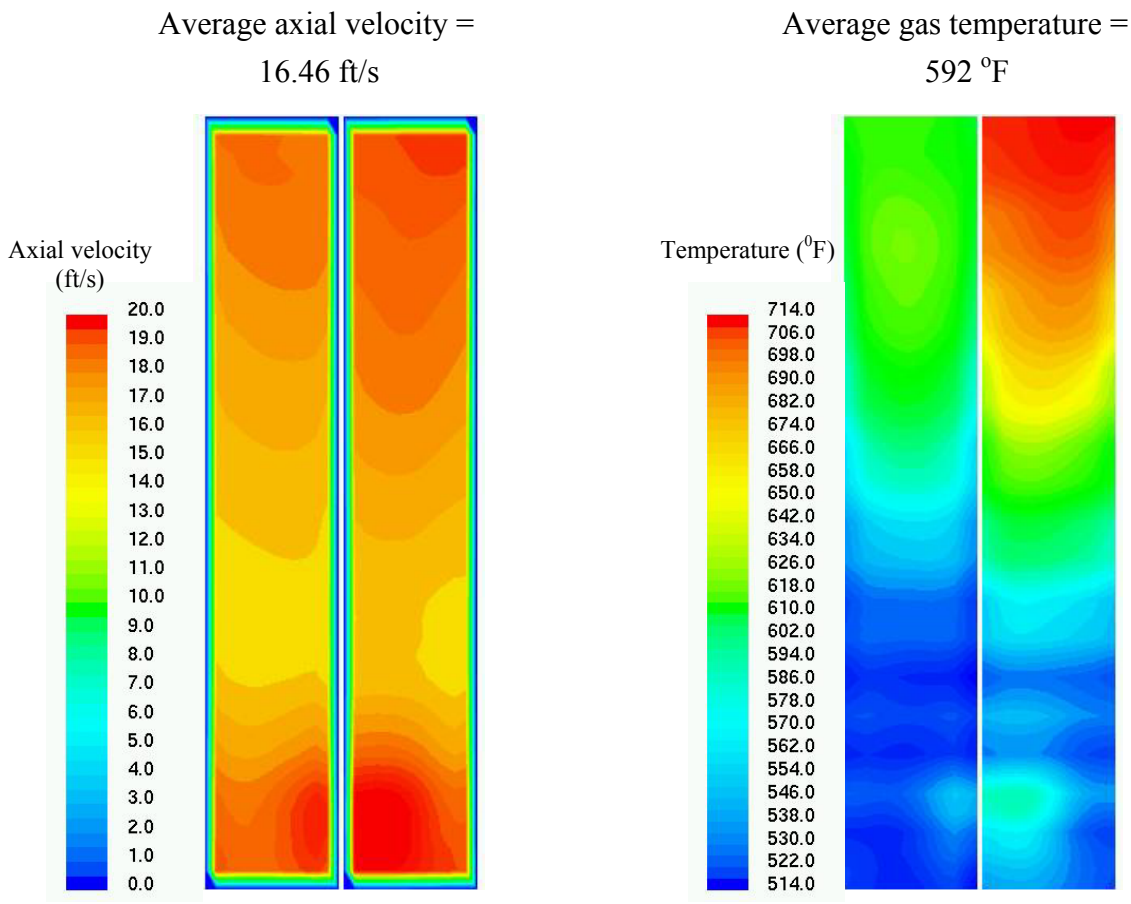

Figure 6-17: Contours of gas axial velocity component (ft/s) and gas temperature (°F) leaving HPEV3 (Box 1), unfired case

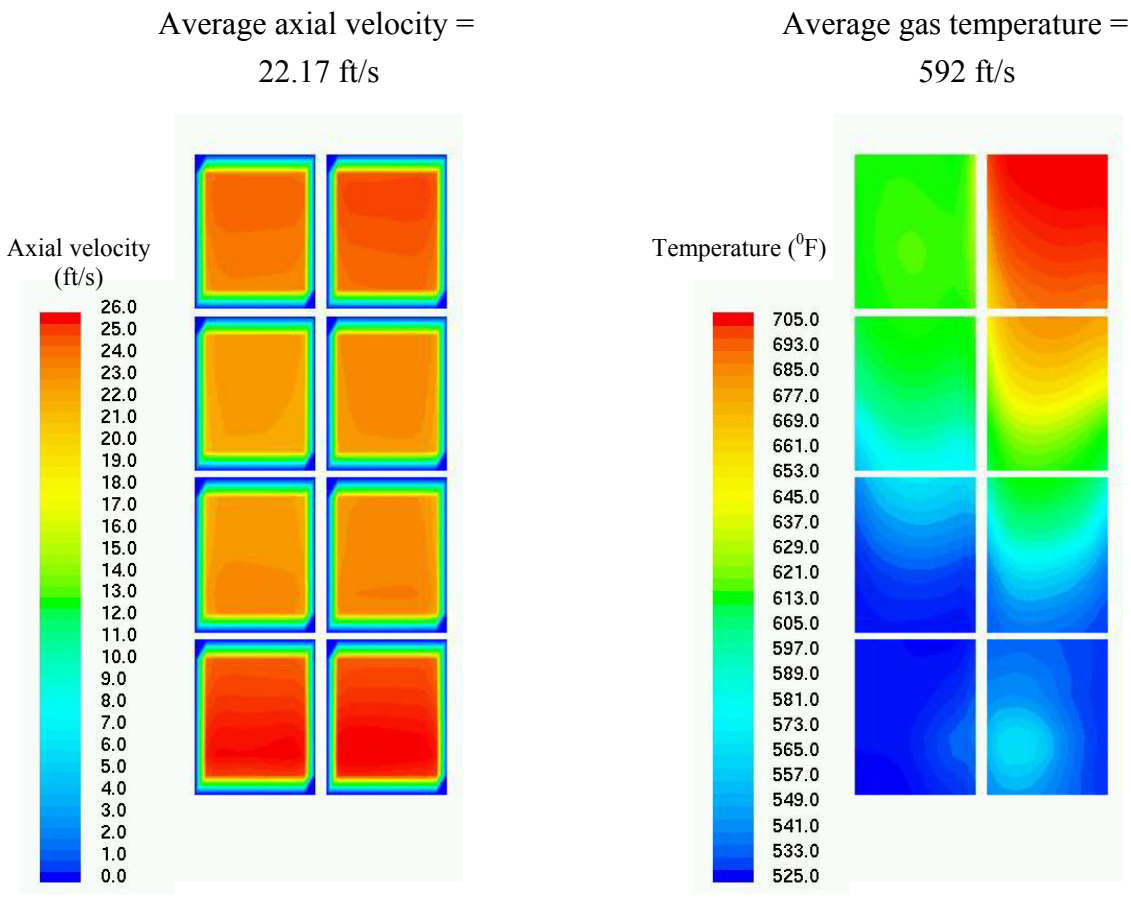

Figure 6-18: Contours of gas axial velocity component (ft/s) and gas temperature (^{o}F) entering CO catalyst, unfired case

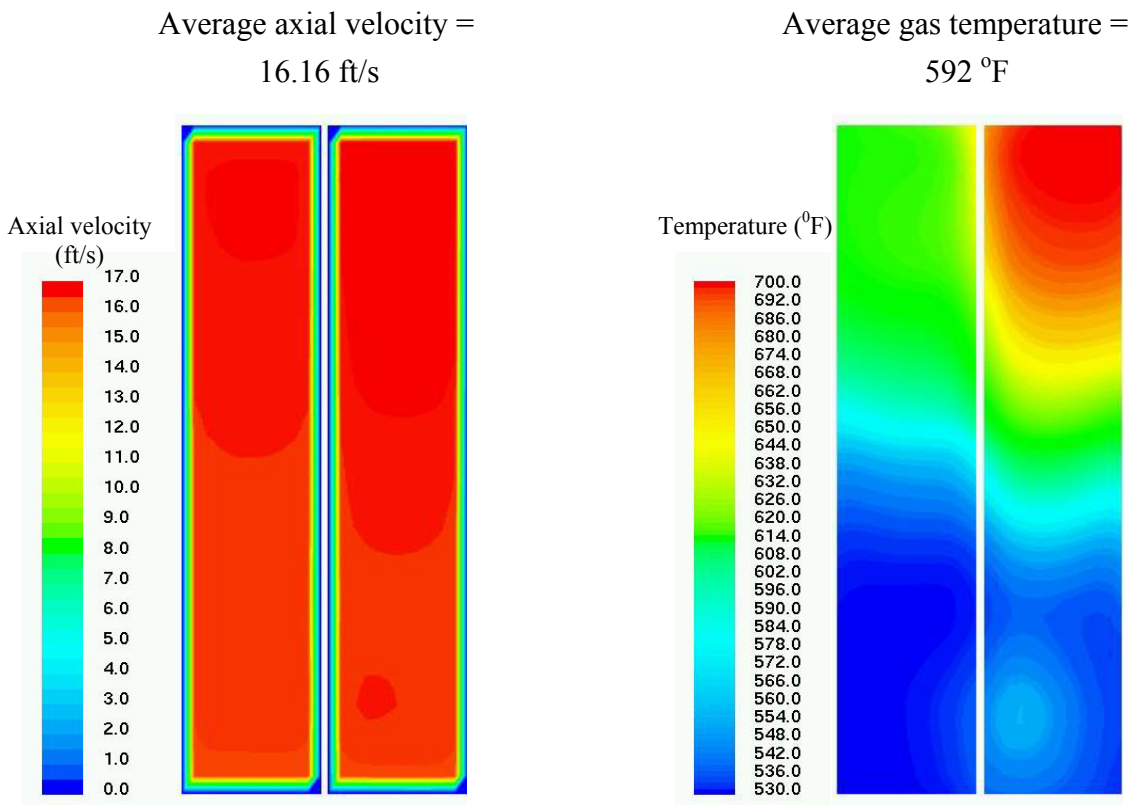

a) Entering SCR catalyst

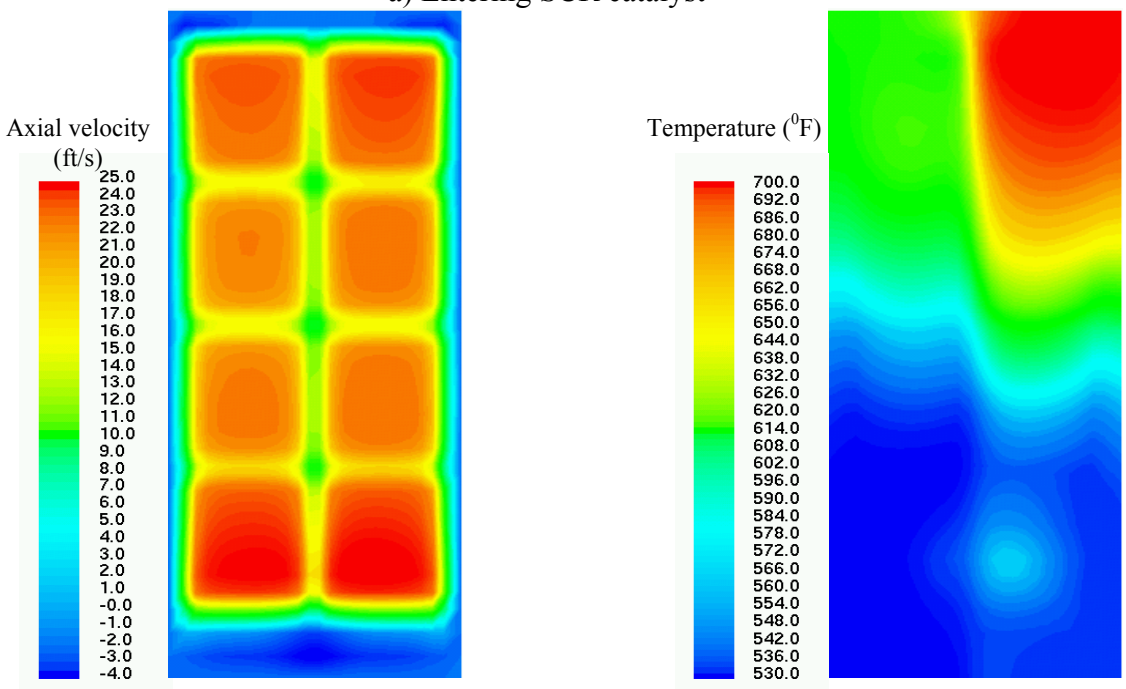

b) at AIG location

Figure 6-19: Contours of gas axial velocity component (ft/s) and gas temperature (°F) entering SCR Catalyst, unfired case

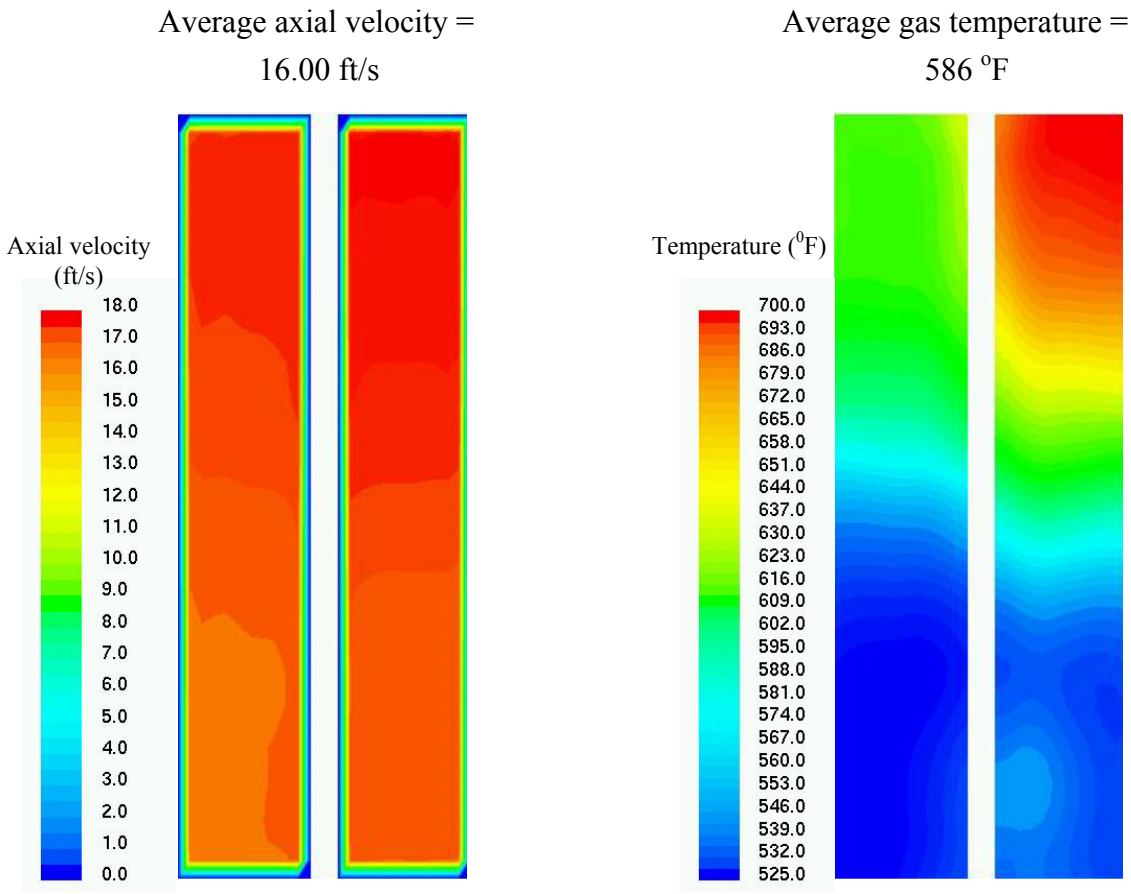

Figure 6-20: Contours of gas axial velocity component (ft/s) and gas temperature (°F) entering HPEC1 (Box2), unfired case

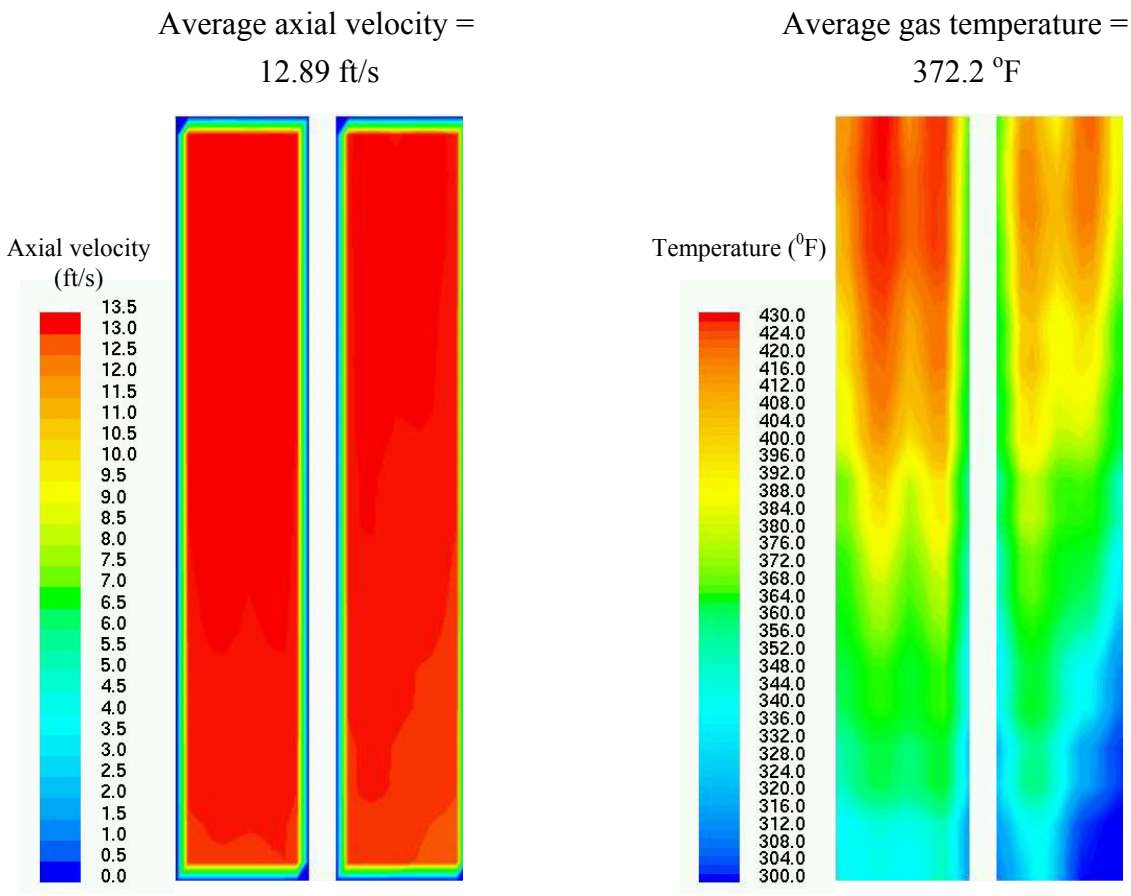

Figure 6-21: Contours of gas axial velocity component (ft/s) and gas temperature (°F) leaving LPEV1 (Box 2), unfired case

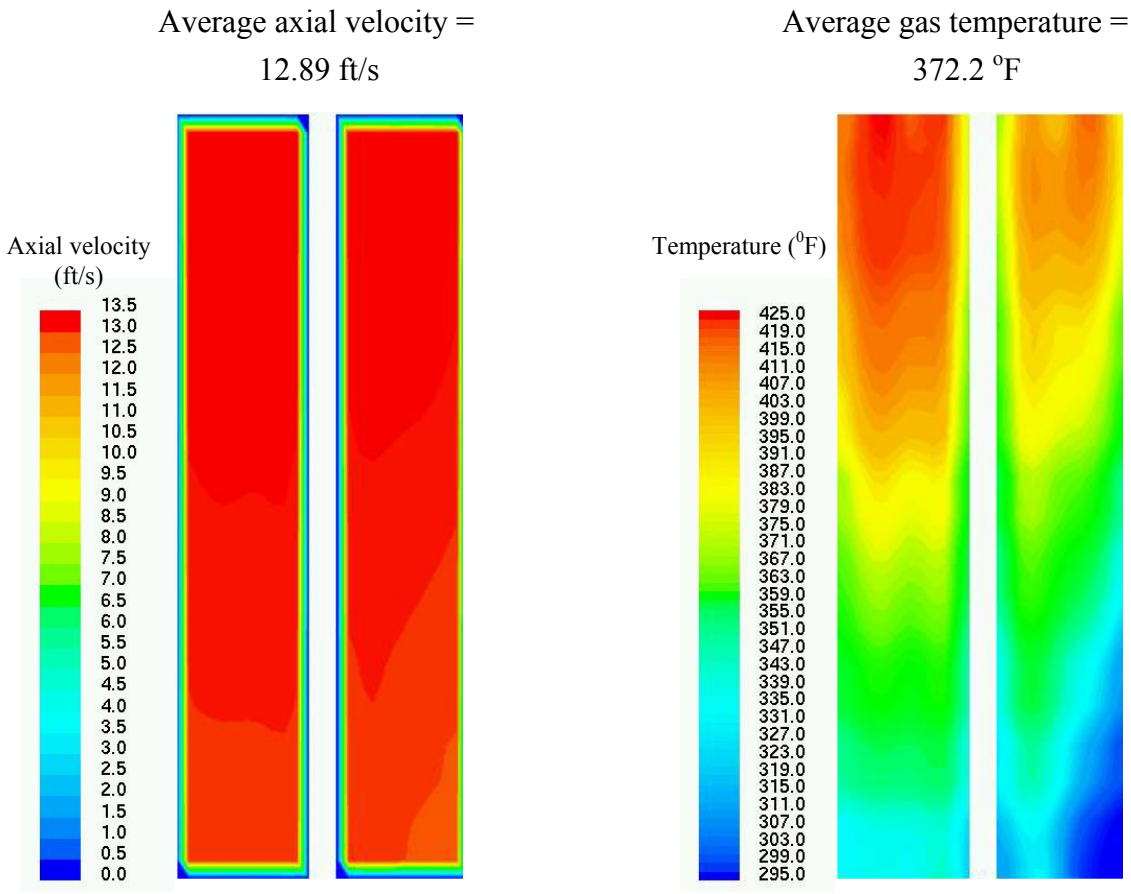

Figure 6-22: Contours of gas axial velocity component (ft/s) and gas temperature (°F) entering LPEV2 (Box 3), unfired case

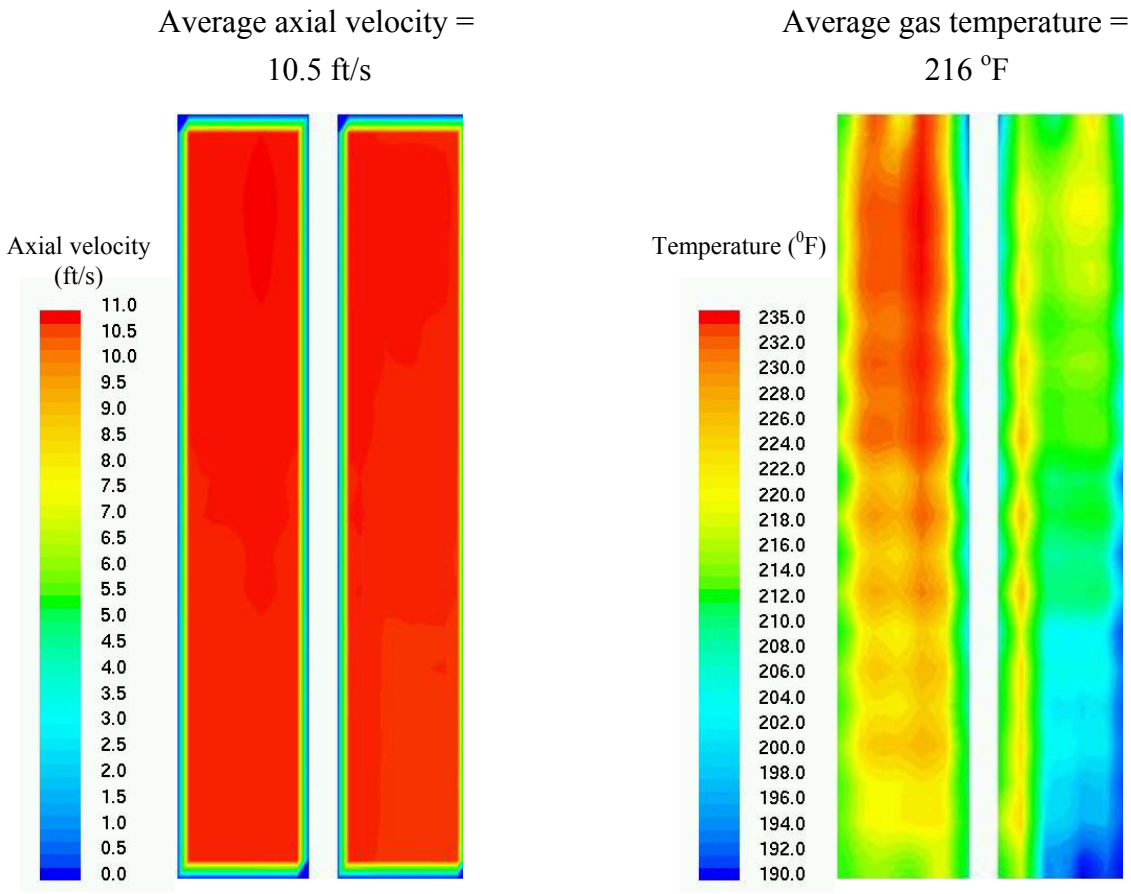

Figure 6-23: Contours of gas axial velocity component (ft/s) and gas temperature (°F) leaving WPHR6 (Box 3), unfired case

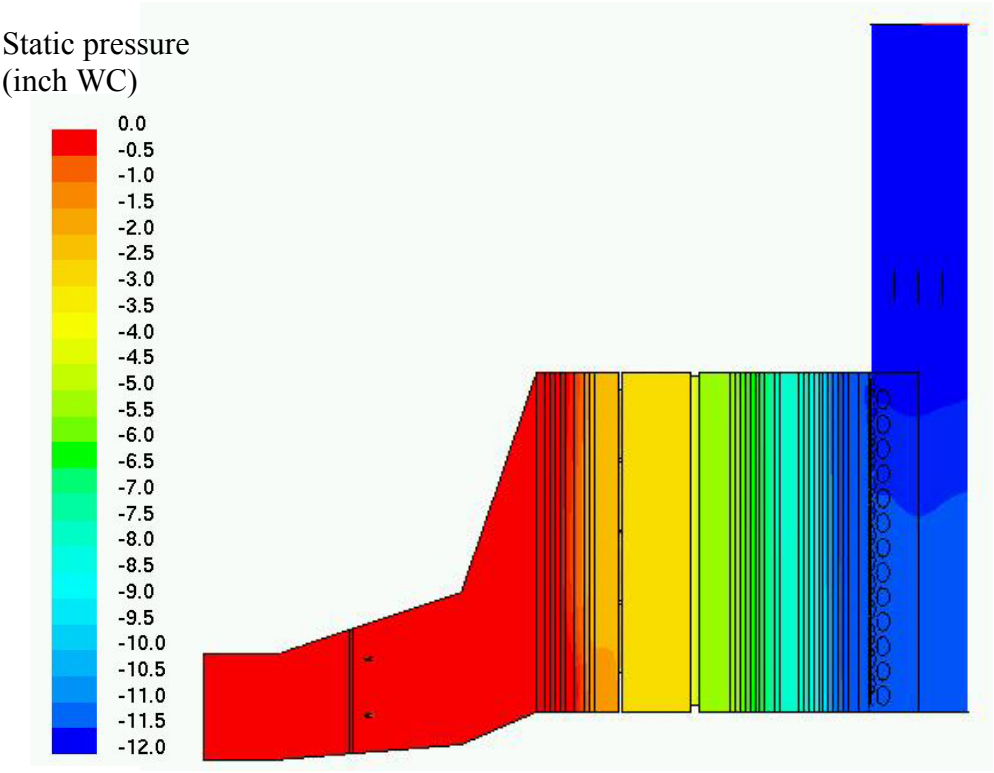

Figure 6-24: Static pressure contour along mid section of model (inch WC), unfired case

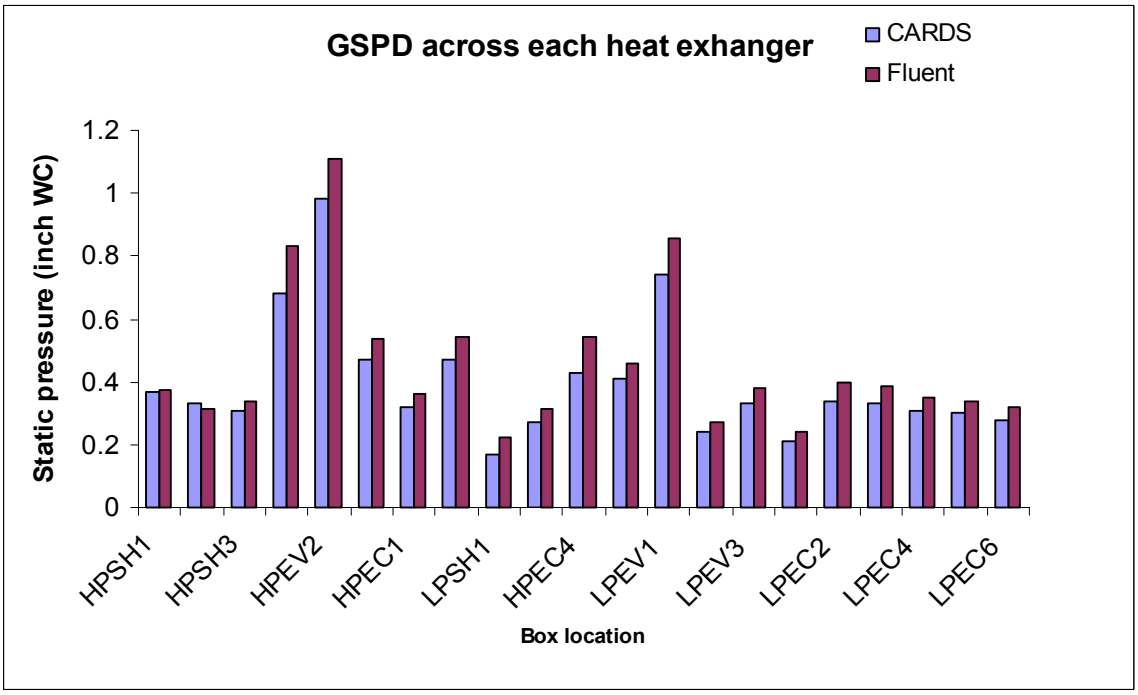

a) Comparison of module GSPD (Fluent Vs CARDS)

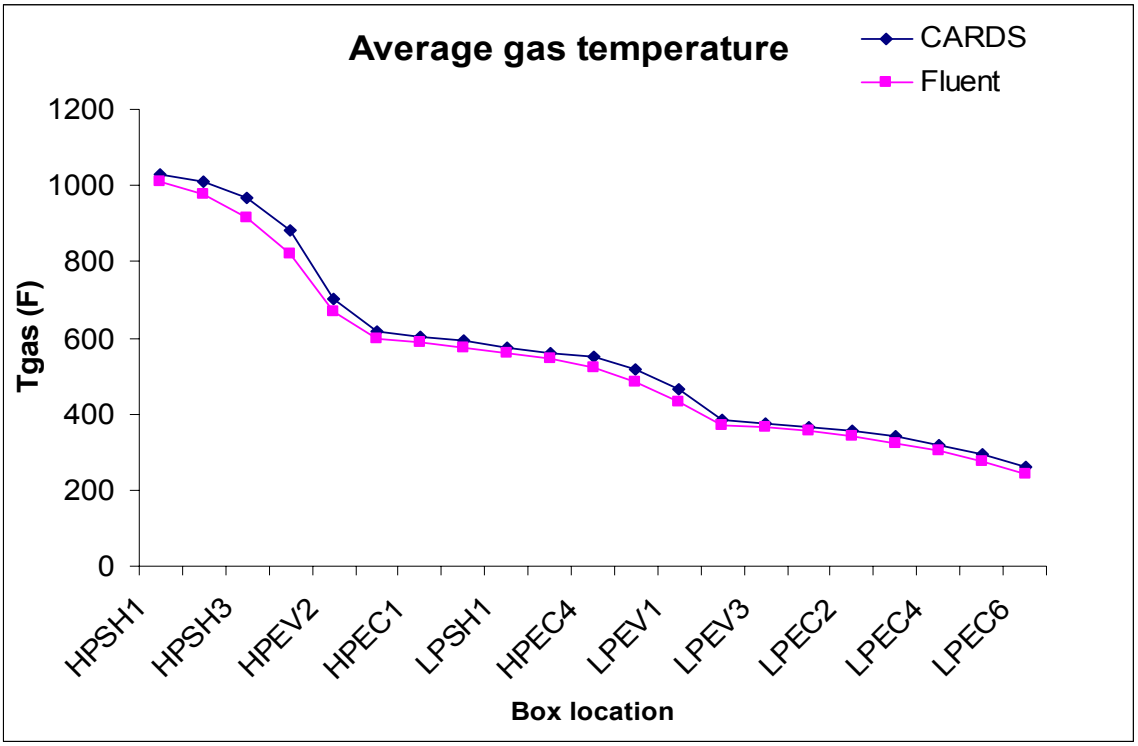

b) Comparison of average gas temperature (Fluent Vs CARDS)

Figure 6-25: Pressure drop and average gas temperature comparison charts, unfired case

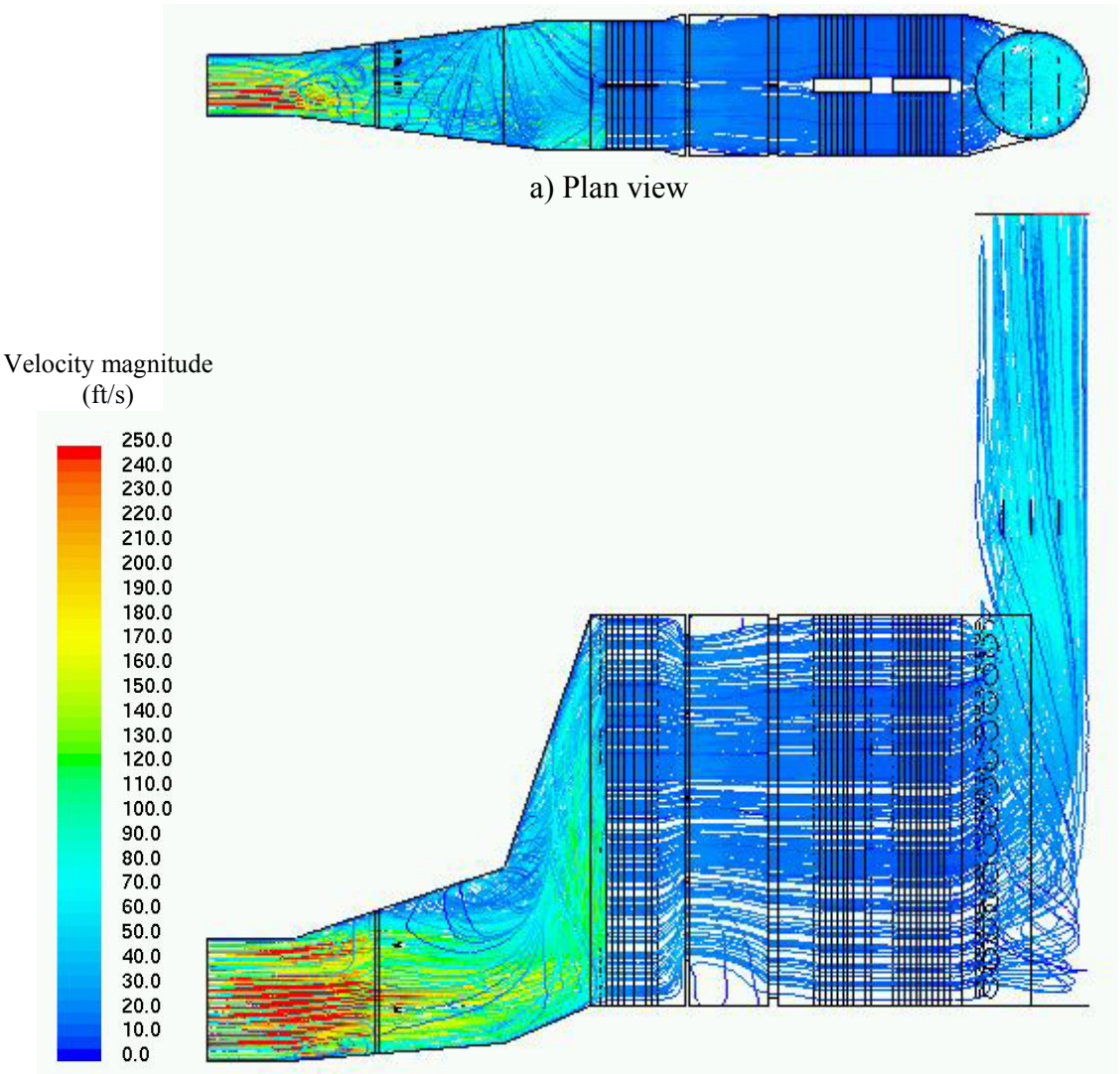

Figure 6-26: Stream traces colored by velocity magnitude, modified fired case

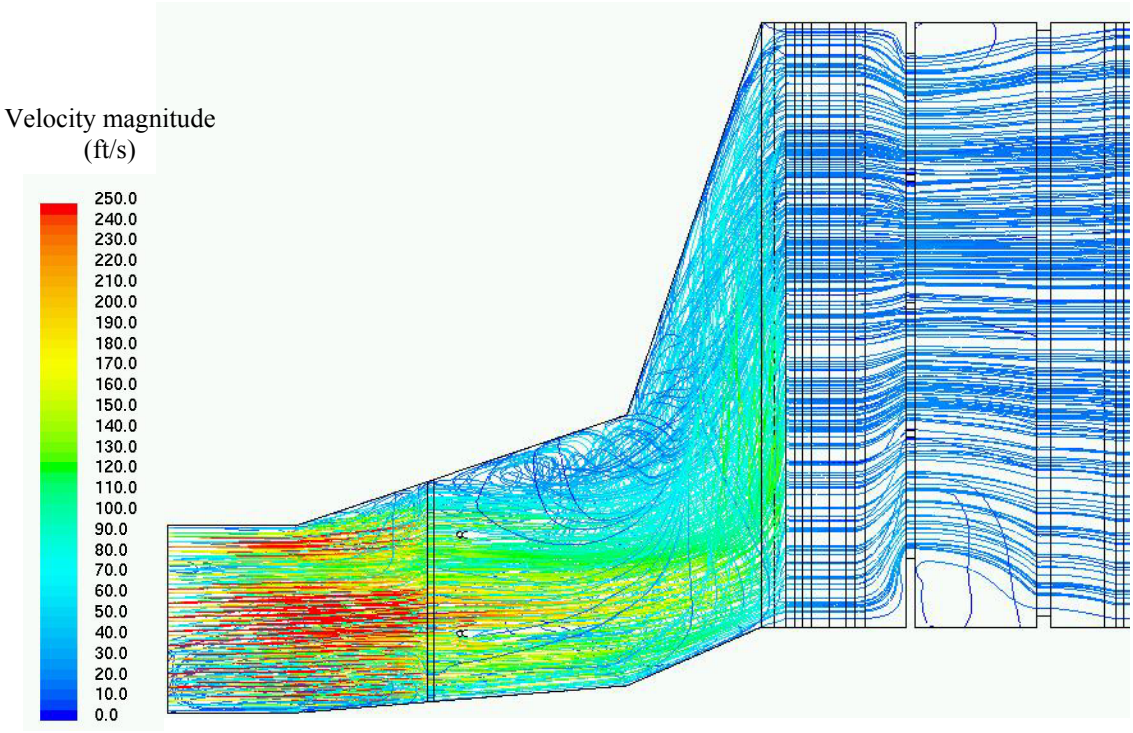

Figure 6-27: Details of stream traces colored by gas velocity magnitude (ft/s) in the inlet duct, modified fired case

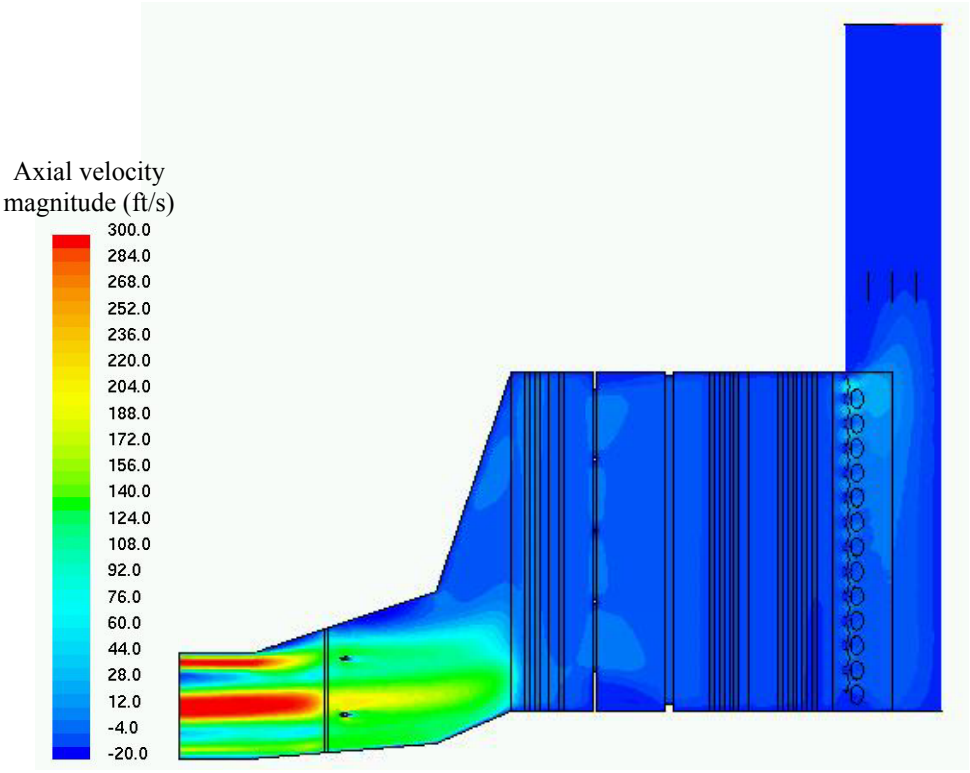

a) Location Z = -15 in

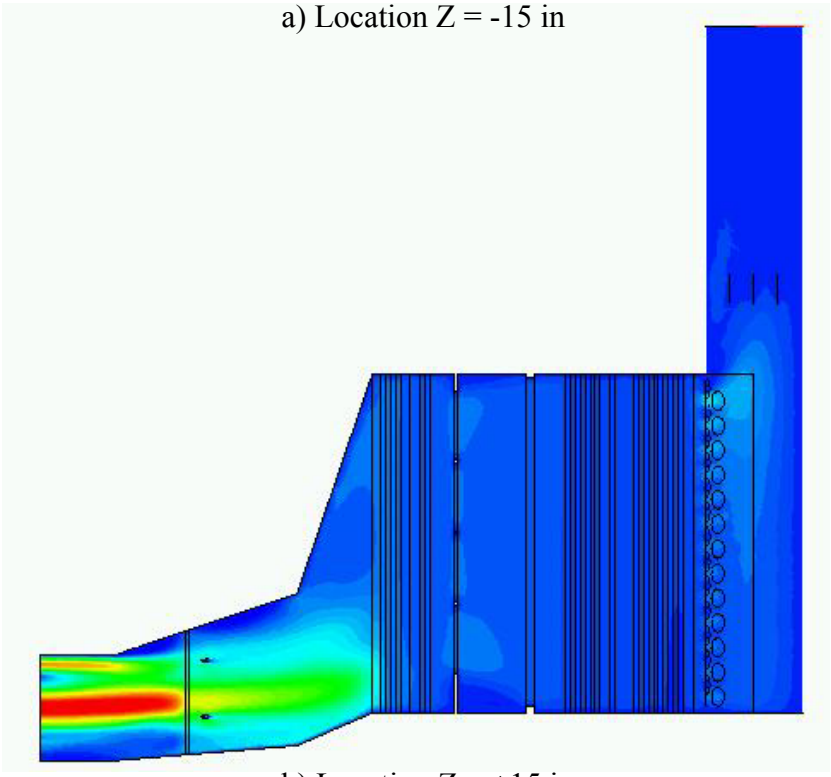

b) Location Z = +15 in

Figure 6-28: Contours of gas axial velocity (ft/s) along the boiler width at locations z= +/- 15 in, modified fired case

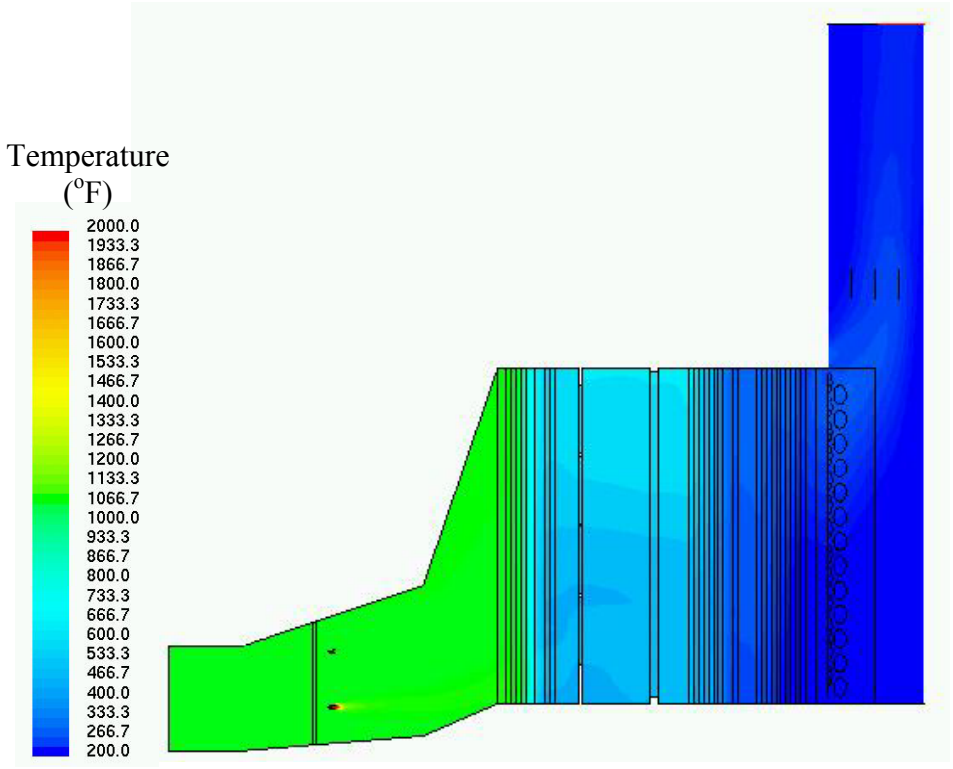

a) Location Z = 15in

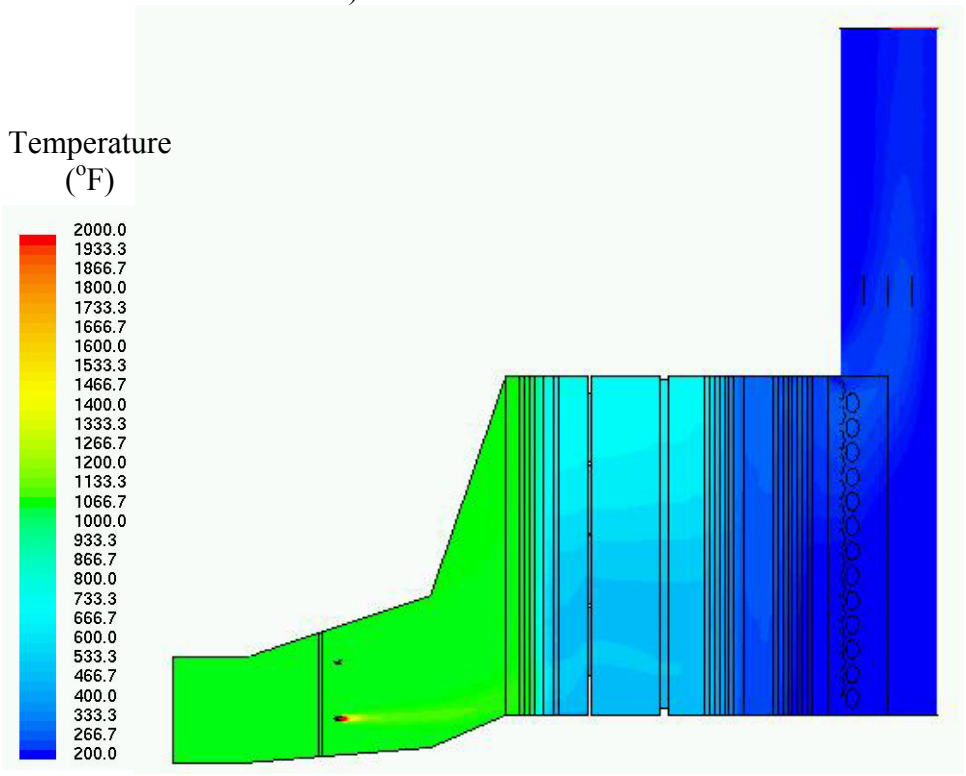

b) Location Z = -15in

Figure 6-29: Contours of gas temperature (°F) along the boiler width at locations z= +/- 15 in., modified fired case

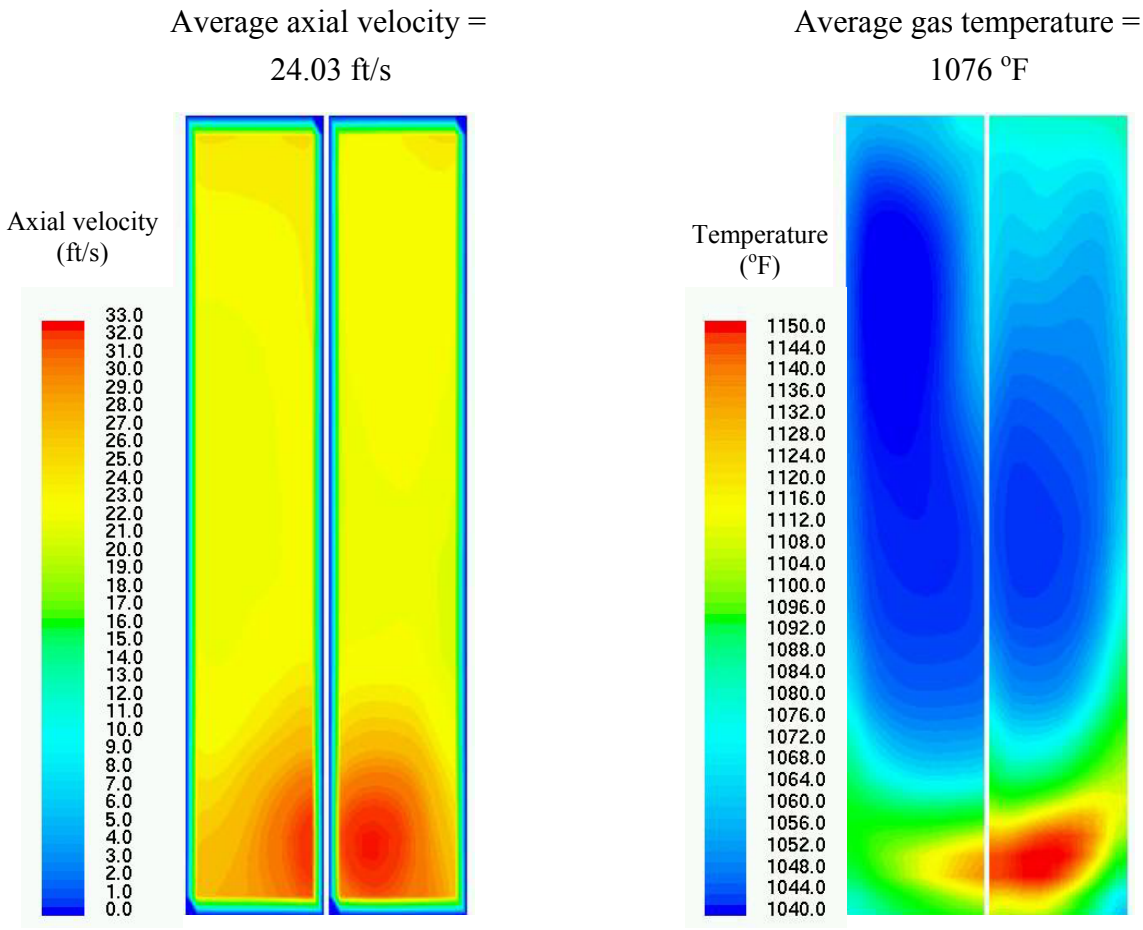

Figure 6-30: Contours of gas axial velocity component (ft/s) and gas temperature (°F) entering HPSH1 (Box 1), modified fired case

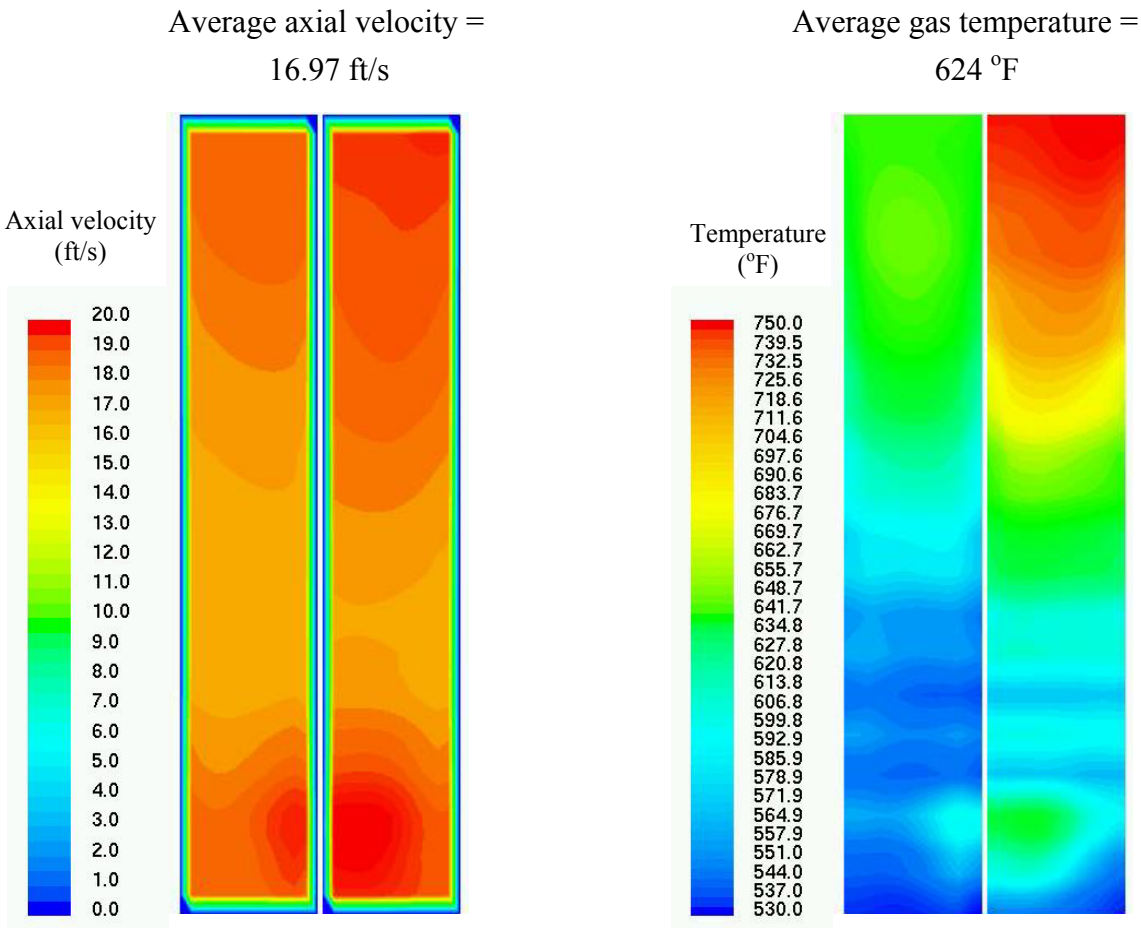

Figure 6-31: Contours of gas axial velocity component (ft/s) and gas temperature (°F) leaving HPEV3 (Box 1), modified fired case

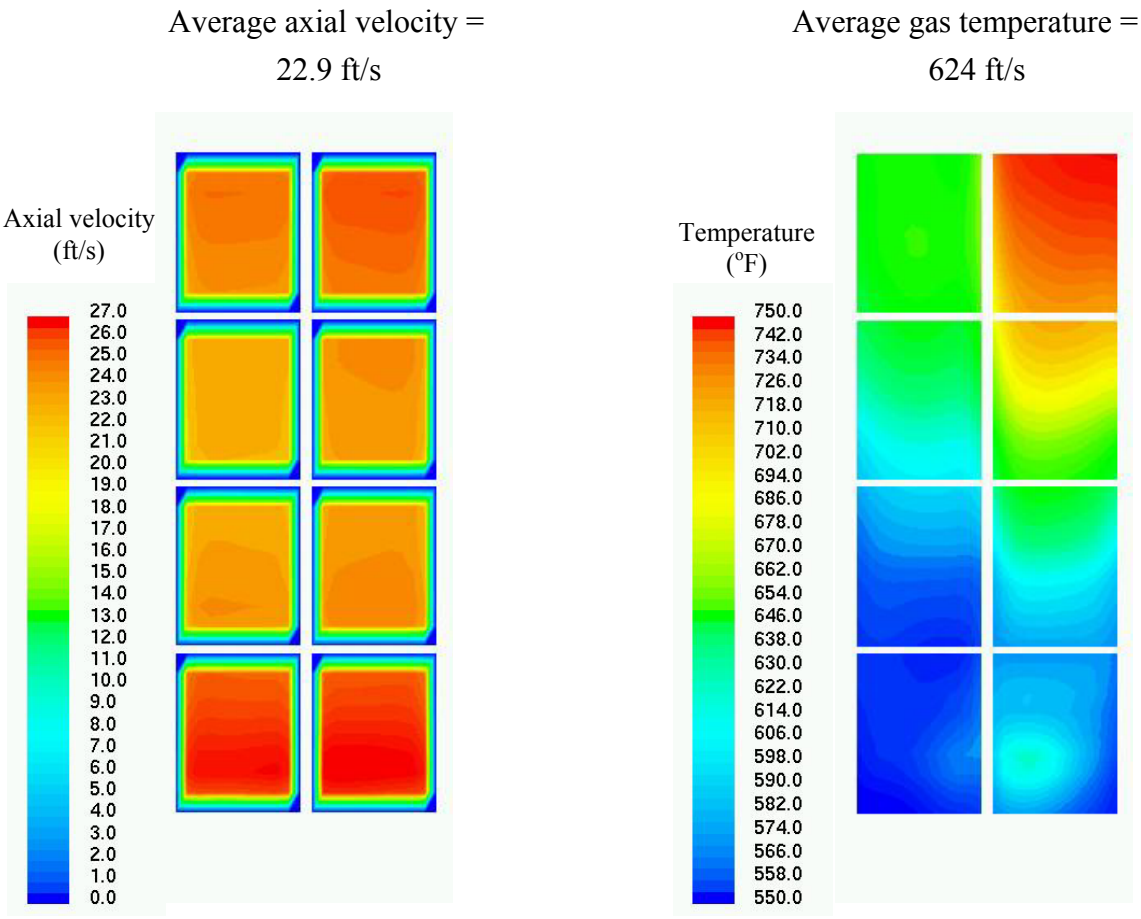

Figure 6-32: Contours of gas axial velocity component (ft/s) and gas temperature (°F) entering CO catalyst, modified fired case

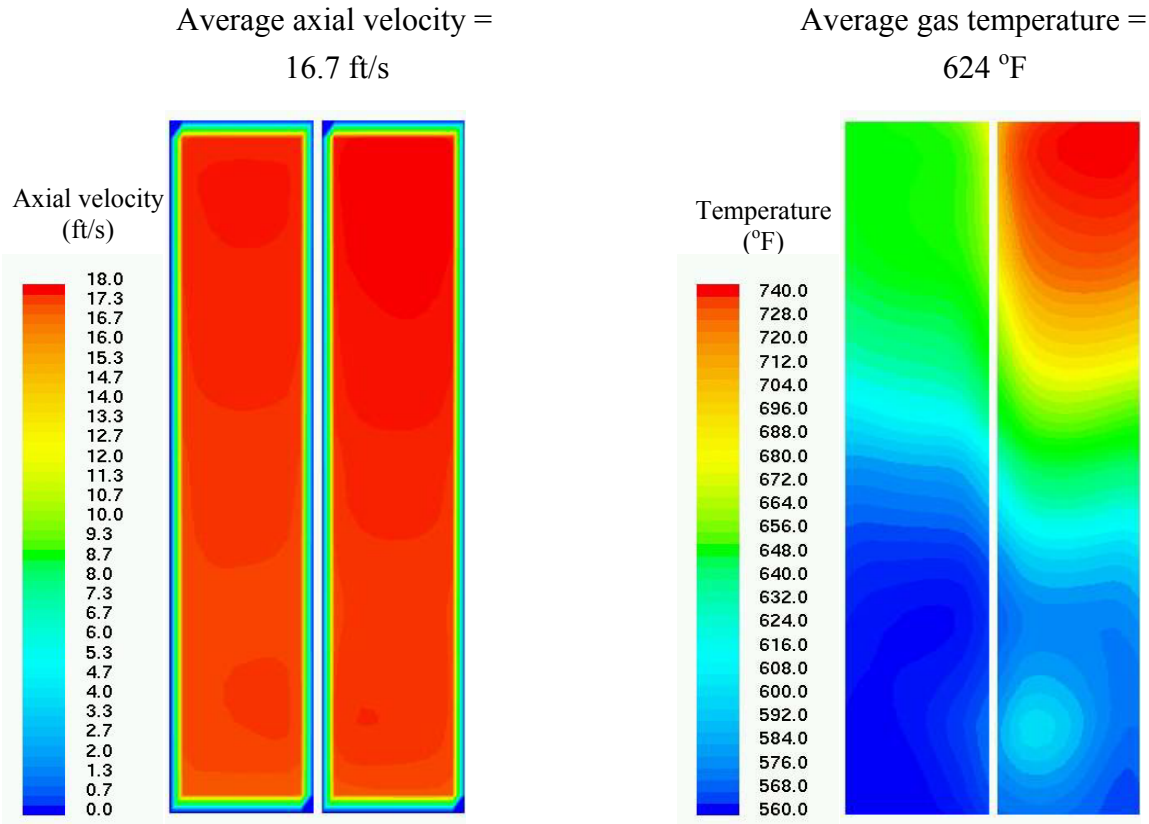

a) Entering SCR catalyst

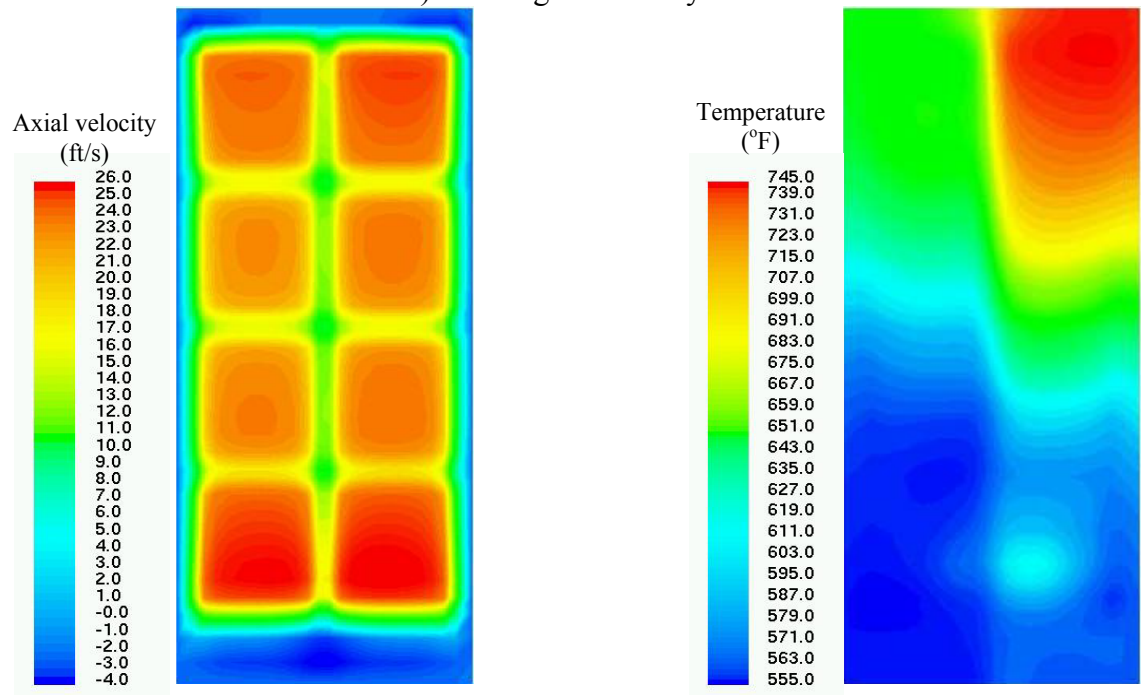

b) at AIG location

Figure 6-33: Contours of gas axial velocity component (ft/s) and gas temperature (°F) for SCR Catalyst, modified fired case

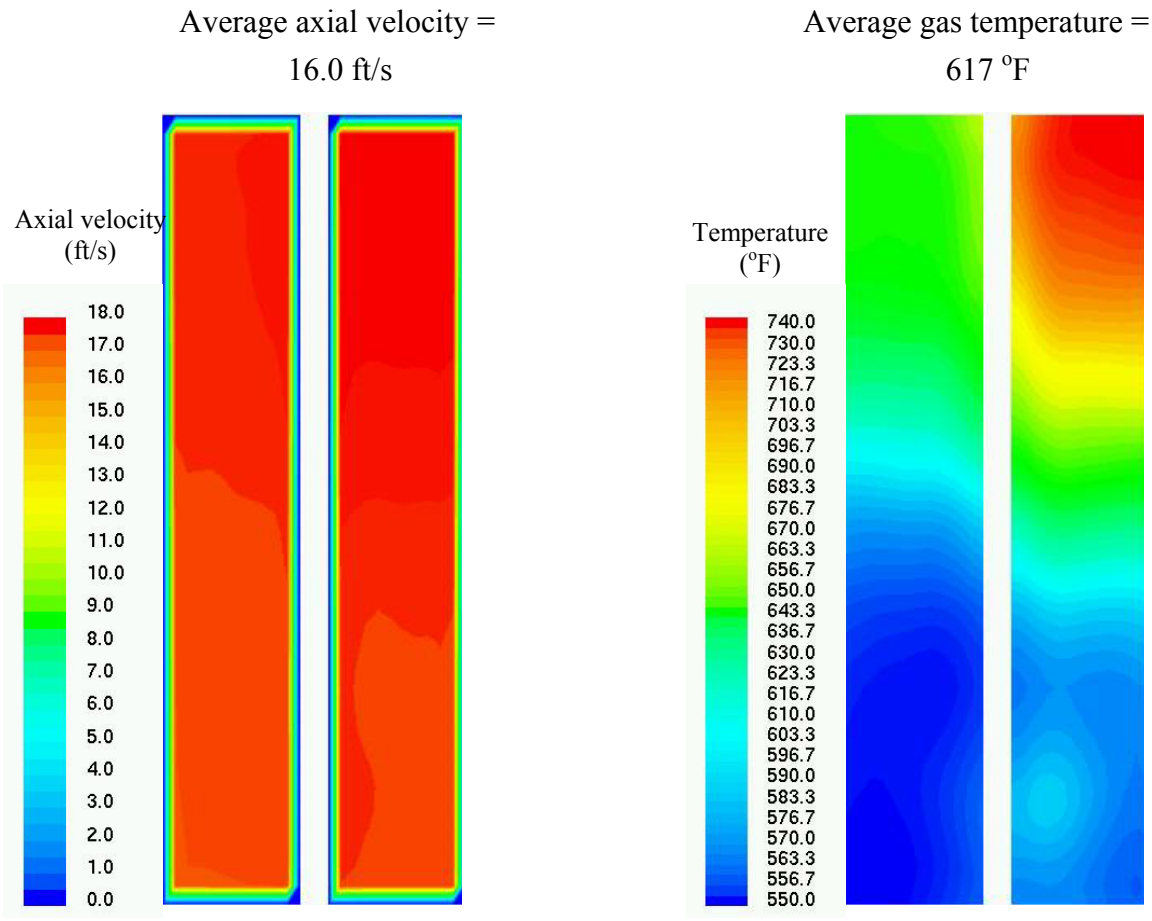

Figure 6-34: Contours of gas axial velocity component (ft/s) and gas temperature (°F) entering HPEC1 (Box 2), modified fired case

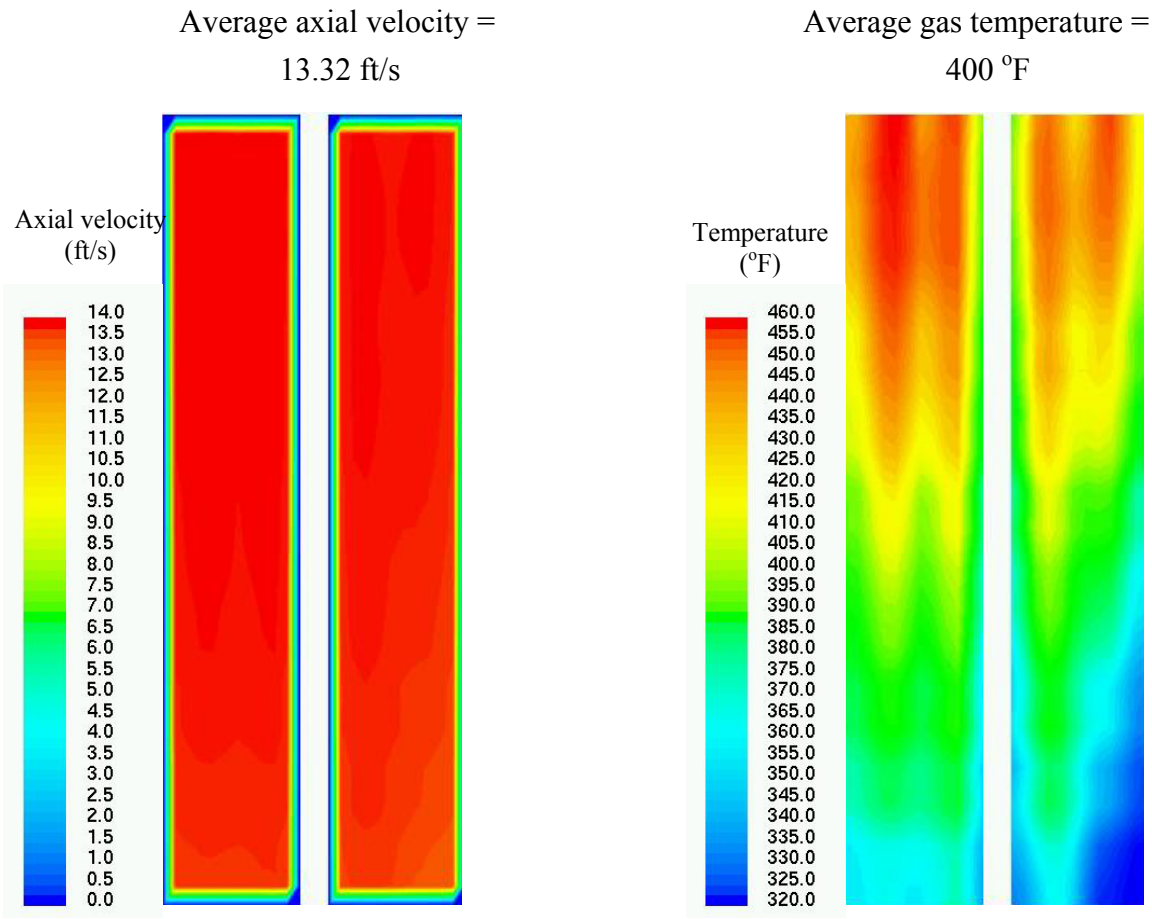

Figure 6-35: Contours of gas axial velocity component (ft/s) and gas temperature (°F) leaving LPEV1 (Box 2), modified fired case

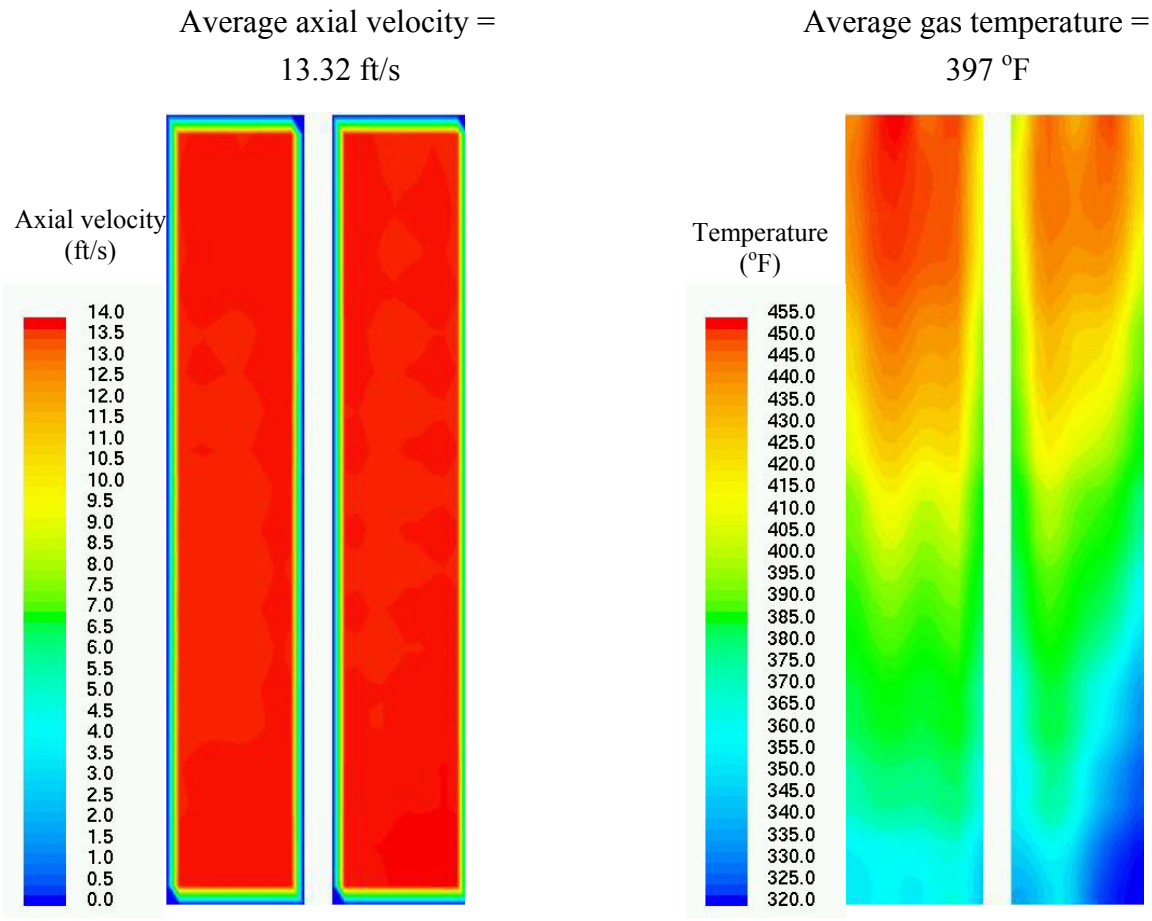

Figure 6-36: Contours of gas axial velocity component (ft/s) and gas temperature (°F) entering LPEV2 (Box 3), modified fired case

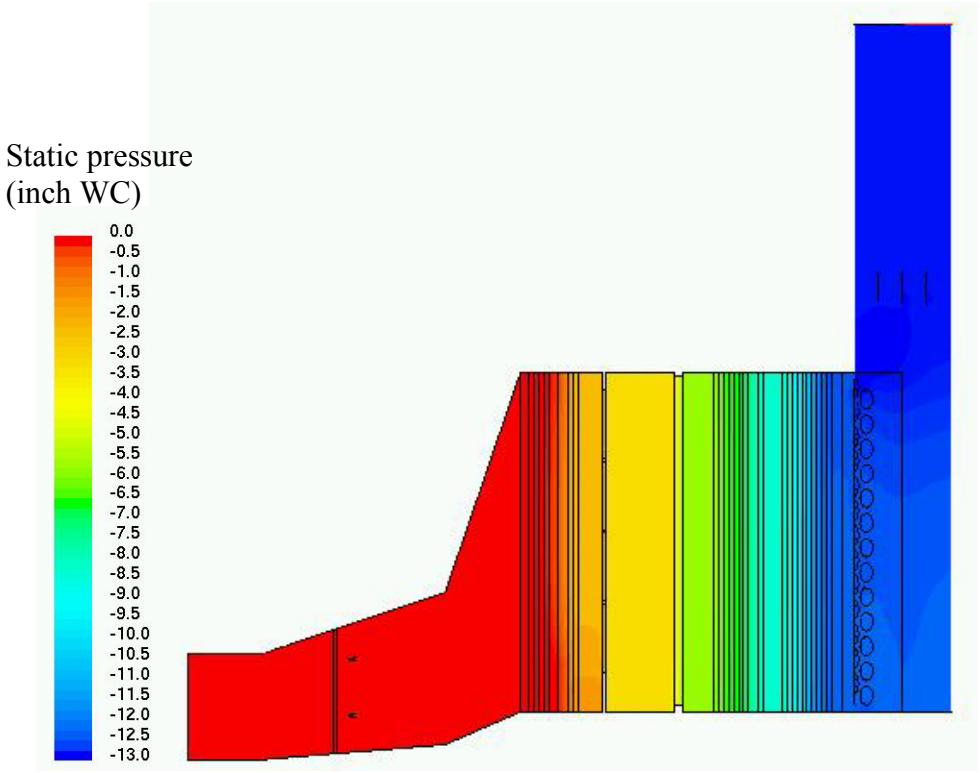

Figure 6-37: Static pressure contour along mid section of model (inch WC), modified fired case

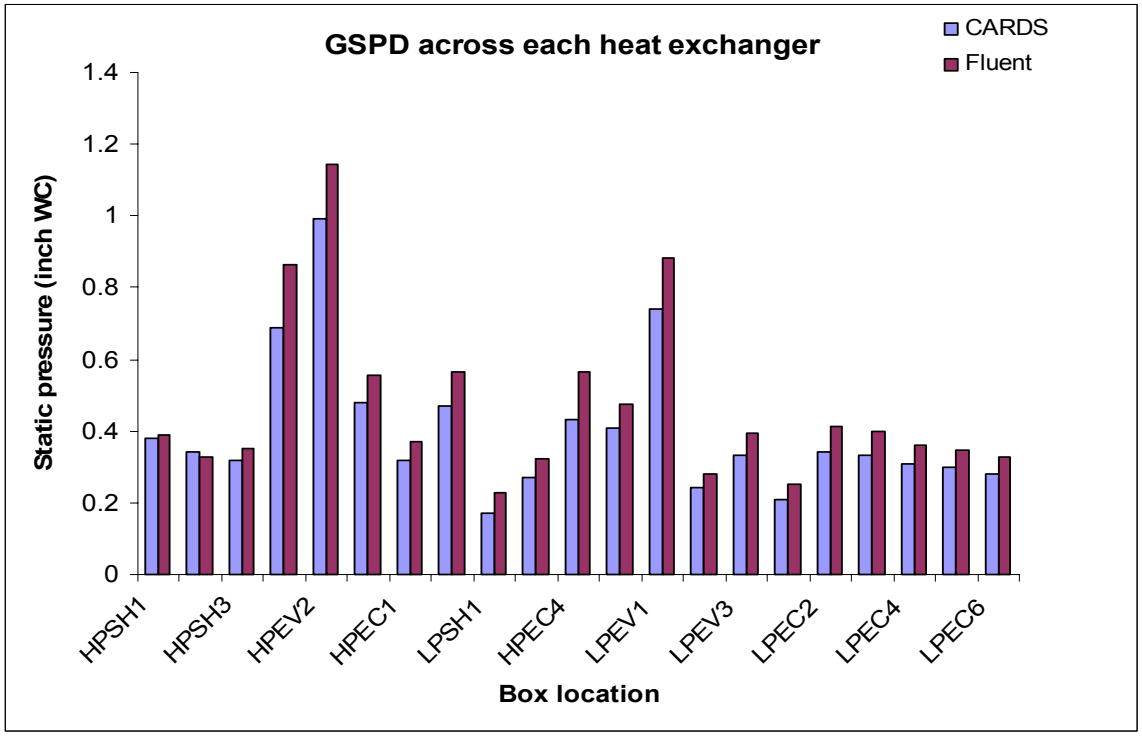

a) Comparison of module GSPD (Fluent Vs CARDS)

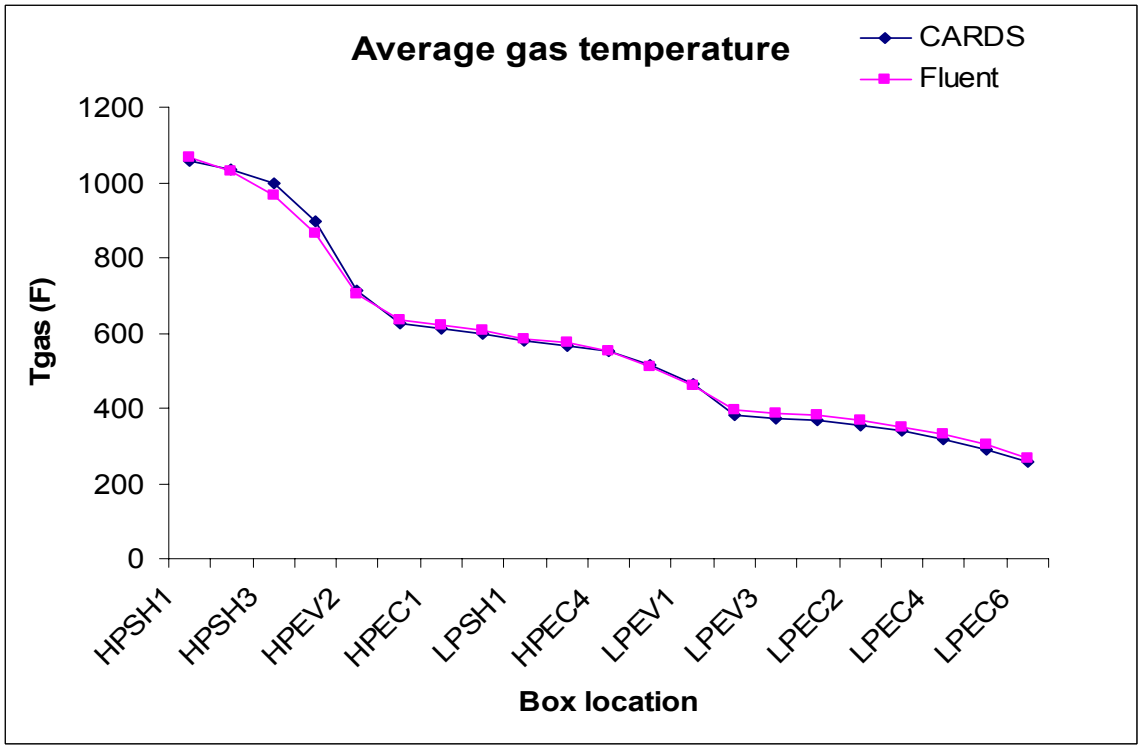

b) Comparison of average gas temperature (Fluent Vs CARDS)

Figure 6-38: Pressure drop and average gas temperature comparison charts, Modified fired case

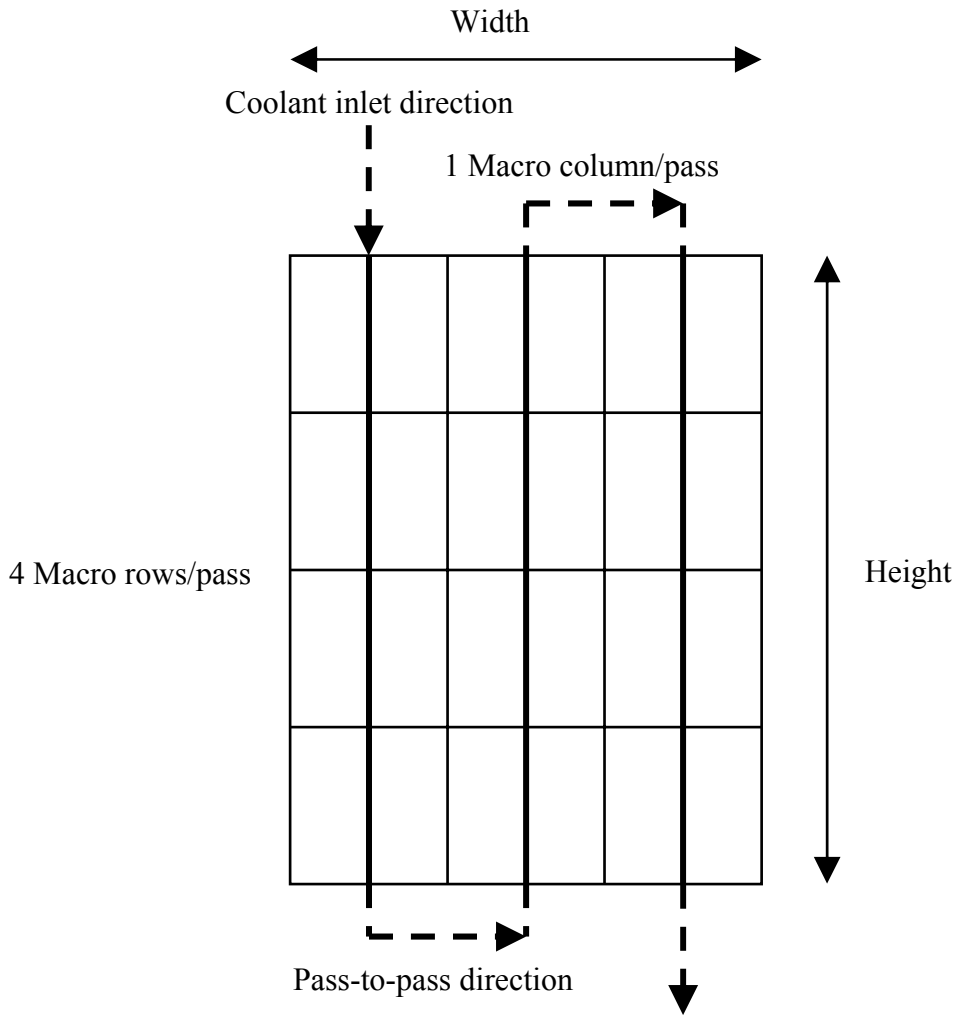

Figure 6-39: Figure showing the macro numbering in heat exchanger with 3 passes [11]

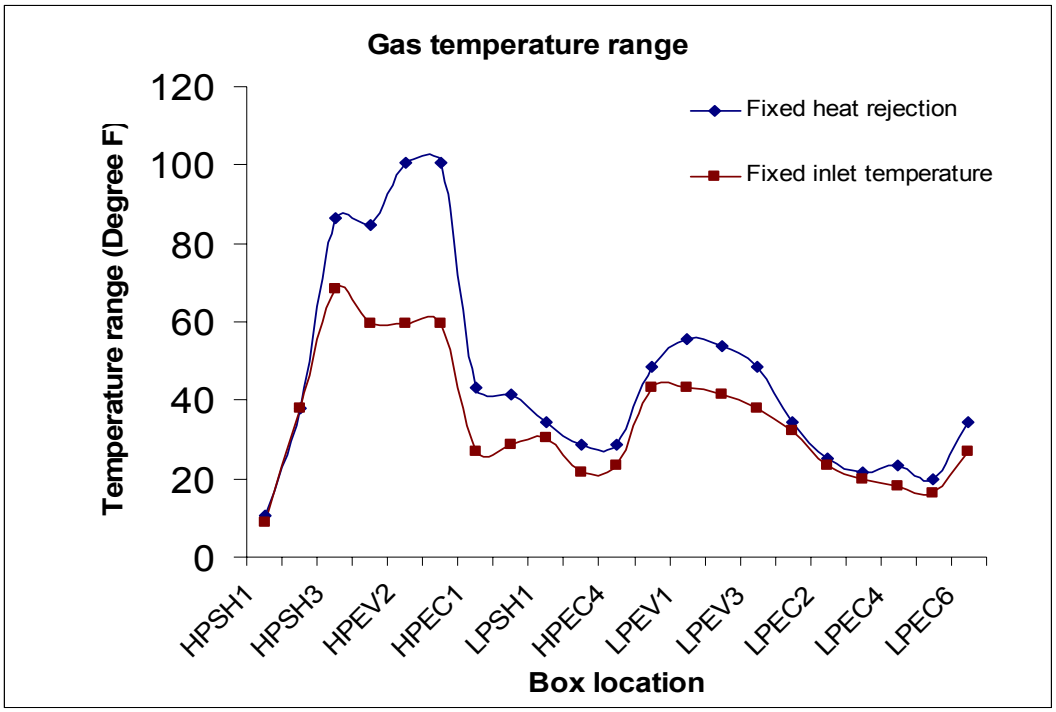

a) Unfired case

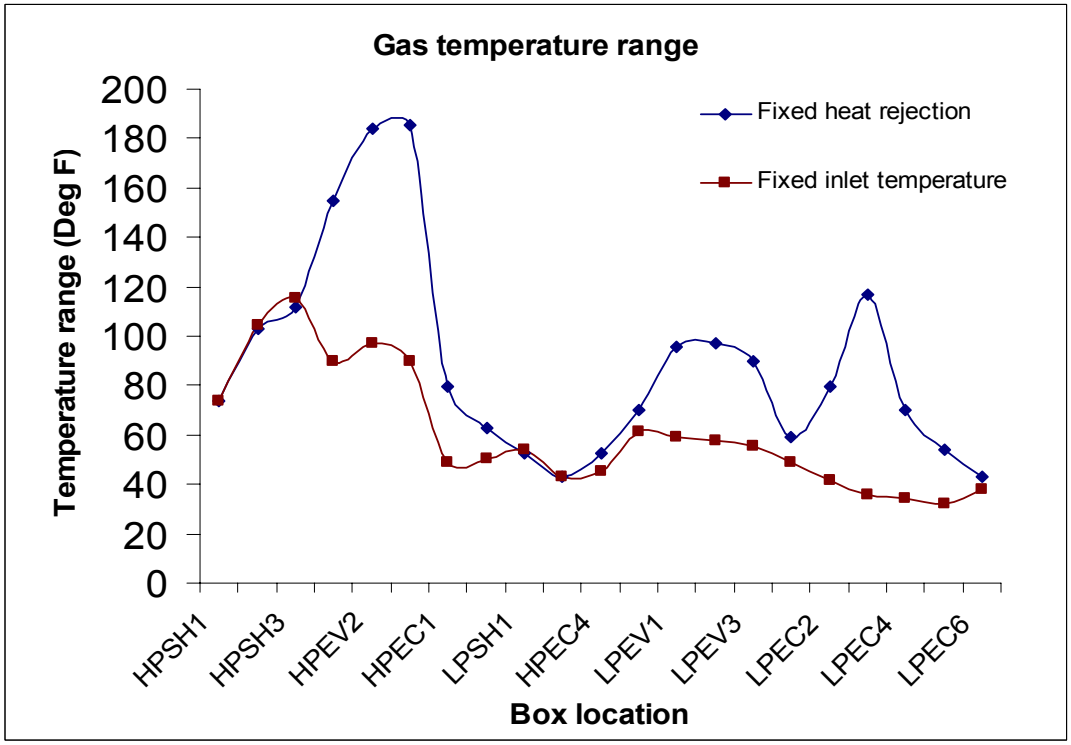

b) Fired case

Figure 6-40: Gas temperature range comparison for fixed heat rejection and fixed coolant inlet temperature

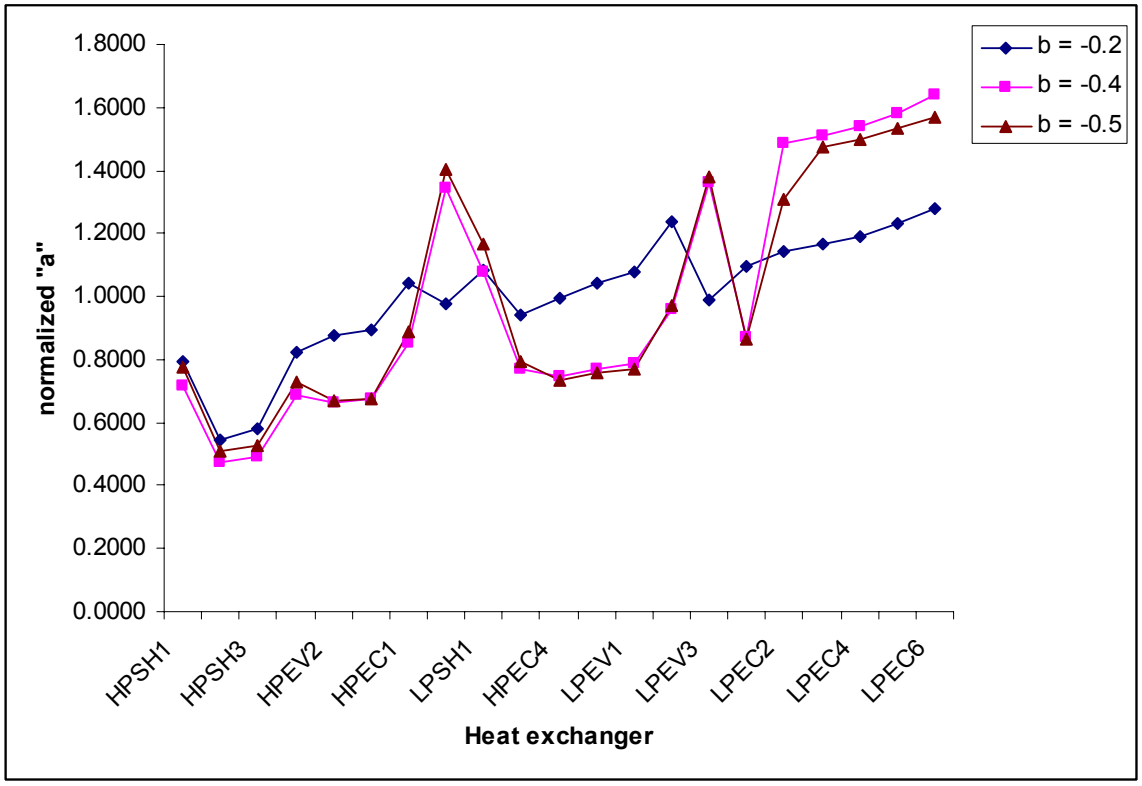

Figure 6-41: Comparison of core friction coefficient values for different values of core friction exponent

Chapter 7

Results and Analysis: Current Creek HRSG

The results for the cases with the inlet and operating conditions shown in chapter 5 for the Current Creek HRSG are presented and discussed in this chapter. The predicted results were analyzed to understand the flow and evaluate the design in the following areas of interest [5]:

- Flow distribution within the inlet duct
- Flow distribution into the burner elements
- Burner performance
- Flow distribution and gas temperature distribution at the heating surface
- Flow distribution into the emission control equipment

Layout of figures

This chapter discusses the simulation results for the Current Creek HRSG. Simulations are carried out for three different cases: a fired case, a modified design fired case, and a modified design unfired case. Figures relating to the fired case are shown from figures 7-1 through 7-13. Figure 7-1 shows the details of stream traces within the

model, colored by velocity magnitude. Figure 7-2 shows the gas velocity contours colored by the velocity magnitude and axial velocity components at different sections in the inlet duct. Figure 7-3 shows the gas velocity contours colored by y and z components of velocities at different sections in the inlet and bypass ducts. Figure 7-4 shows the iso-surface plots of velocities in the inlet duct. Figure 7-5 shows the contours of static pressure variation along the width of the HRSG. Figure 7-6 shows contours of gas velocity distribution along the width of the HRSG. Figure 7-7 shows contours of gas axial velocity distribution along the width of the HRSG. Figure 7-8 shows contours of gas temperature distribution along the width of the HRSG. Figure 7-9 shows contours of gas flow and temperature distribution entering HPSH1 (Box 1). Figure 7-10 shows contours of gas flow and temperature distribution leaving HPSH2 (Box 1). Figure 7-11 shows contours of gas flow distribution upstream of the duct burner. Figure 7-12 shows contours of gas flow and temperature distribution entering the heat exchanger downstream of the burner. Figure 7-13 shows the comparison of gas-side pressure drop in each of the heat exchanger sections and the average gas temperature entering the different heat exchangers with the CARDS predictions.

Figures 7-14 to 7-19 show the simulation results for the burner sub-model study. Figure 7-14 shows the different burner configurations modeled in the sub-model study. Figures 7-15 and 7-16 show the temperature contour comparison between the different configurations. Figure 7-17 shows temperature contours at different sections along the length for the three configurations. Figure 7-18 shows the contours of velocity magnitude along the length of the three configurations. Figure 7-19 shows the contours of axial

velocity magnitude along the length of the three configurations. Figure 7-20 shows the revised burner array configuration.

Results for the modified design, fired case are shown in figures 7-21 through 7-36. Figure 7-21 shows the stream traces within the model colored by velocity magnitude. Figure 7-22 shows the gas velocity contours colored by velocity magnitude along the width of the HRSG. Figure 7-23 shows the gas axial velocity contours along the boiler width of the HRSG. Figure 7-24 shows the contour of gas temperature along the width of the HRSG. Figure 7-25 shows contours of gas flow and temperature distribution entering HPSH1 (Box 1). Figure 7-26 shows contours of gas flow and temperature distribution leaving HPSH2 (Box 1). Figure 7-27 shows contours of gas flow distribution upstream of the duct burner. Figure 7-28 shows contours of gas flow and temperature distribution entering HPSH3 (Box 2). Figure 7-29 shows contours of gas flow and temperature distribution leaving HPEV4 (Box 2). Figure 7-30 shows contours of gas flow and temperature distribution at the AIG location. Figure 7-31 shows contours of gas flow and temperature distribution entering the SCR catalyst. Figure 7-32 shows contours of gas flow and temperature distribution entering IPSH1 (Box 3). Figure 7-33 shows contours of gas flow and temperature distribution entering HPEC3 (Box 4). Figure 7-34 shows contours of gas flow and temperature distribution entering LPEV3 (Box 5). Figure 7-35 shows the static pressure contour along the width of the HRSG. Figure 7-36 shows the comparison of gas-side pressure drop in each of the heat exchanger sections and the average gas temperature entering the different heat exchanger to that of CARDS for the modified design, fired case. Figure 7-37 shows the comparison of gas-side pressure drop

in each of the heat exchanger sections and the average gas temperature entering the different heat exchanger to that of CARDS for the modified design, unfired case.

7.1 HRSG inlet conditions and inlet duct

The gas velocity distribution in the inlet duct is important, as the inlet duct directs the gas flow from the GT to the heat exchanger surfaces. A uniform distribution of flow into the heat exchangers is desired for good thermal performance. The regions of back flow in the inlet duct are to be limited [5]. For the Current Creek model, the exhaust gas velocity profile entering the inlet of the HRSG is shown in figures 4-6 and 4-7. This HRSG is designed to operate with the axial exhaust GT, with swirl in the flow. It is identified that the inlet flow conditions for this model are sufficient enough and do not require any flow control devices in the inlet duct. Velocity distribution at different sections in the bypass duct and inlet is shown in figures 7-2, and 7-3. Results show that the inlet duct design is sufficient enough to limit back flow in the expansion part without affecting the mail flow into the heat exchangers. It is also clear that the expansion of the high velocity core is uniform and the walls of the inlet duct are not exposed to high velocity, high temperature gases, as shown in figure 7-4. The variation of static pressure is shown in figure 7-5. It is evident that there is a gain in the pressure when the flow is passing through the expansion part before entering the heat exchangers, as expected.

7.2 Flow distribution into first heat exchanger surface

Gas flow and temperature distribution into the heat exchangers are the primary design criteria, since a uniform distribution of mass and heat flux into the tube banks

results in stable performance of the system. The initial distribution into the first heat exchanger also influences the distribution into the heat exchangers downstream [5].

The gas velocity distribution at the first heat exchanger surface for the original configuration and fired case is shown in figure 7-9. It is observed that around 91% (90.8%) of the velocities are with in +/-20% of the average velocity. These conditions meet the requirements (VPI) for the acceptable flow distribution. The gas temperature distribution at the first heat exchanger surface is shown in figure 7-9; the temperature variation observed in this figure is around 30 ^{o}F across the surface. Lower values of temperature at the top are the result of the large vertical motion of the gas in that region.
It is observed that the flow requirements at the first heat exchanger surface are satisfied and meet the requirements set by VPI.

7.3 Conditions at the duct burner

The burner arrangement for supplementary firing in the Current Creek model includes six duct burners provided with 14 wing baffles distributed evenly through the boiler area. The burner is located between the two heat exchanger boxes as shown in figure 3-2. For the ideal performance of the burner, the gas flow distribution entering the burners should meet some requirements, flow is to be uniform, with the some minimum velocity and vectors normal to the burner plane. The purpose of the baffles is to increase the flow velocity and to direct the gas flow into the burners. The velocity profile 18 in. upstream of the burner is shown in figure 7-11. It can be observed that the effect of the baffles is seen on the flow with some vertical moment of the flow at this plane. The average velocity at this plane is observed to be 20.77 ft/s with 95% of velocity values

falling within +/-25% of the average velocity. The temperature distribution leaving HPSH2 (Box 2)/entering the burner is shown in figure 7-10. The average gas temperature is observed to be 1045 ^{o}F, which is high enough for auto ignition of the fuel.

The conditions downstream of the burner are also studied. Figure 7-12 shows the gas velocity and temperature distribution entering the heat exchanger downstream of the burner. It is observed that the temperature distribution entering this section averages 1556^{o}F, which is in agreement with the heat input parameters based upon the fuel addition and the heating value of the fuel, but the peak temperatures in this plane is very high, up to 2400^{o}F. These high temperature peaks might cause structural damage to the heat exchanger sections and affect the performance of the entire system. It is concluded from the analysis that the initial burner design is not sufficient enough for the safe operation of the HRSG. The flow conditions downstream of this section are not discussed for this case. A sub-model study is carried out to improve the burner design and reduce the temperature peaks at the plane entering the heat exchanger downstream of the burner.

7.4 Burner sub-model study

Instead of considering the complete model, to improve the performance of the burner, a sub-model study is carried out considering only a single burner element with two wing baffles one above the burner duct and one below is considered. The section considered for the analysis extends between the exit of the heat exchanger module box 1 (HPSH2) through the exit of the heat exchanger module box 2 (HPEV4).

An important condition necessary for ideal performance of the burner is the velocity distribution of the gas flow entering the burner. Velocity distribution should be uniform and high enough with enough turbulence to provide proper mixing of the fuel with the gas. A second requirement is that the temperature should be high enough to self ignite the fuel. In this case, the temperature of the exhaust gas is high enough for auto-ignition. Considering the temperature contour downstream of the burner two configurations of the burner are tested. The first configuration, represented as test configuration 1, blocks the gaps provided in the baffle section, thereby increasing the gas velocity entering the burner. The second configuration suggested by engineers from the industry based upon their experience is that in addition to the blockage of the gaps in the wing baffles, an additional notch is provided on the two baffles spanning the middle 40% of the burner length. This suggestion is made based upon the temperature peaks observed downstream of the burner for the original configuration.

The inputs to the sub-model are taken from the results for the fired case of the original design. Average values of velocity and turbulence parameters are used as inputs for the sub-model. The resulting temperature contours along the burner mid section are shown in figure 7-14. It is evident that the high temperature peaks in the middle of the boiler section are reduced in the test configurations. It can be seen that for the same average temperature (i.e. same amount of fuel input), temperature peaks are reduced from 3350^{o}F for original configuration to 2400^{o}F for test configuration 1 and 2100^{o}F for test configuration 2. The temperature contour downstream of the burner for the original configuration indicates that the mixing of the fuel with the gas is not complete and high temperature peaks are concentrated in the middle with low temperature zones located

near the walls. The temperature contours downstream of the burner for the test configuration 1 in figure 7-16 shows better temperature distribution, which indicates better mixing of the exhaust gases with the fuel and the burnt gases. The temperature contours downstream of burner for test configuration 2 show that the temperature is uniform when compared with the other two cases. This can be explained by the use of the velocity contour plots in the direction of flow. Figure 7-18 shows the contours of velocity magnitude along the width of the sub-model. Figure 7-19 shows the contours of axial velocity components along the width of the sub-model. It can be observed from these figures that the magnitude of velocity is small in the original case compared to the test configurations. From figure 7-18 at the location z=0 for the original configuration, the flow of the exhaust gases is directed towards the center of the model and not spreading much. For the test configuration 2 we observe that the flow is diverging, providing enough recirculation and allowing proper mixing of the gas with the burnt gases. This can be seen in the temperature contour shown in figure 7-17. The temperature contour for test configuration 2 also explains the slight high temperature peaks seen at the walls in figure 7-16. This is because of the large recirculation region created in the middle section of the burner, and flow moving towards the outer side and can be seen in figure 7-17 at location z=10ft.

The conclusion from the burner sub-model study is that the existing burner configuration can be replaced by the test configuration 2. The results indicate that the improvement in temperature contour and reduction in temperature peaks downstream of burner are clear. The next step is to see the impact of this change in the burner design in the full HRSG model. Figure 7-20 shows the changes in the burner array configuration

from the original to the revised configuration. The results for the fired case and unfired cases with the revised burner configuration are discussed in the following sections.

7.5 Revised configuration

It is observed that the initial design of the duct burner array is not sufficient for ideal performance. A sub-model study is completed to identify the improved design of the duct burner which gives ideal performance, adding required heat energy evenly without high temperature peaks at the heat exchanger sections downstream of burner. A configuration is identified and this configuration is tested in the full model. In addition to the changes in the baffle openings an additional modification is made. The gaps at the top and bottom baffles are also reduced as shown in figure 7-20. The following section discusses the results for the modified burner design, fired case.

7.5.1 HRSG inlet conditions and inlet duct

Stream traces for the revised configuration, fired case, are shown in figure 7-21. The discussion of flow in the inlet duct for the original burner configuration showed that the initial design of the inlet duct is sufficient to meet the flow requirements into the first heating surfaces. As the changes in the design are done downstream of the heat exchanger module box 1, the effect of these changes on the flow in the inlet duct is minimum, and this is evident from the stream traces plots. The flow conditions at the inlet to the first heat exchanger surface also show no change and satisfy the flow requirements set by VPI. However, flow distribution downstream of the heat exchanger module box 1 needs to be studied for the revised configuration.

7.5.2 Conditions at the duct burner

The burner arrangement is shown in figure 7-20. The gas flow requirements required for good performance of the burner are discussed in section 7-3. The velocity profile 1.5 ft. upstream of the burner is shown in figure 7-27. The average axial velocity at the location 1.5 ft. upstream of the burner is observed to be 19.84 ft/s with 95% of velocity values falling with in +/-25% of the average velocities. The temperature contour also shows small deviations less than 10 ^{o}F from the average value.

The conditions downstream of the burner are studied. Figure 7-28 shows the gas velocity and temperature distribution entering the heat exchanger downstream of the burner. It is observed that the temperature distribution entering this section averages 1556 ^{o}F, which is in agreement with the heat input parameters based upon the fuel addition and the heating value of the fuel, with the peak temperatures in this plane reduced to 1950 ^{o}F compared to the 2400 ^{o}F for the original configuration - a clear improvement. The temperature contour shows better mixing of the exhaust gases with the burnt gases downstream of the duct burner. The low temperature zones are located at the bottom wall of the plane, as the opening at the bottom wall allows large amount of exhaust gas without changing the flow parameters in this region.

7.5.3 Flow at the SCR system

The velocity distribution entering the SCR catalyst and the location of the SCR ammonia injection grid (AIG) are discussed in this section. Results for the revised configuration fired case are shown in this section; results for the unfired case are also analyzed, and the flow conditions at key locations in the model are tabulated in table 7-1.

The gas distribution at the AIG location is shown in figure 7-30, and the gas distribution entering the SCR is shown in figure 7-31. At the AIG location, the velocity profile is found to be uniform, with 92% of the velocity values falling within +/-15% of the average velocity. Predicted gas temperature variations at the AIG plane fall within a range of +/-55 ^{o}F from the average value. In the unfired case (not shown), the temperature distribution ranges from lower values near the floor to the higher values at the top of the unit. This is because of the upward flow of water and steam through both the evaporator and super heater tube modules upstream of the AIG.

Gas distribution at the face of the SCR is shown in figure 7-31. In this plane the variation is observed to be very large because of the effect of the walls. However, in the plane just upstream of the SCR catalyst, the flow conditions required for the flow distribution into the catalyst are satisfied. Table 7-1 indicates similar trends of flow in both the cases, fired and unfired, indicating that the velocity requirements for the SCR catalyst are satisfied.

7.5.4 Flow distribution through the downstream heat exchangers

The flow distribution into the first heat exchanger surface (Box 1), burner section, and the heat exchanger tube module (Box 2) downstream of the burner are discussed in the previous sections. The flow distribution downstream of the SCR catalyst is also important; studying this flow pattern helps us to understand the effect of blockages provided to support the catalyst blocks in the flow area. The gas velocity distribution entering the heat exchanger modules box 3, 4, and 5 is shown in figure 7-32, figure 7-33 and figure 7-34. These figures show that the velocity is relatively low and uniform

through out the heat exchanger modules down stream of the SCR catalyst ranging from 8ft/s to 14ft/s with low velocities near the walls. The temperature distribution at this location is also observed to be as expected because of the water/steam flow directions.

The comparison of the predicted gas-side pressure drop in each of the heat exchangers and the average gas temperature entering each of the heat exchanger sections to the CARDS predictions is shown in figure 7-36 for the revised configuration, fired case and in figure 7-37 for the revised configuration, unfired case. It is observed that the results from the flow modeling using Fluent are in agreement with the CARDS predictions.

Velocity evaluations	***Fired case***	***Modified fired case***	***Modified unfired case***
Avg. gas velocity entering HPSH1 (ft/s)	20.62	20.5	20.5
%HPSH1 area within 20% V_{avg}	90.8%	90.8%	90.8%
Max. axial velocity at HPSH1 (% of V_{avg})	24.8(121%)	24.8(121%)	24.8(121%)
Avg. gas velocity before burner (ft/s)	19.8	19.8	19.4
% area before burner within 25% V_{avg}	94.05	96.7	96.7
Avg. gas velocity entering HPSH3 (ft/s)	24.0	24.0	19.2
% HPSH3 area within 20% V_{avg}	73.3	73.3	73.3
Avg. gas velocity at AIG (ft/s)	13.57	13.6	12.2
%AIG area within 15% V_{avg}	91.5%	91.5%	92%
Avg. gas velocity before SCR (ft/s)	12.4	12.4	11.1
%SCR area within 15% V_{avg}	81.5%	81.5%	88.3%
Avg. gas velocity entering SCR (ft/s)	14.1	14.1	12.6
%SCR area within 15% V_{avg}	56%	56%	55.7%
Avg. gas velocity entering IPSH1 (ft/s)	13.7	13.7	12.3
Avg. gas velocity entering HPEC3 (ft/s)	11.4	11.4	10.6
Avg. gas velocity entering LPEV3 (ft/s)	9.6	9.6	9.1

Table 7-1: Summary of Velocity evaluations at key locations, Current Creek model

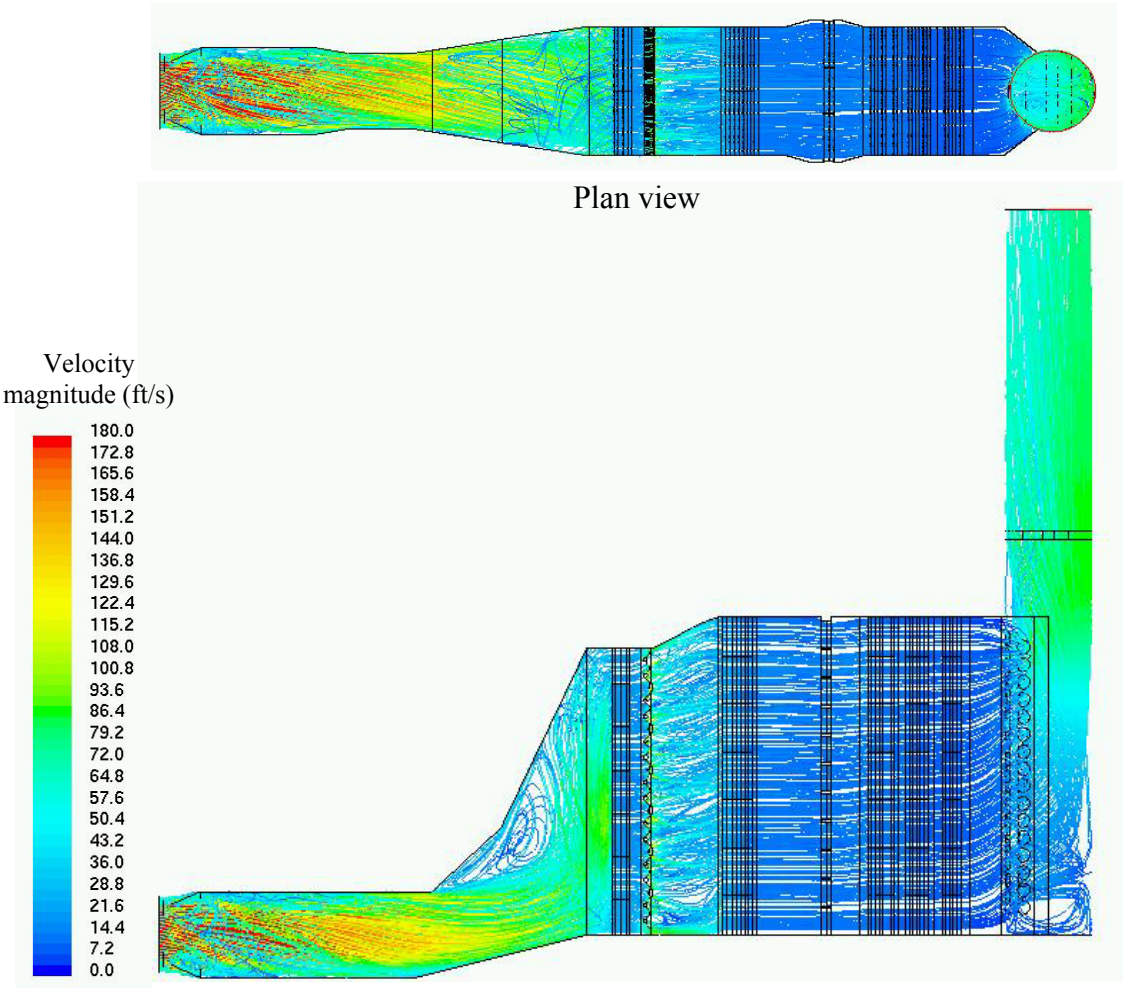

Figure 7-1: Stream traces colored by velocity magnitude, fired case

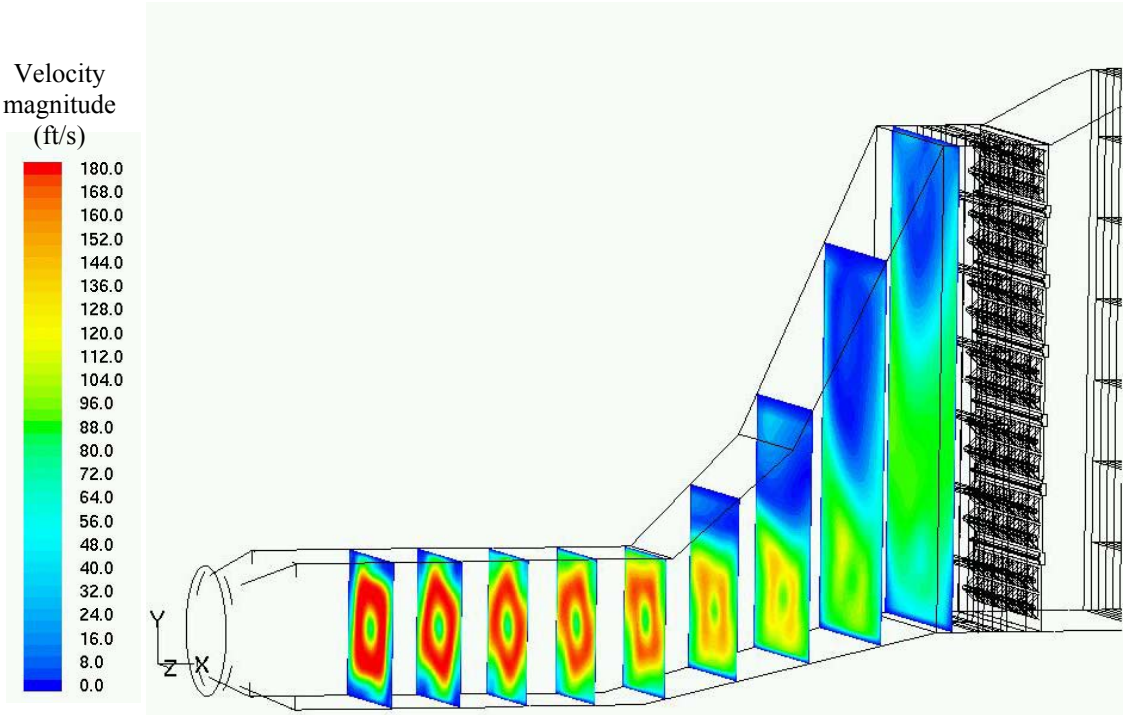

a) Contours of gas velocity magnitude (ft/s)

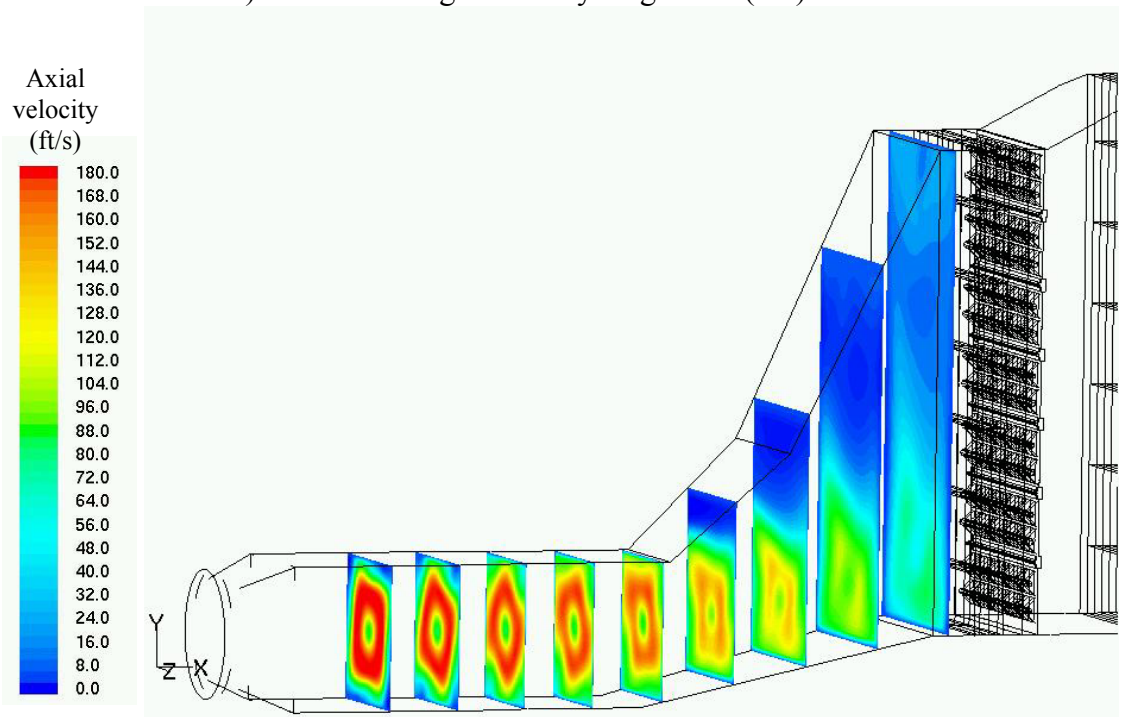

b) Contours of gas axial velocity (ft/s)

Figure 7-2: Contours of gas velocity magnitude (ft/s) and axial velocity of gas in the inlet duct and bypass duct, fired case

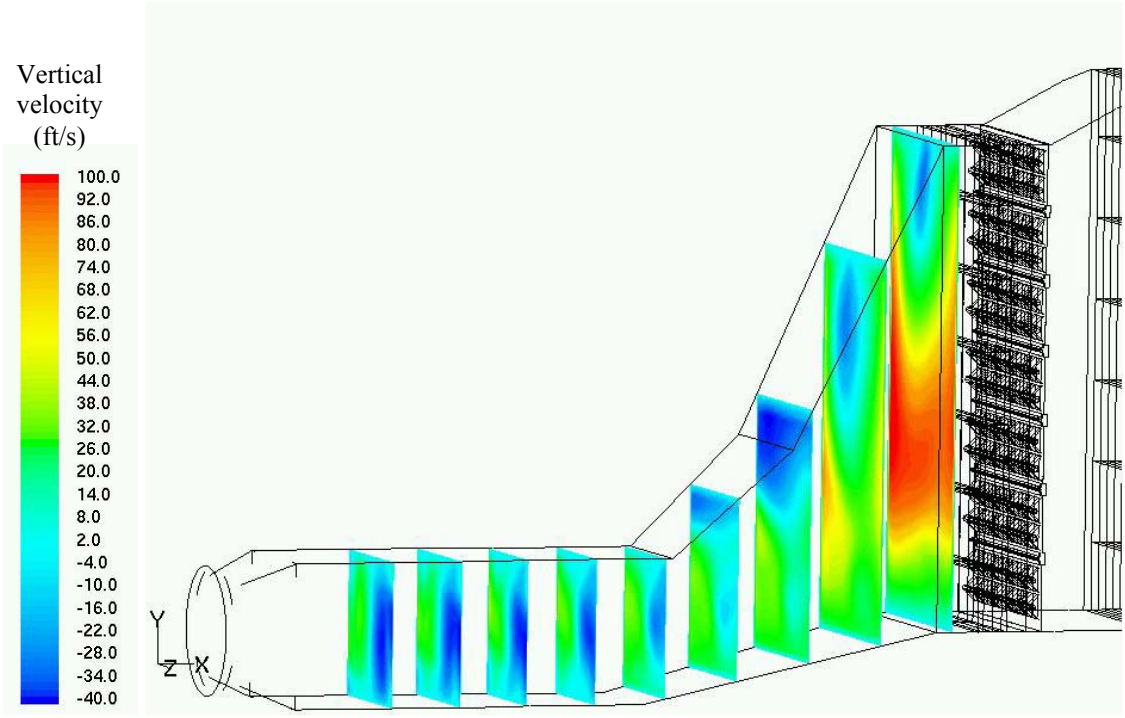

a) Contours of gas vertical velocity (ft/s)

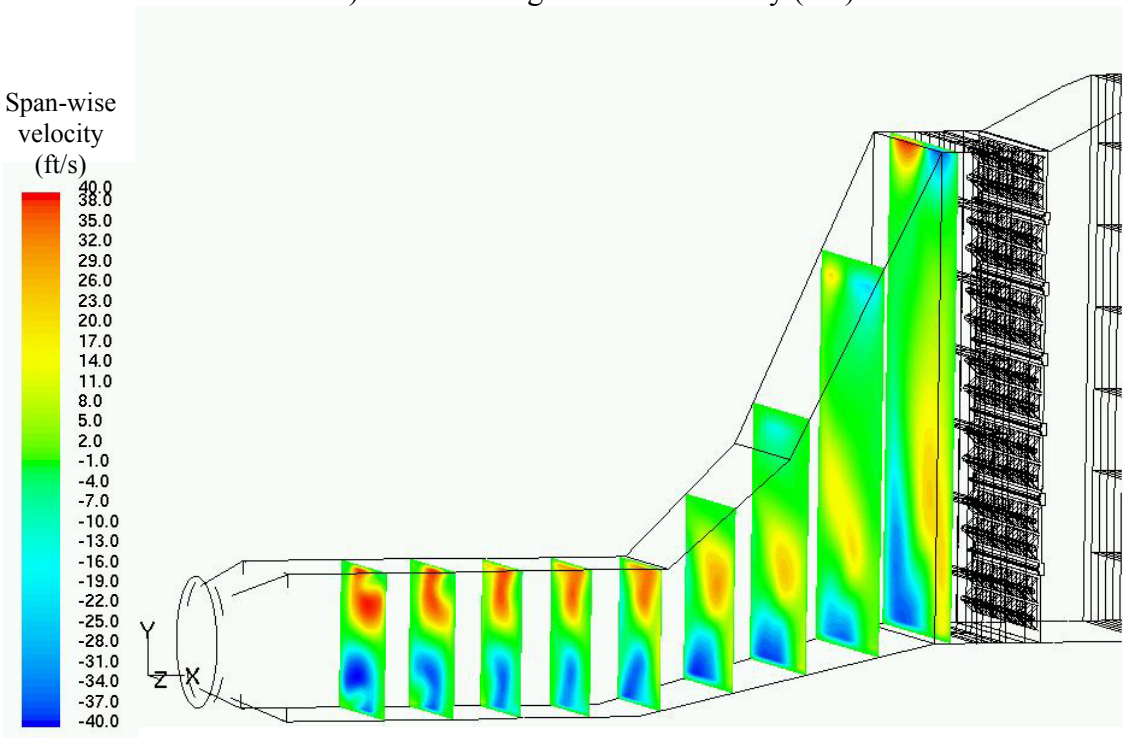

b) Contours of gas span wise velocity (ft/s)

Figure 7-3: Contours of gas vertical velocity (ft/s) and span wise velocity in the inlet duct and bypass duct, fired case

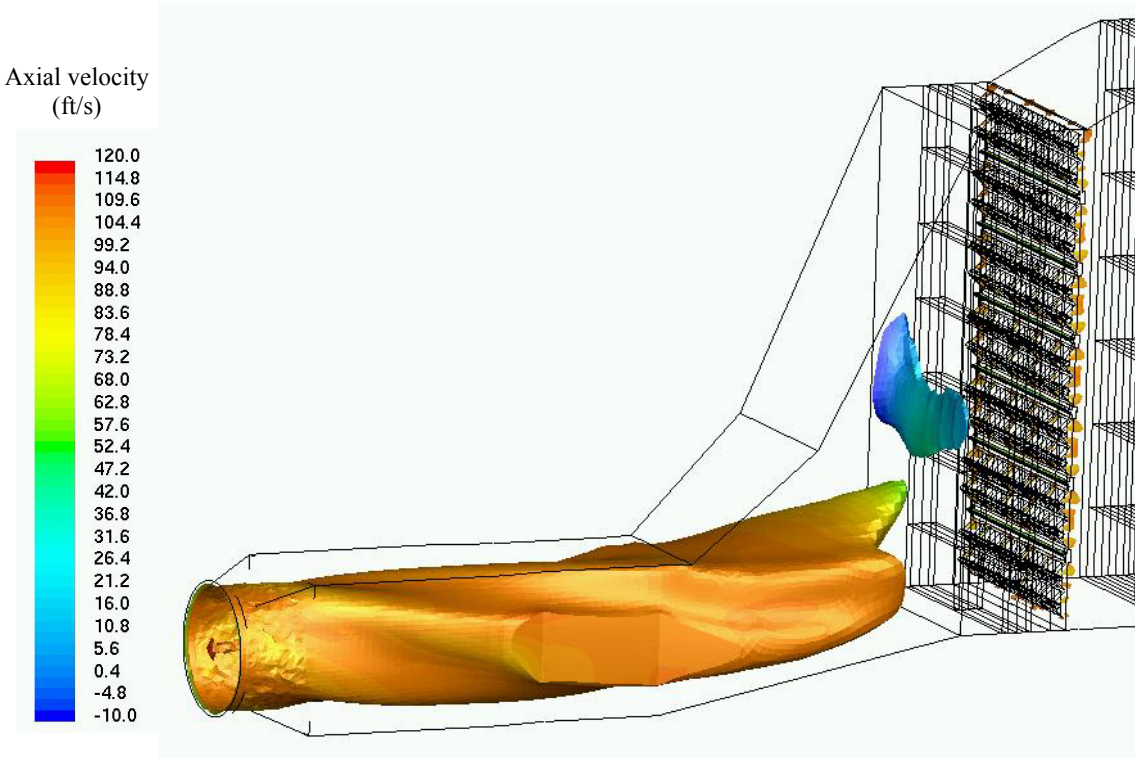

a) 100 ft/s iso-surface of velocity magnitude

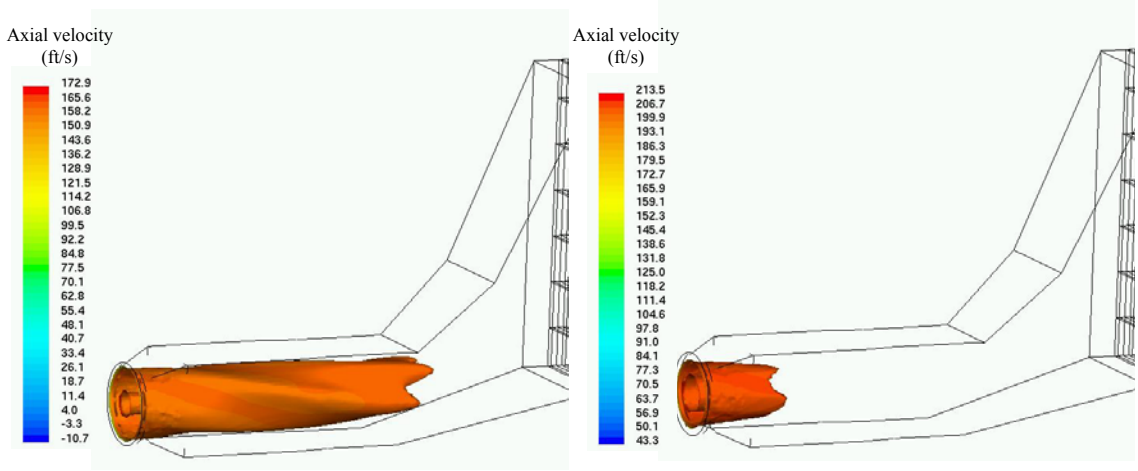

b) 150 ft/s iso-surface of velocity magnitude c) 200 ft/s iso-surface of velocity magnitude

Figure 7-4: Constant value surfaces of gas velocity magnitude at 100 ft/s, 150 ft/s and 200 ft/s shaded by axial component of gas velocity, fired case

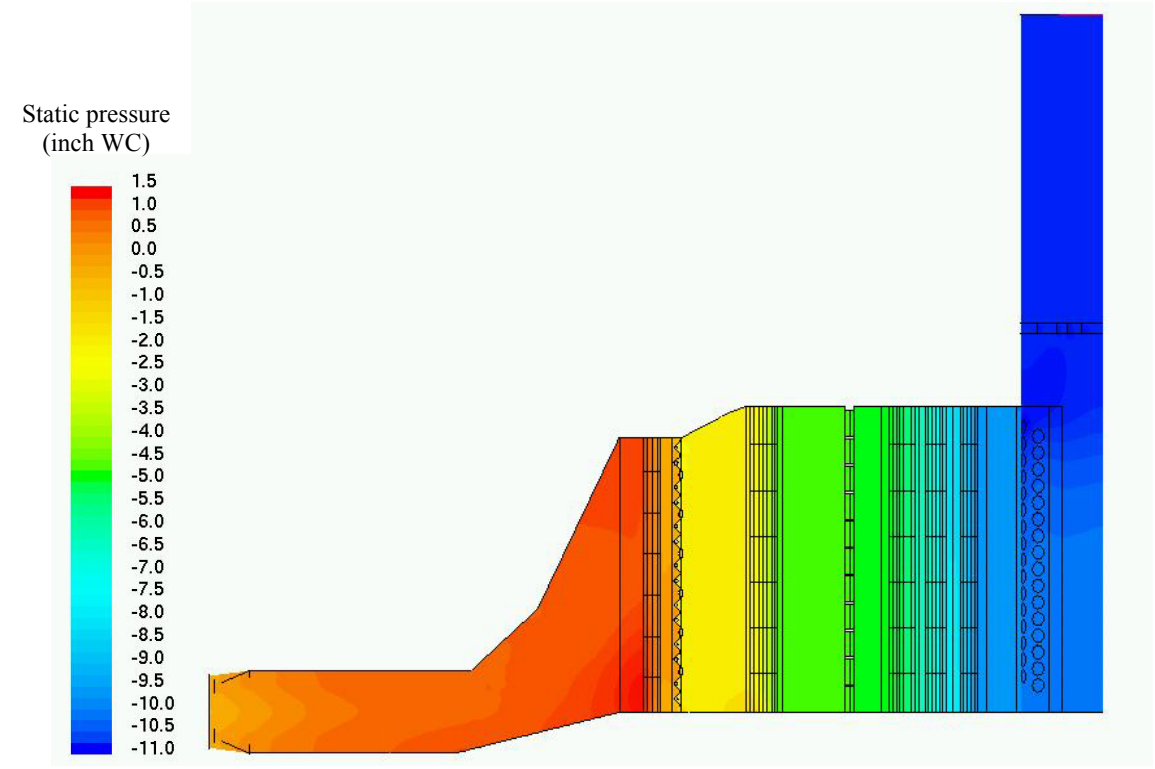

a) Boiler z-mid plane

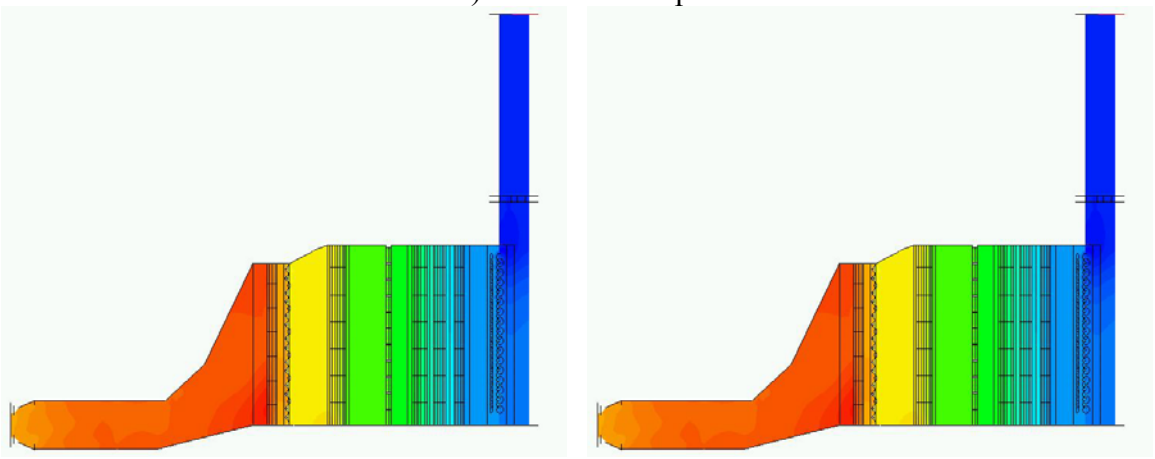

b) left -40 inches offset, right +40 inches offset

Figure 7-5: Contours of static pressure (inch WC) on HRSG mid-plane and on planes +/- 40 inches offset from mid plane, fired case

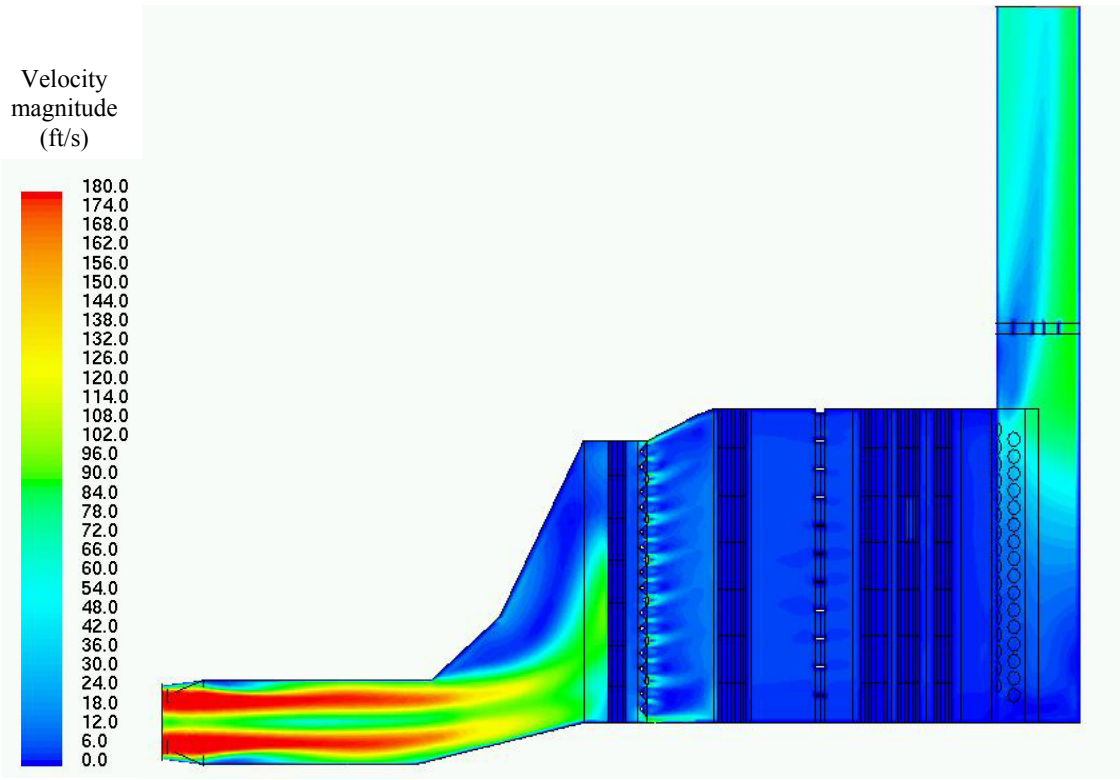

Figure 7-6: Contours of gas velocity magnitude (ft/s) on HRSG mid-plane, fired case

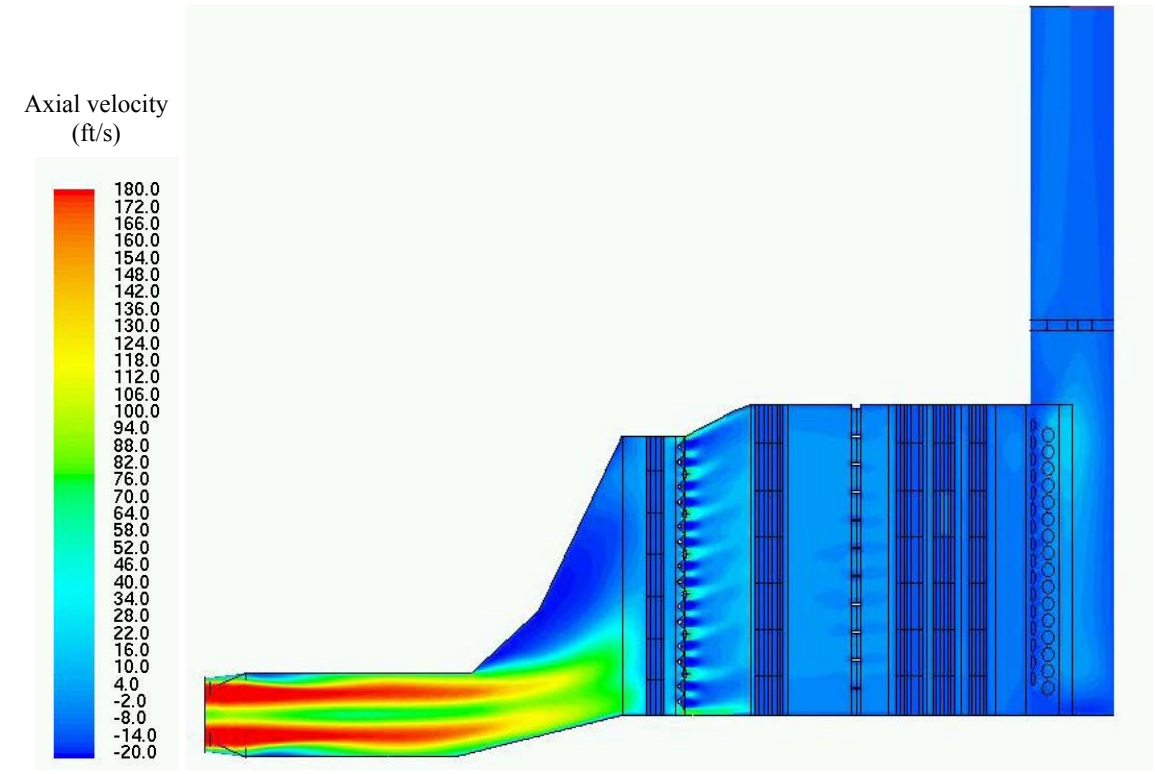

b) Boiler z-mid plane

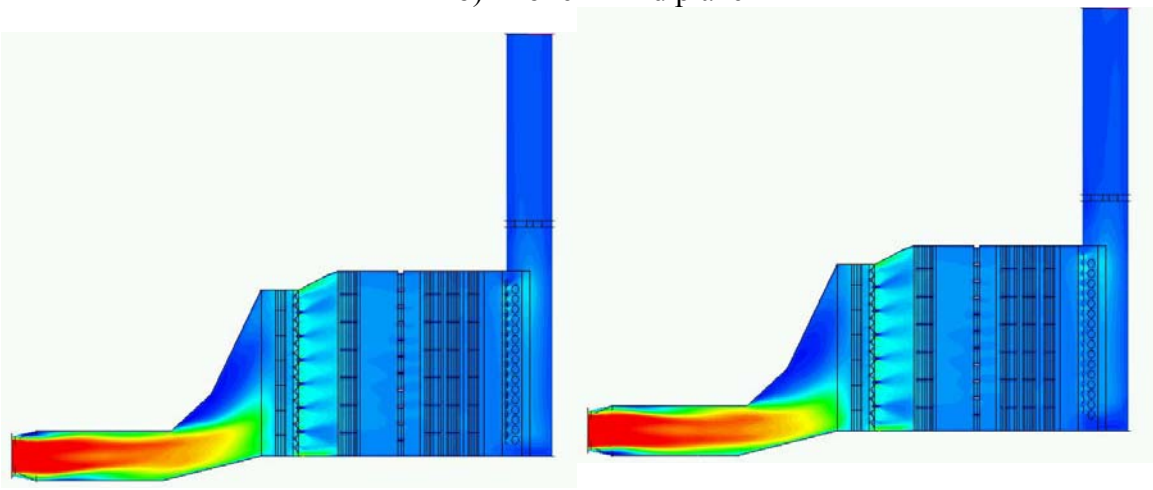

b) left -40 in. offset, right +40 in. offset

Figure 7-7: Contours of gas axial velocity (ft/s) on HRSG mid-pane and on planes +/-40 inches offset from mid-plane, fired case

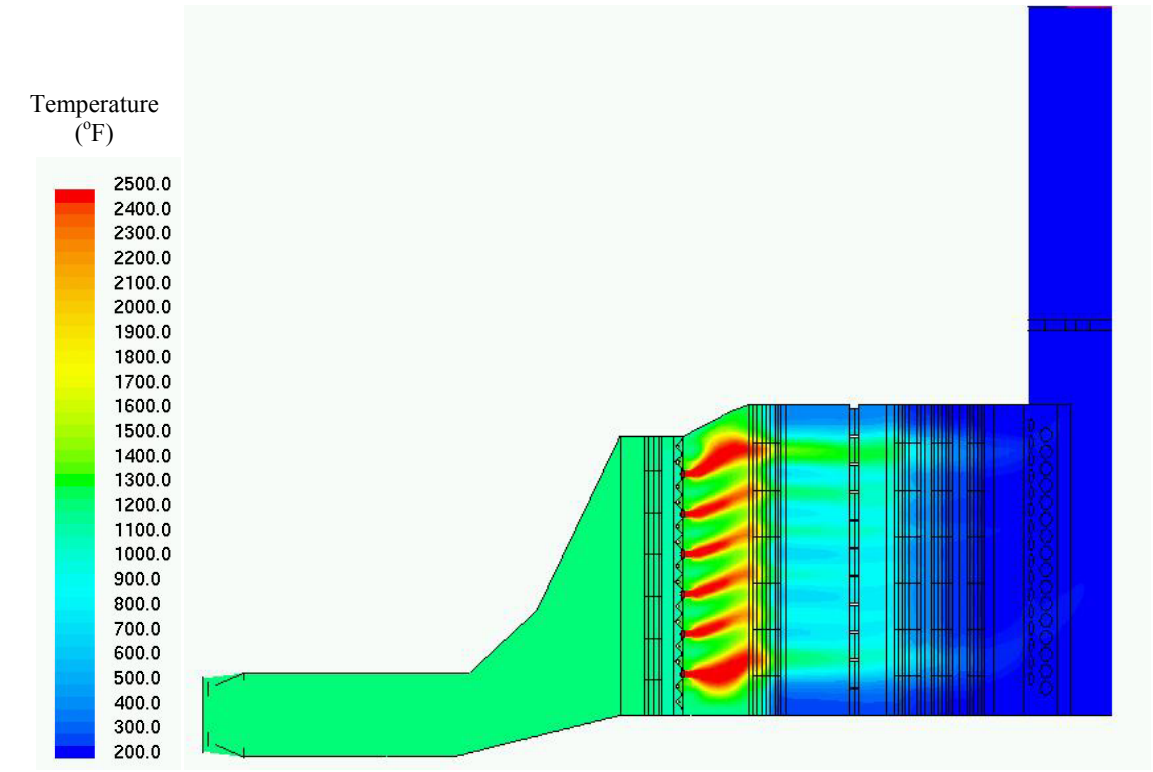

a) Boiler z-mid plane

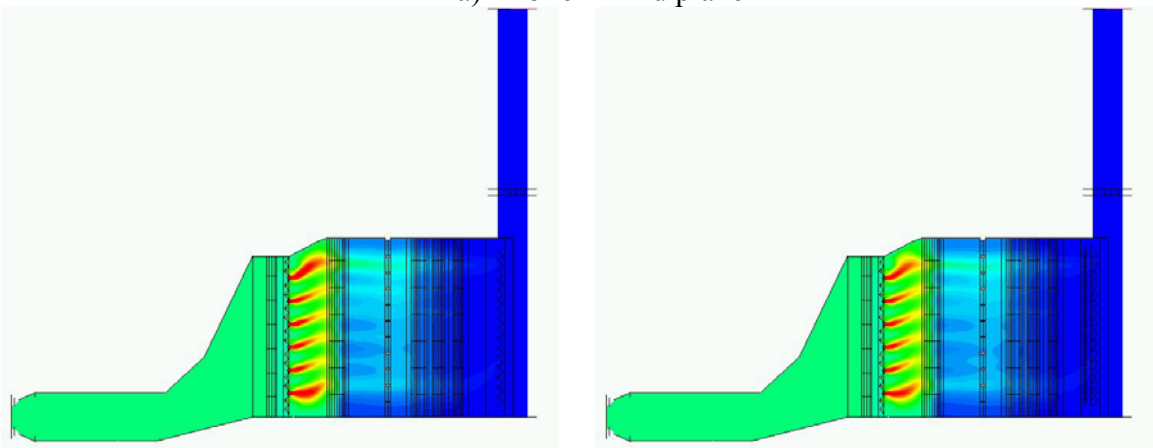

b) left -40 inches offset, right +40 inches offset

Figure 7-8: Contours of gas temperature (°F) along the boiler mid-plane and on planes at locations z= +/- 40 inches, fired case

Average axial velocity = 20.62 ft/s

Average gas temperature = 1113 ^{o}F

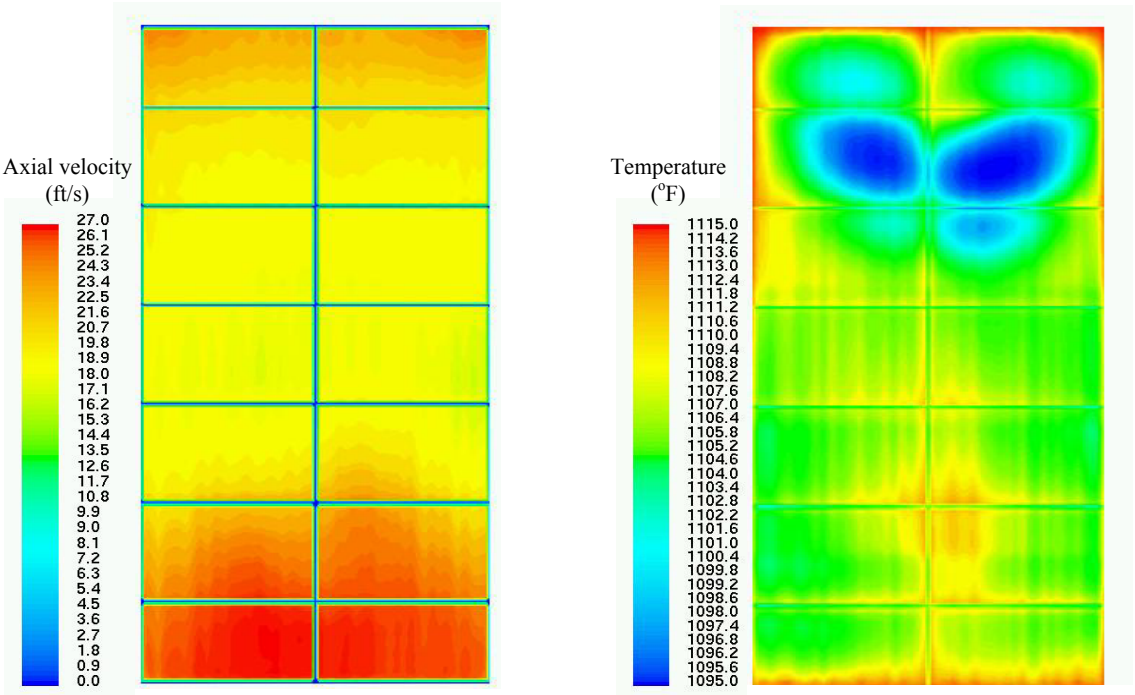

Figure 7-9: Contours of gas axial velocity component (ft/s) and gas temperature (^{o}F) entering HPSH1 (Box 1), fired case

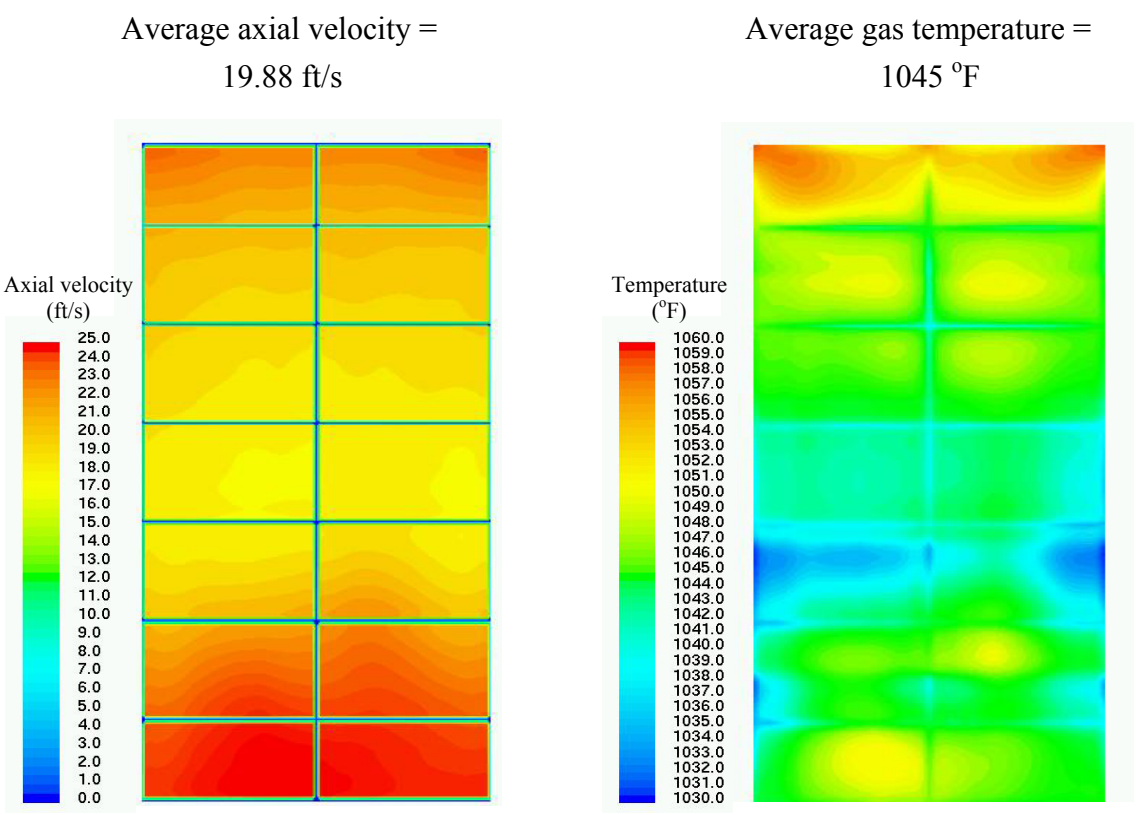

Figure 7-10: Contours of gas axial velocity component (ft/s) and gas temperature (°F) leaving HPSH2 (Box 1), fired case

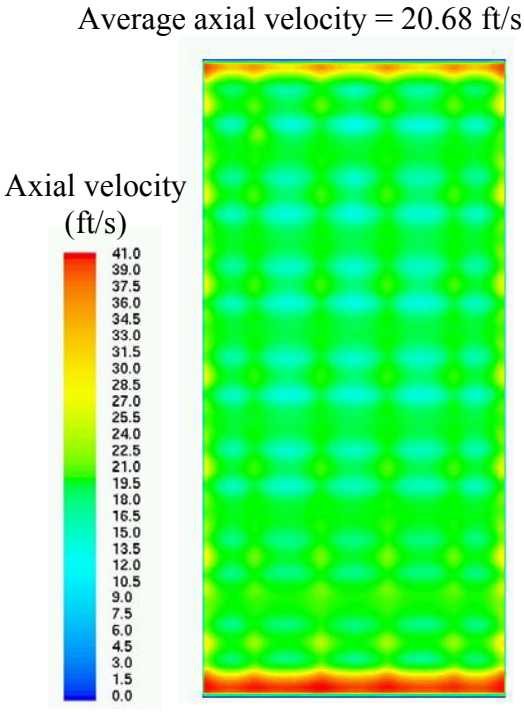

Figure 7-11: Contours of gas axial velocity component (ft/s) upstream of burner, fired case

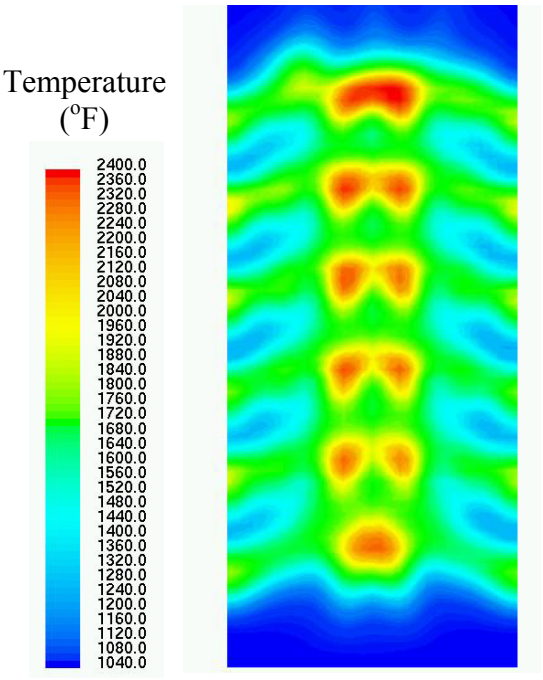

Figure 7-12: Contours of gas temperature (°F) entering heat exchanger downstream of burner, fired case

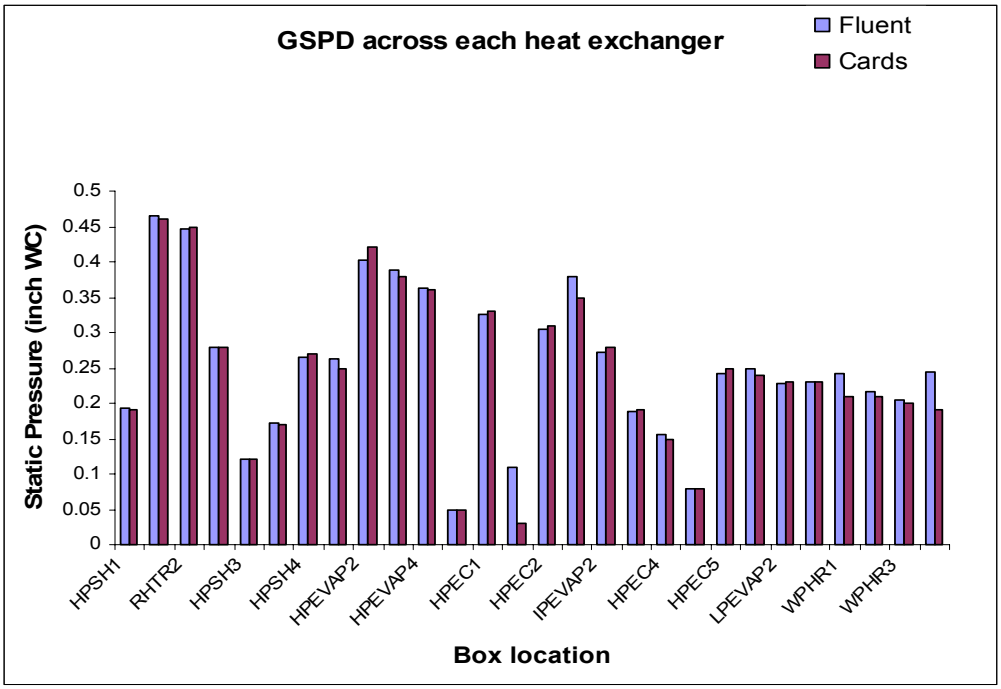

a) Comparison of module GSPD (Fluent Vs CARDS)

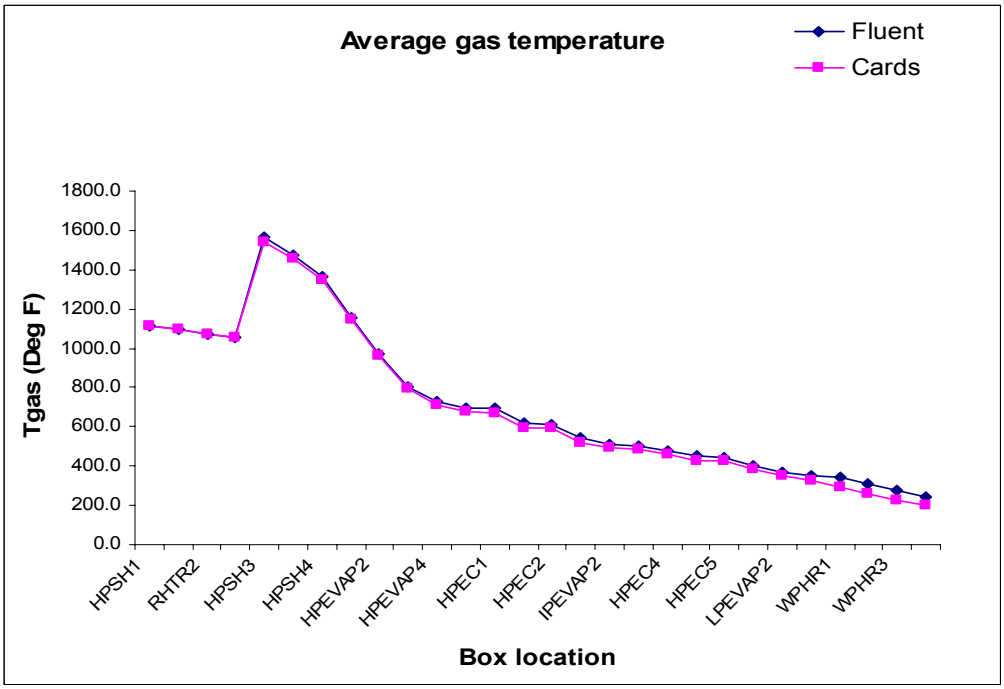

a) Comparison of average gas temperature (Fluent Vs CARDS)

Figure 7-13: Pressure drop and average gas temperature comparison charts, fired case

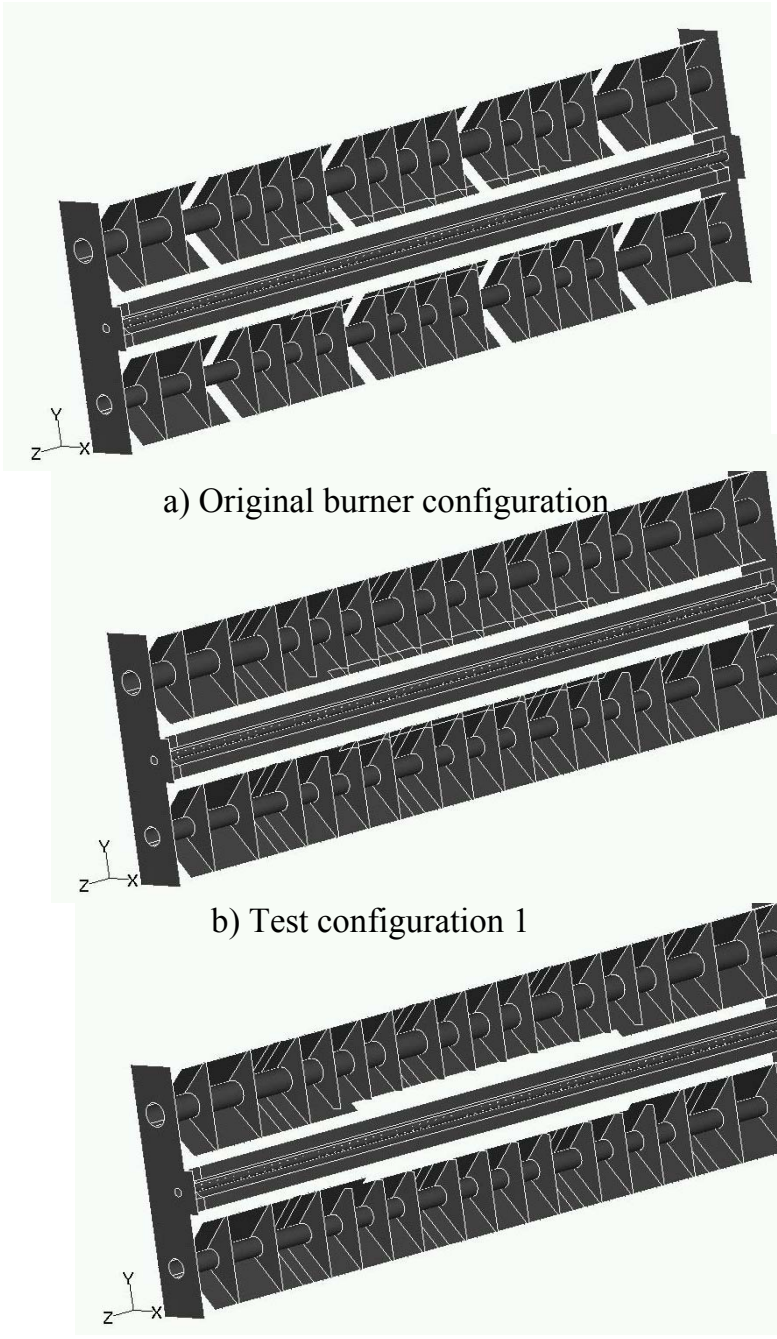

a) Original burner configuration

b) Test configuration 1

c) Test configuration 2

Figure 7-14: Burner configurations for sub-model study

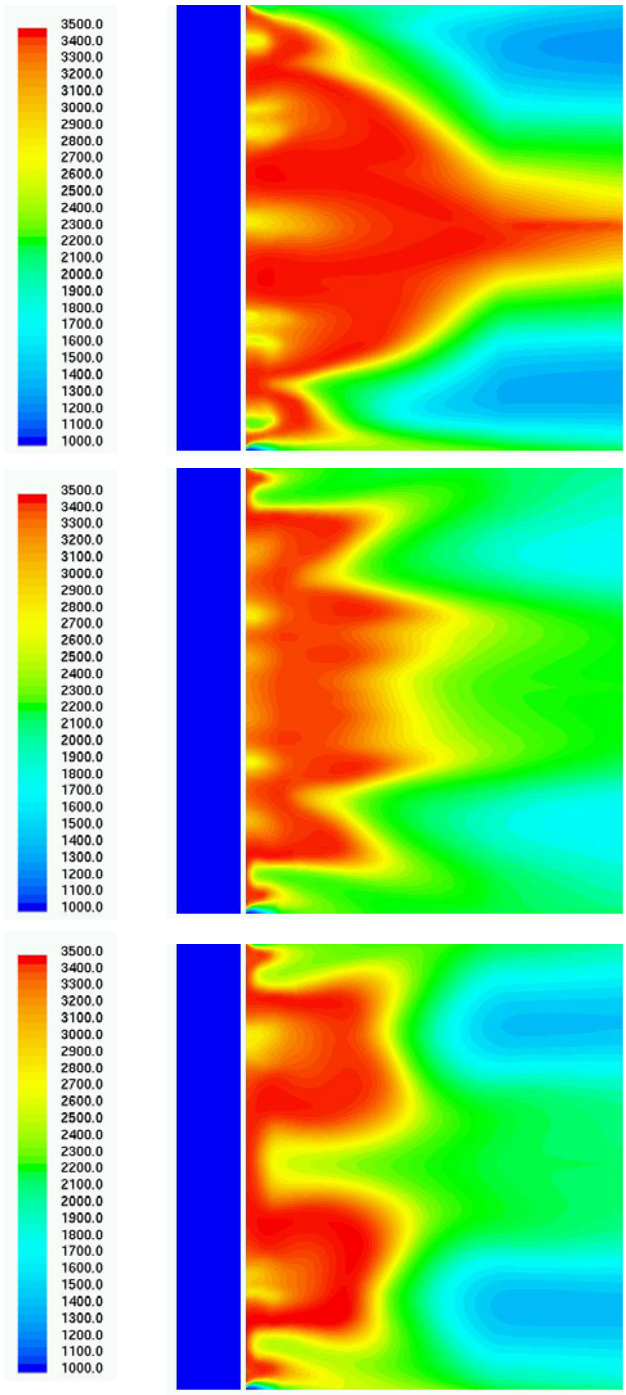

a) Original burner configuration

b) Test configuration 1

c) Test configuration 2

Figure 7-15: Temperature contour (^{o}F) comparison between different burner configurations, sub-model study

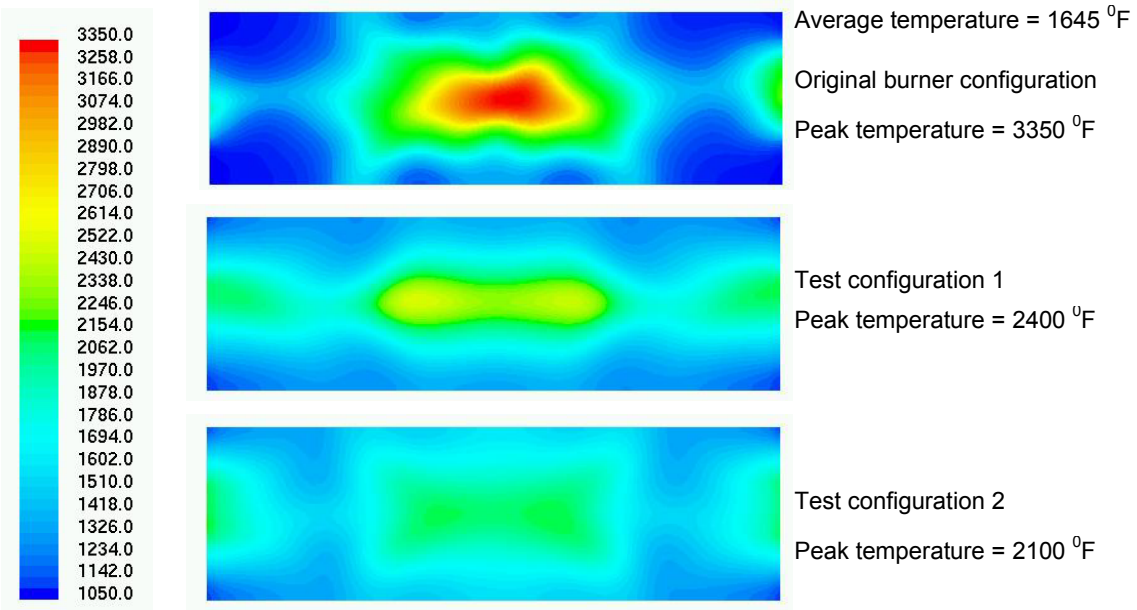

Figure 7-16: Temperature contour (^{o}F) comparison downstream of burner, sub-model study

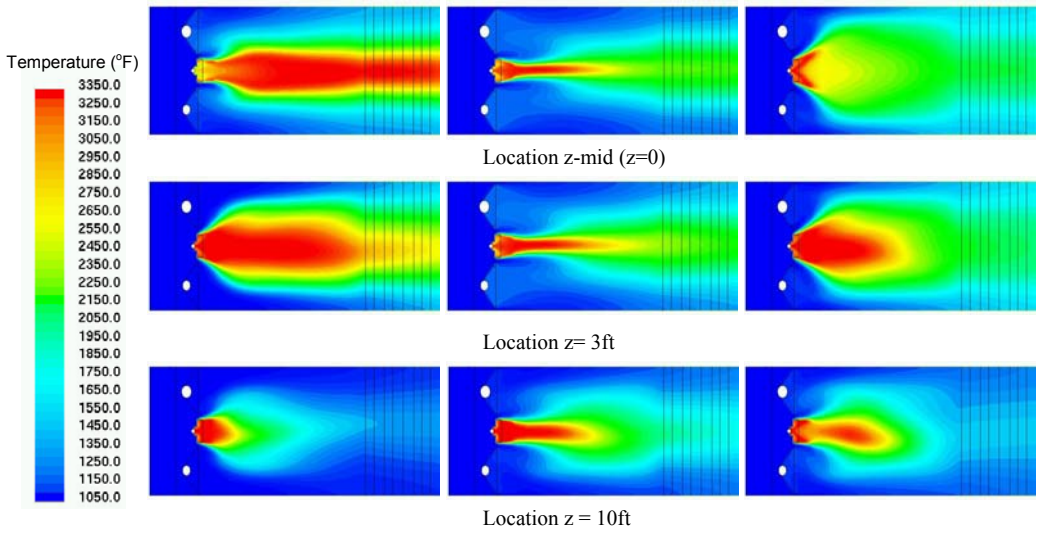

Original configuration Test configuration 1 Test configuration 2

Figure 7-17: Temperature contours (^{o}F) at different sections in sub-model

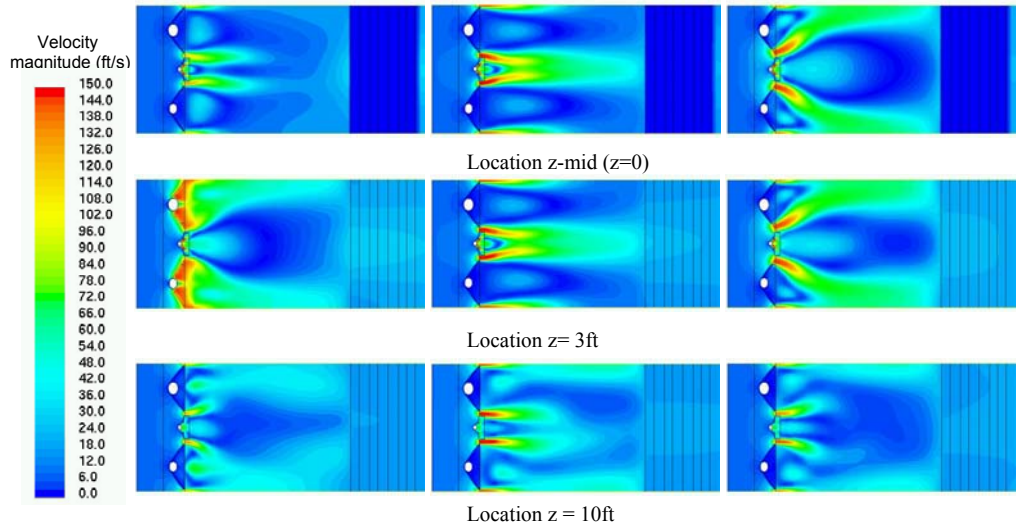

Figure 7-18: Velocity magnitude contours at different sections in sub-model

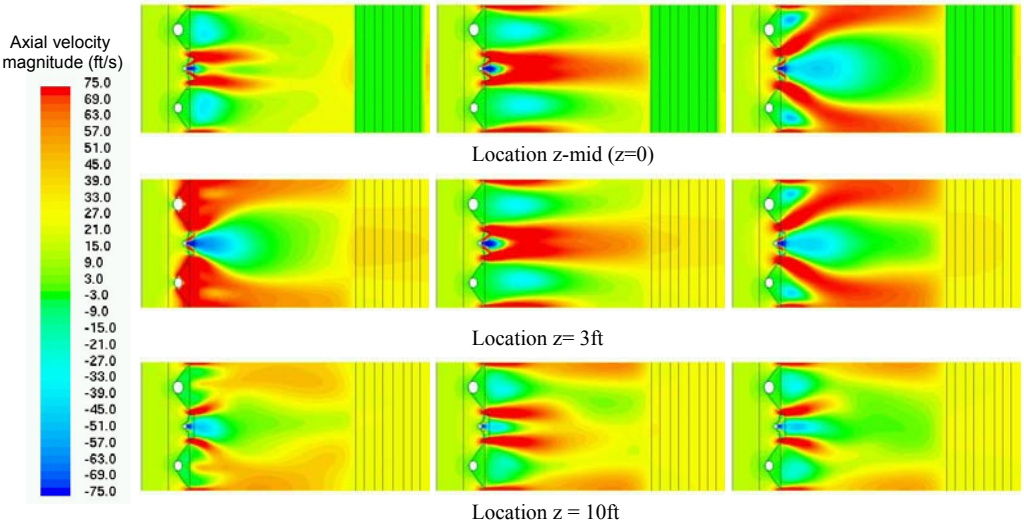

Figure 7-19: Axial velocity magnitude contours at different sections in sub-model

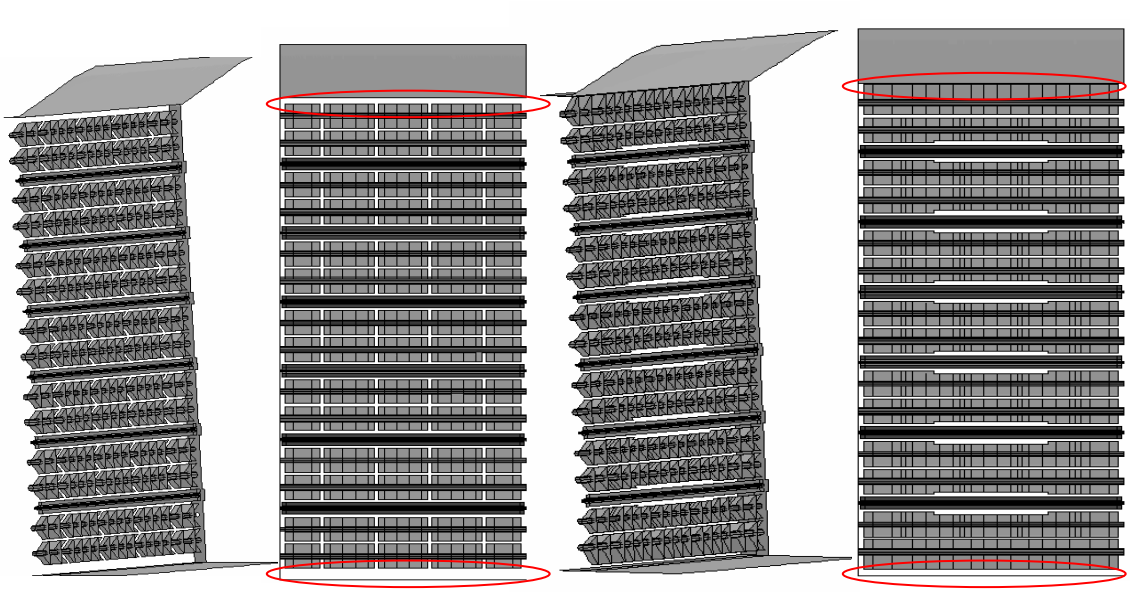

a) Original burner array configuration b) Revised burner array configuration

Figure 7-20: Revised burner configuration for Current Creek model

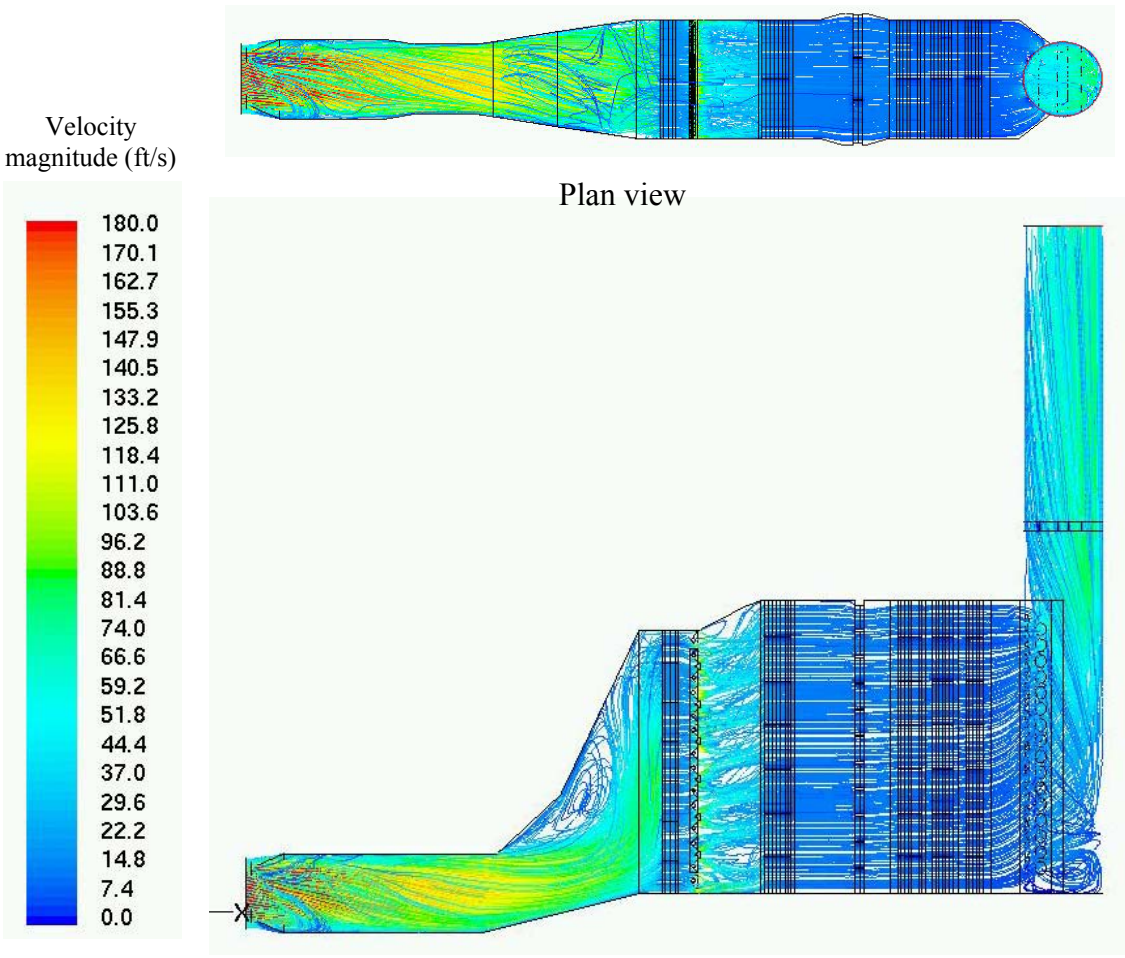

Figure 7-21: Stream traces colored by velocity magnitude, modified burner geometry, fired case

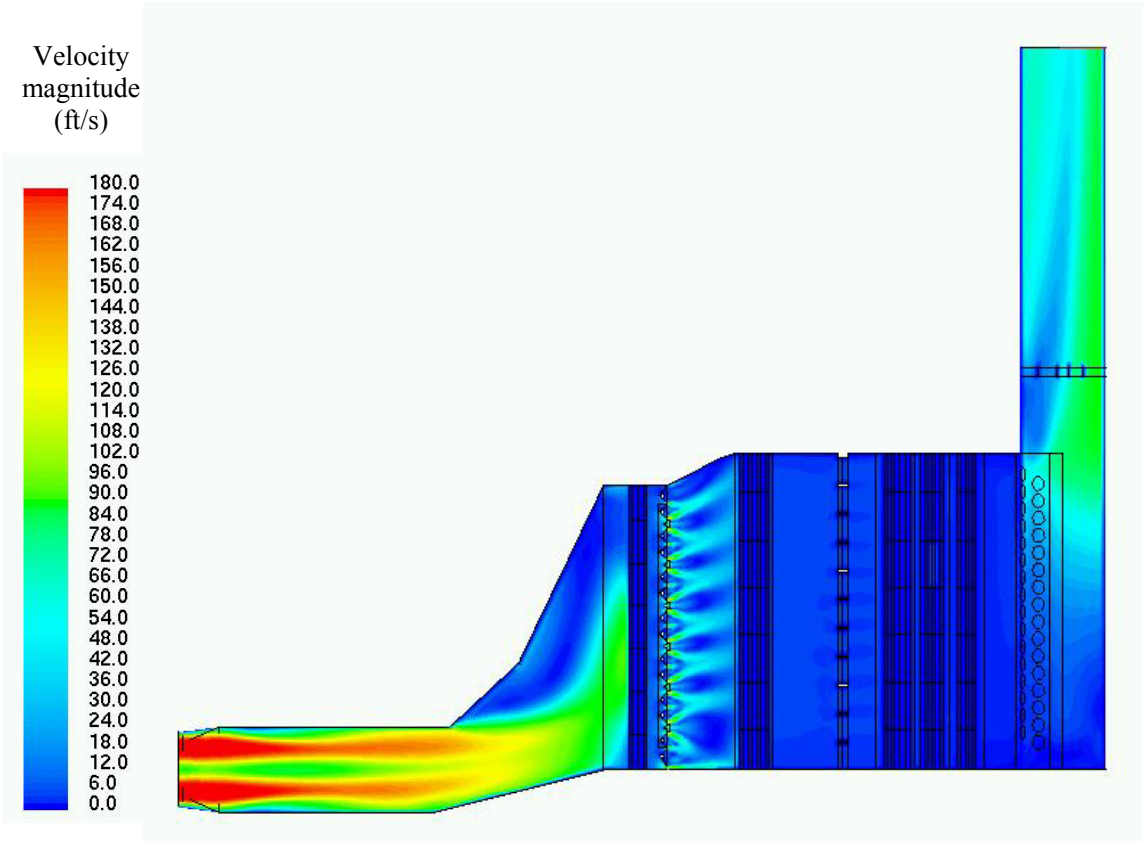

Figure 7-22: Contours of gas velocity magnitude (ft/s) on HRSG mid-plane, modified burner geometry, fired case

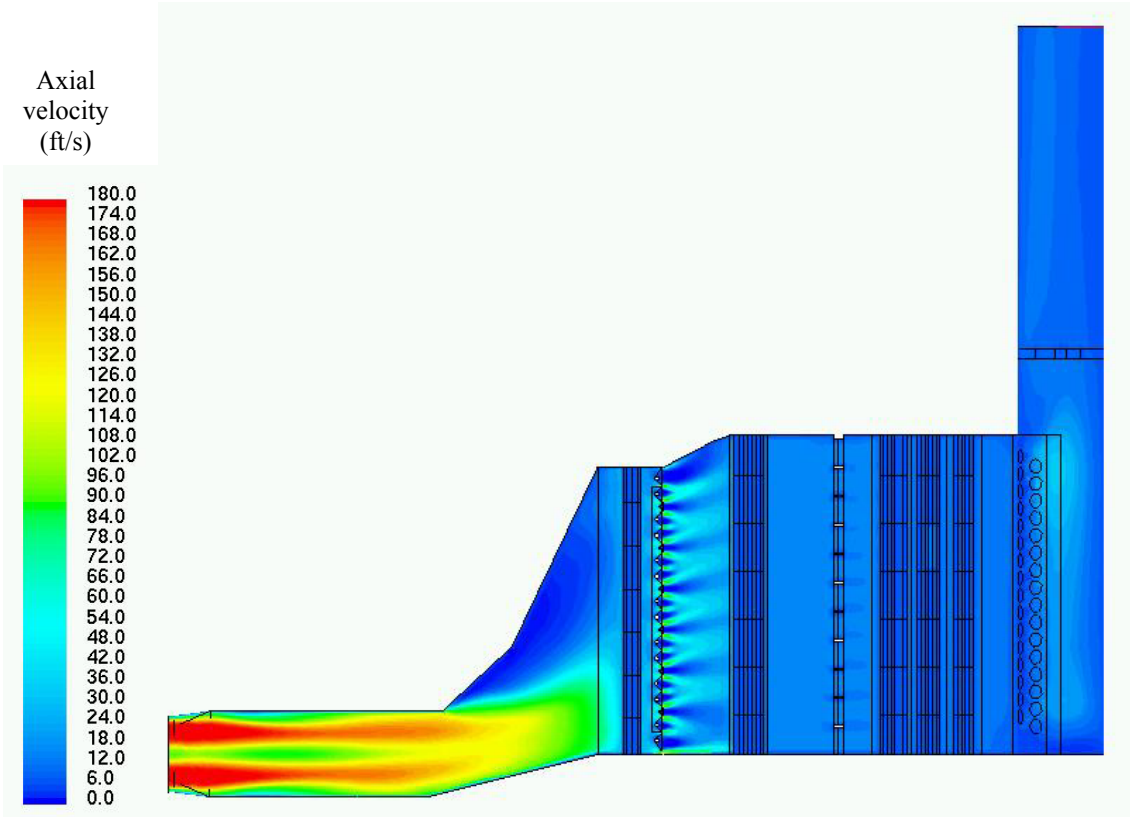

a) Boiler z-mid plane

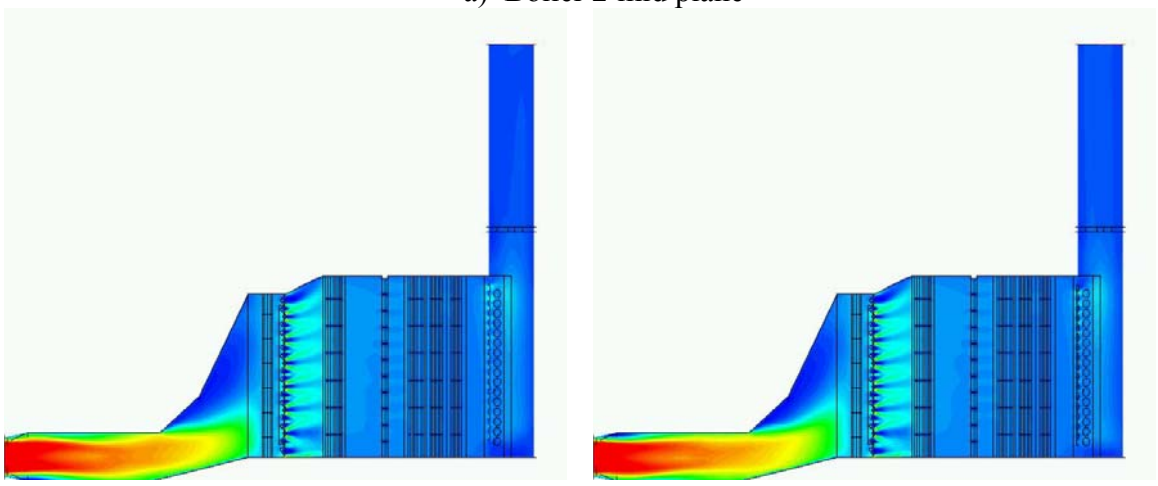

b) left -40 inches offset, right +40 inches offset

Figure 7-23: Contours of gas axial velocity (ft/s) on boiler mid-plane and on plane z = +/-40 inches offset from mid, modified burner geometry, fired case

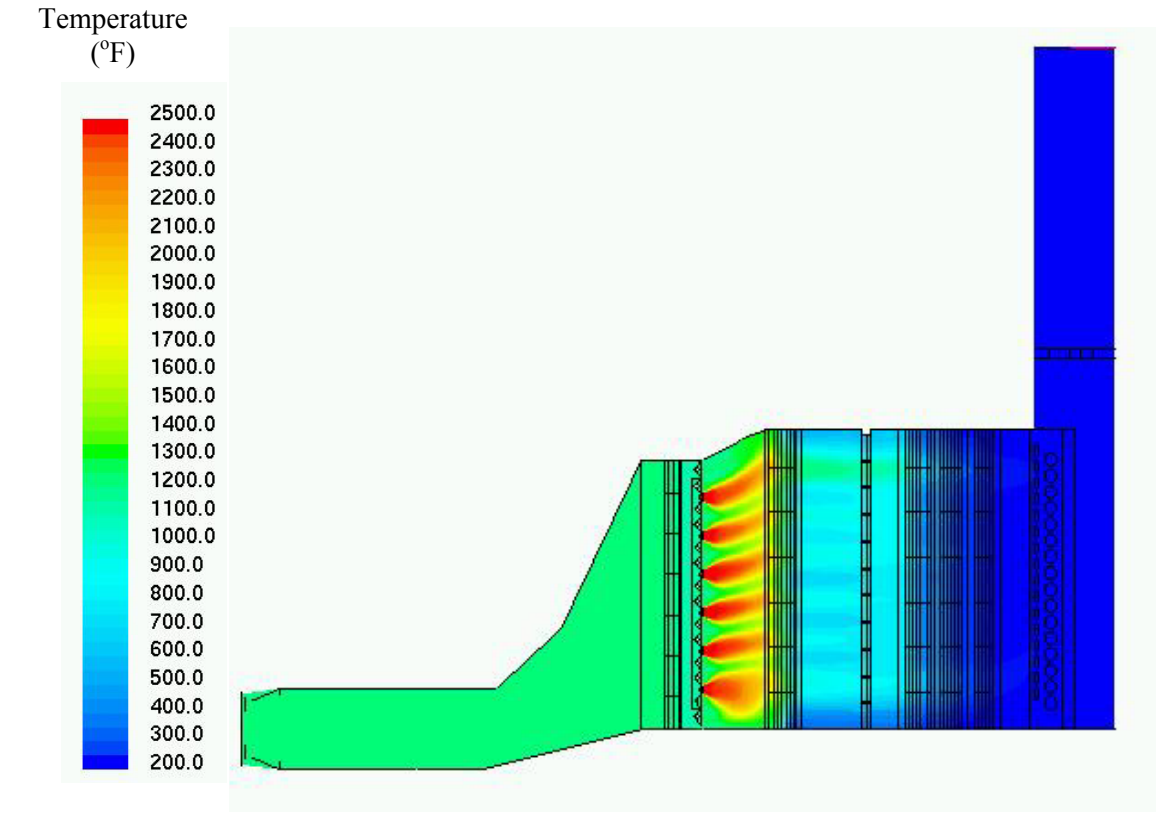

a) Boiler z-mid plane

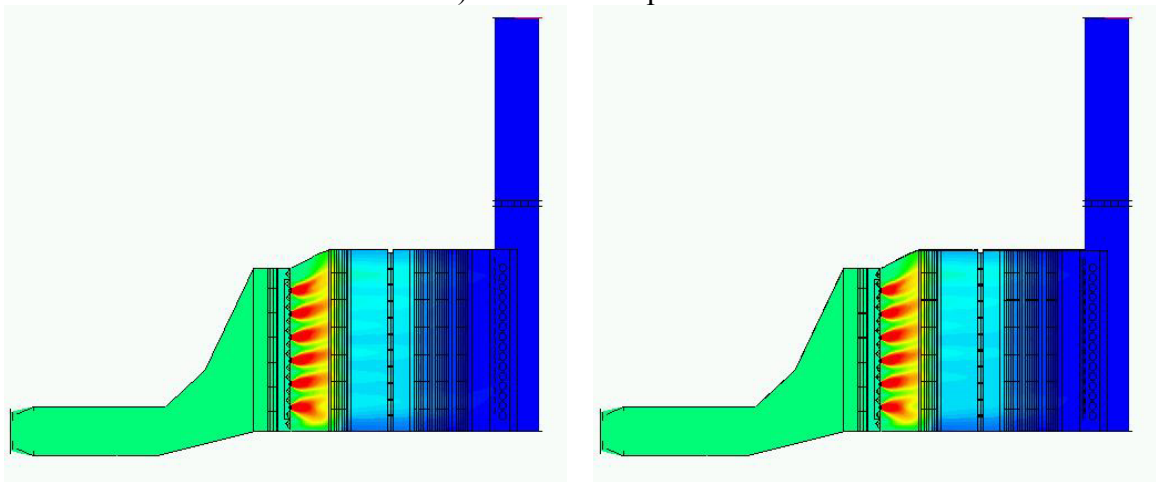

b) left -40 inches offset, right +40 inches offset

Figure 7-24: Contours of gas temperature (°F) on boiler mid-plane and on plane z= +/- 40 inches offset from mid, modified burner geometry, fired case

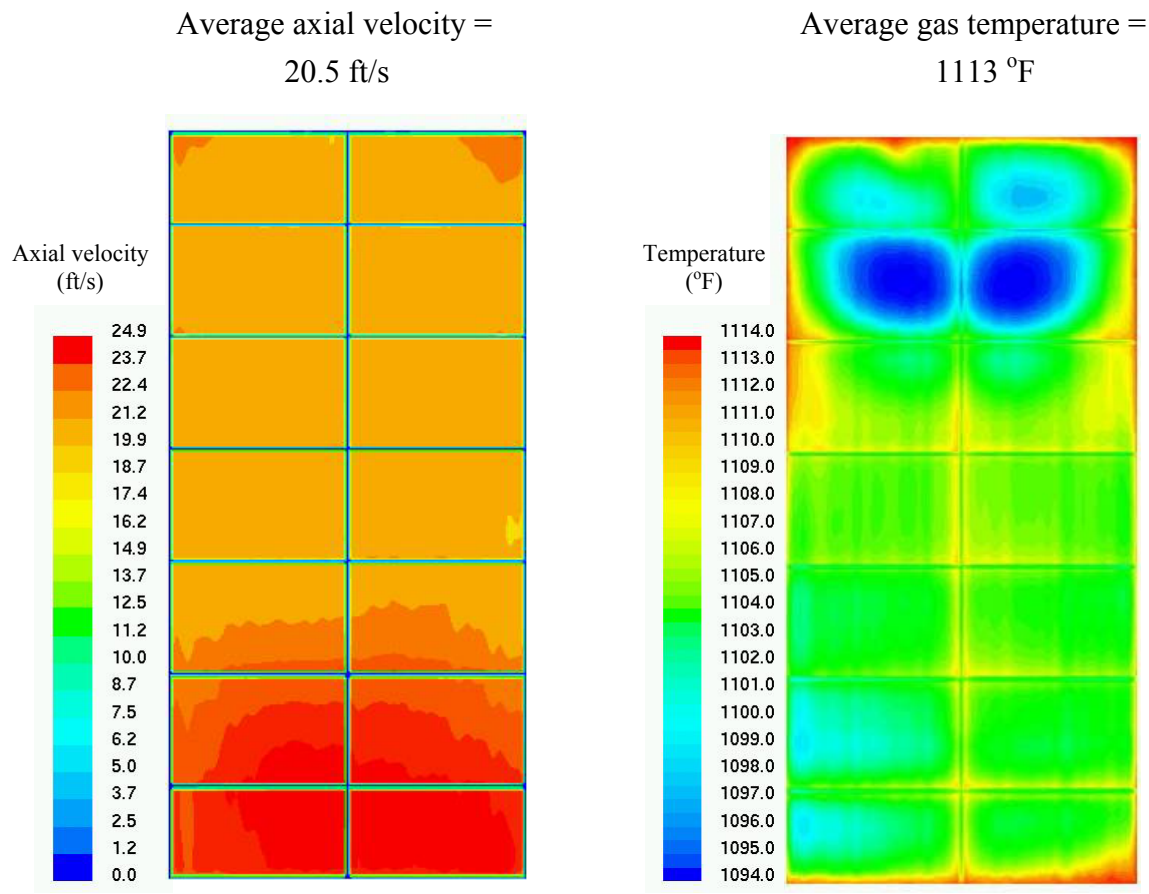

Figure 7-25: Contours of gas axial velocity component (ft/s) and gas temperature (°F) entering HPSH1 (Box 1), modified burner geometry, fired case

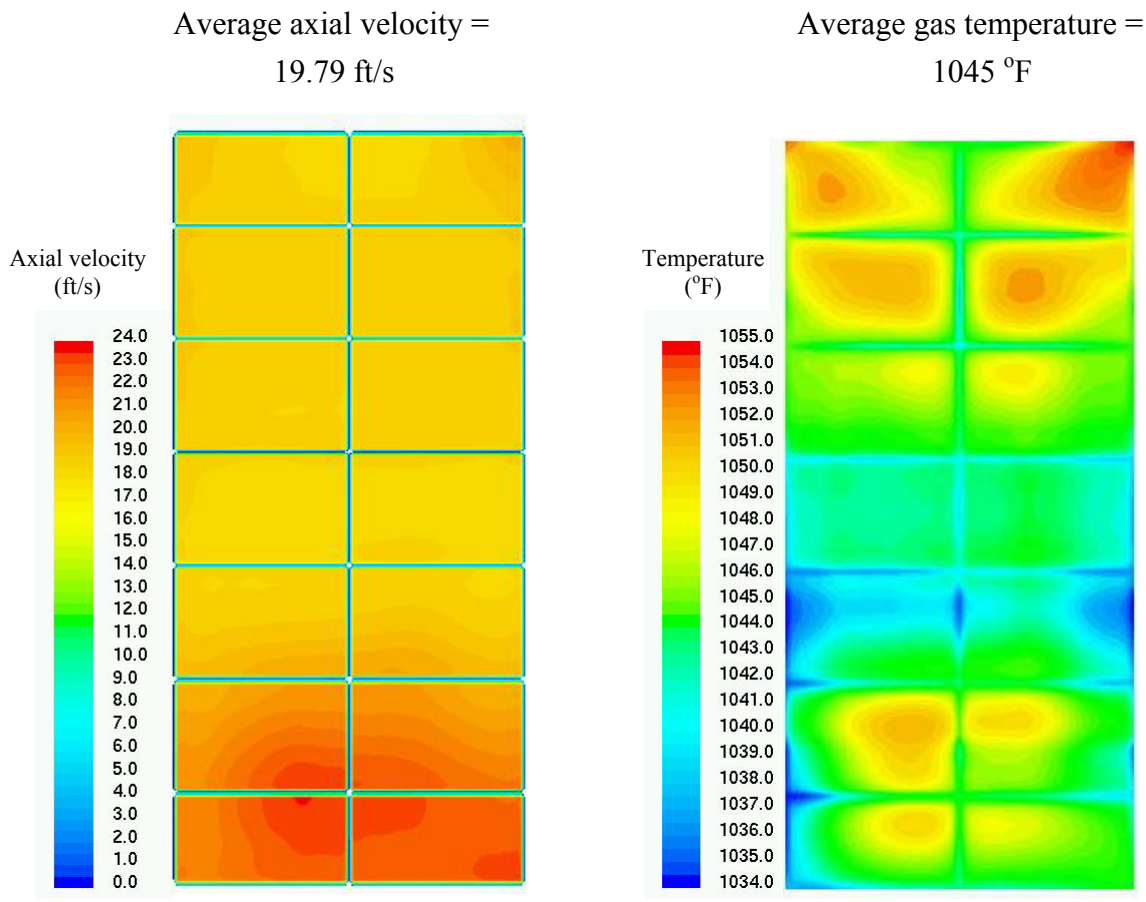

Figure 7-26: Contours of gas axial velocity component (ft/s) and gas temperature (°F) exiting HPSH2 (Box 1), modified burner geometry, fired case

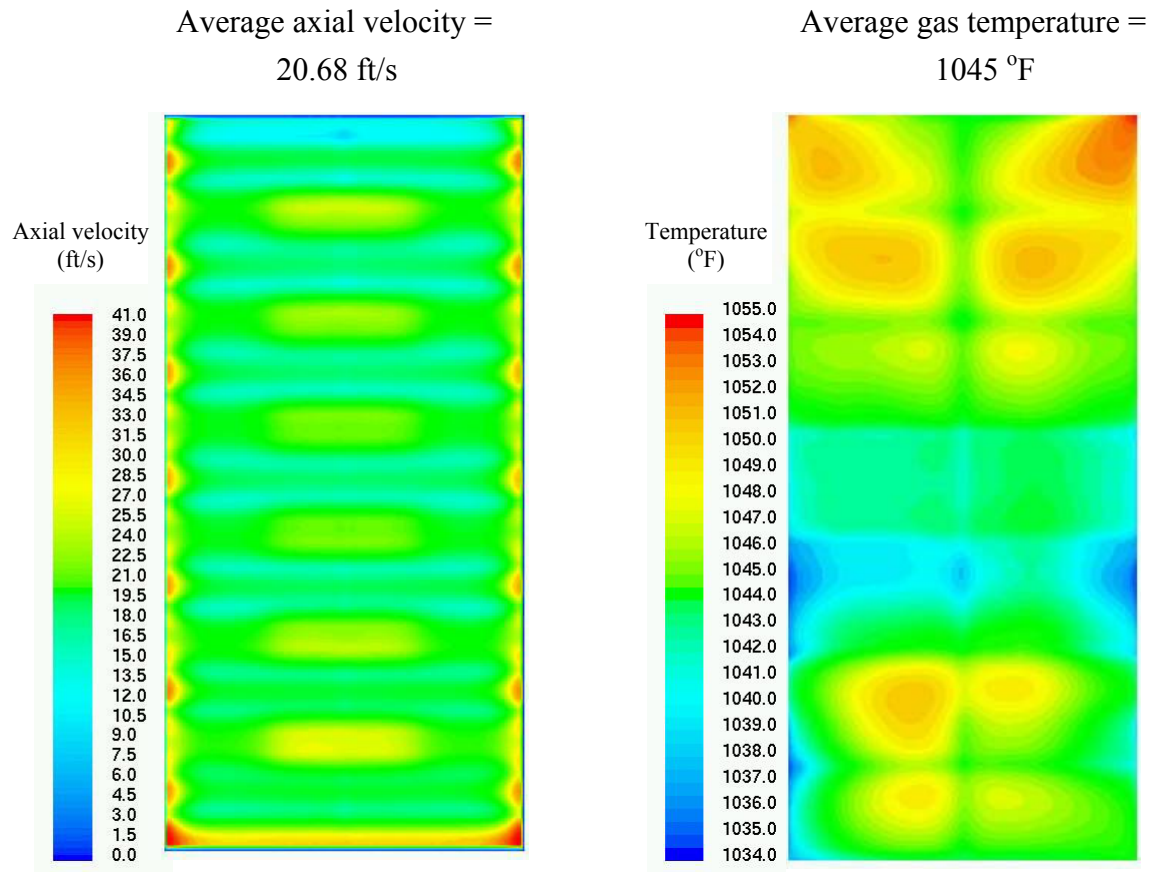

Figure 7-27: Contours of gas axial velocity component (ft/s) and gas temperature (°F) 18 in. upstream of burner, modified burner geometry, fired case

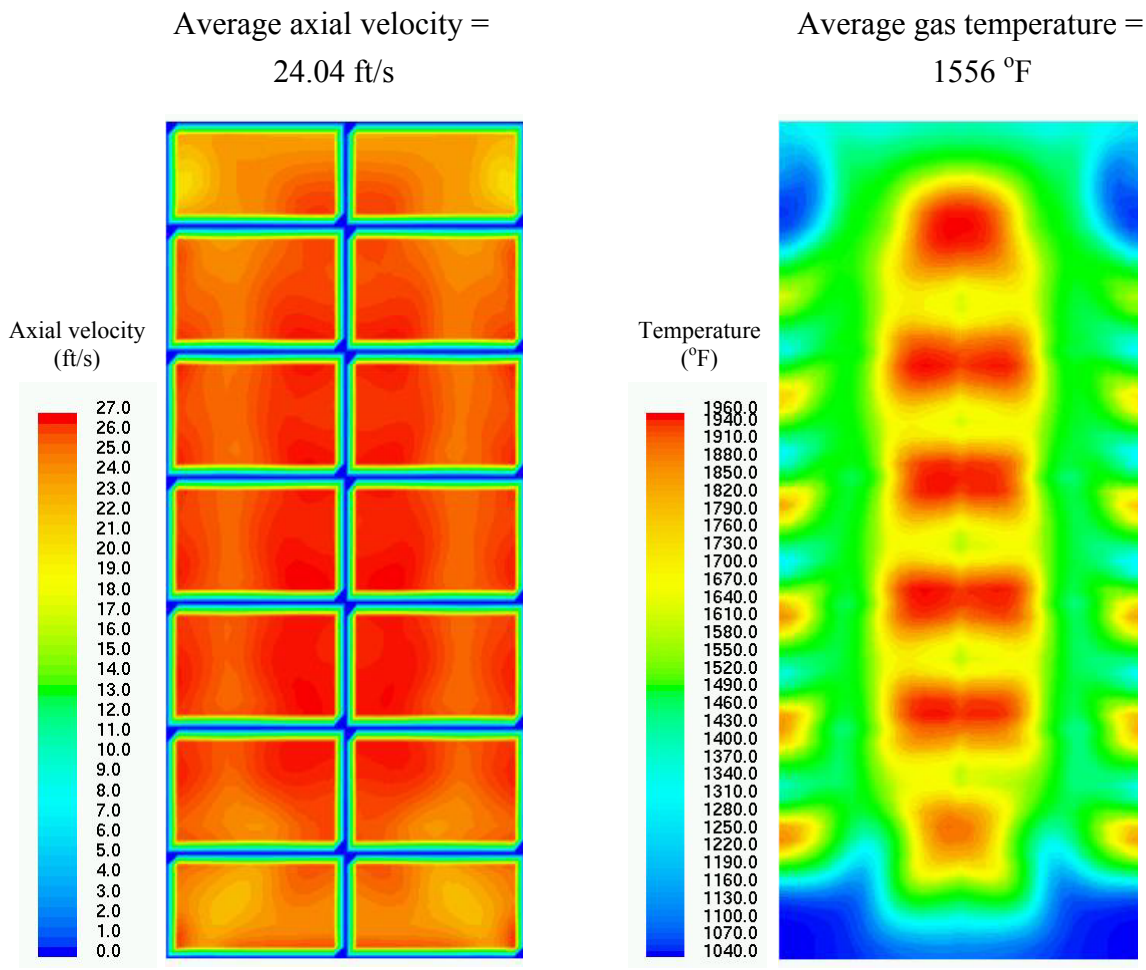

Figure 7-28: Contours of gas axial velocity component (ft/s) and gas temperature (°F) entering HPSH3 (Box 2), modified burner geometry, fired case

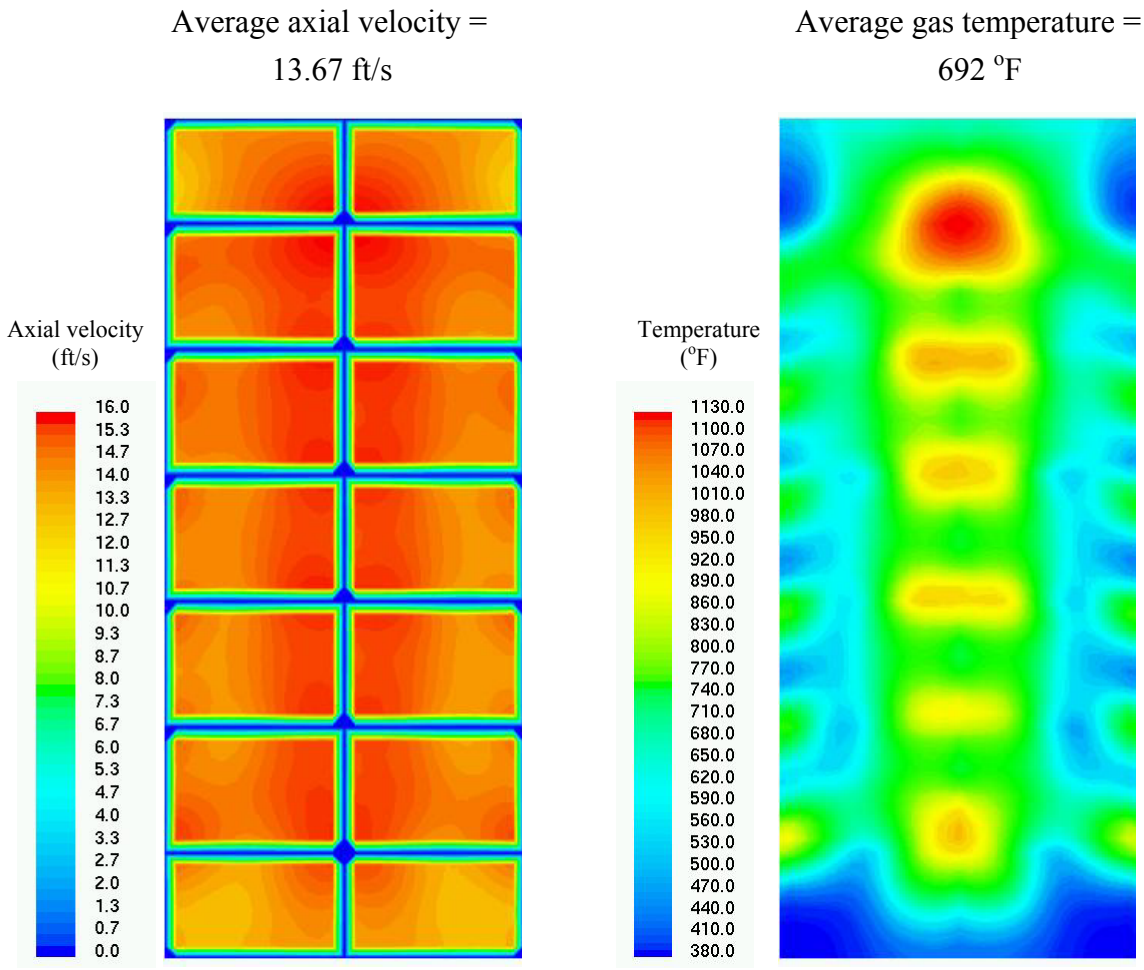

Figure 7-29: Contours of gas axial velocity component (ft/s) and gas temperature (°F) exiting HPEV4 (Box 2), modified burner geometry, fired case

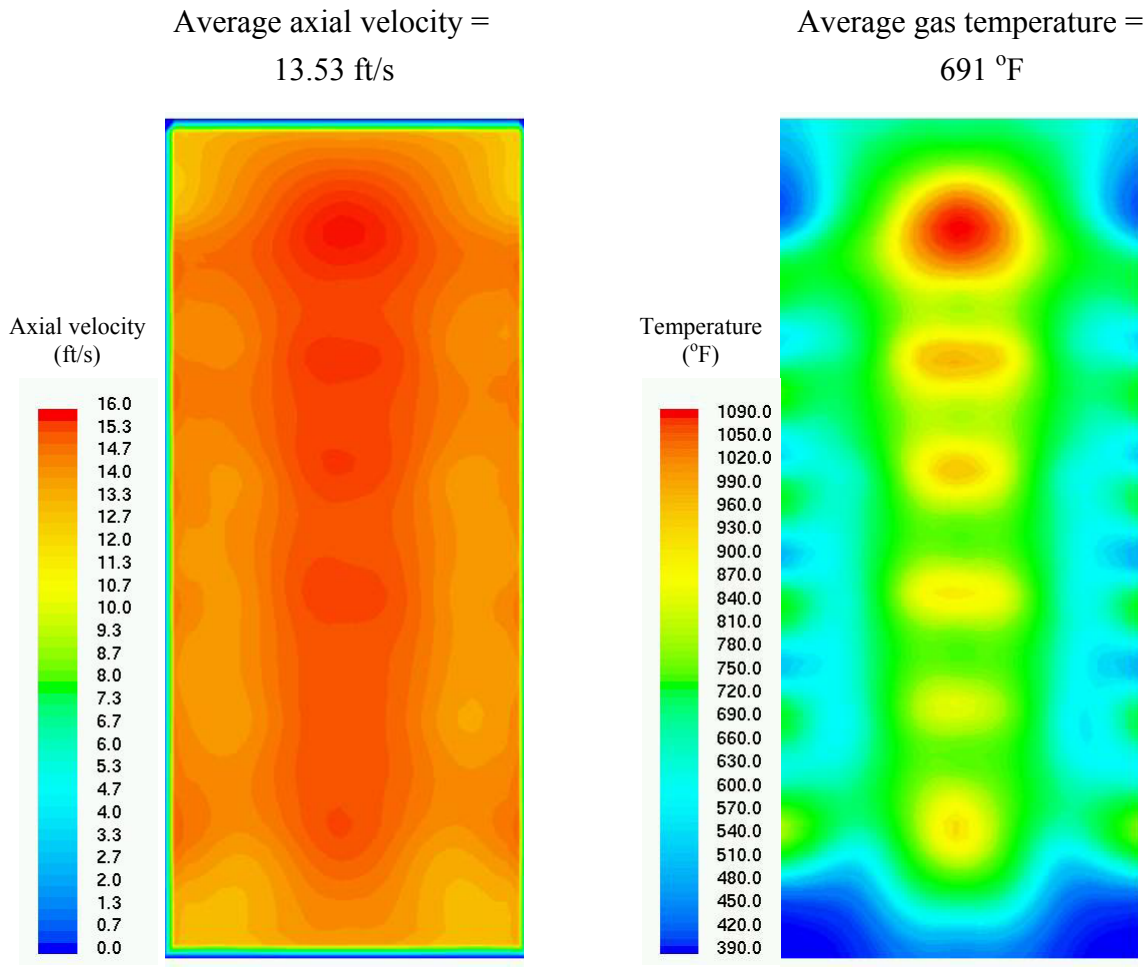

Figure 7-30: Contours of gas axial velocity component (ft/s) and gas temperature (°F) at AIG location, modified burner geometry, fired case

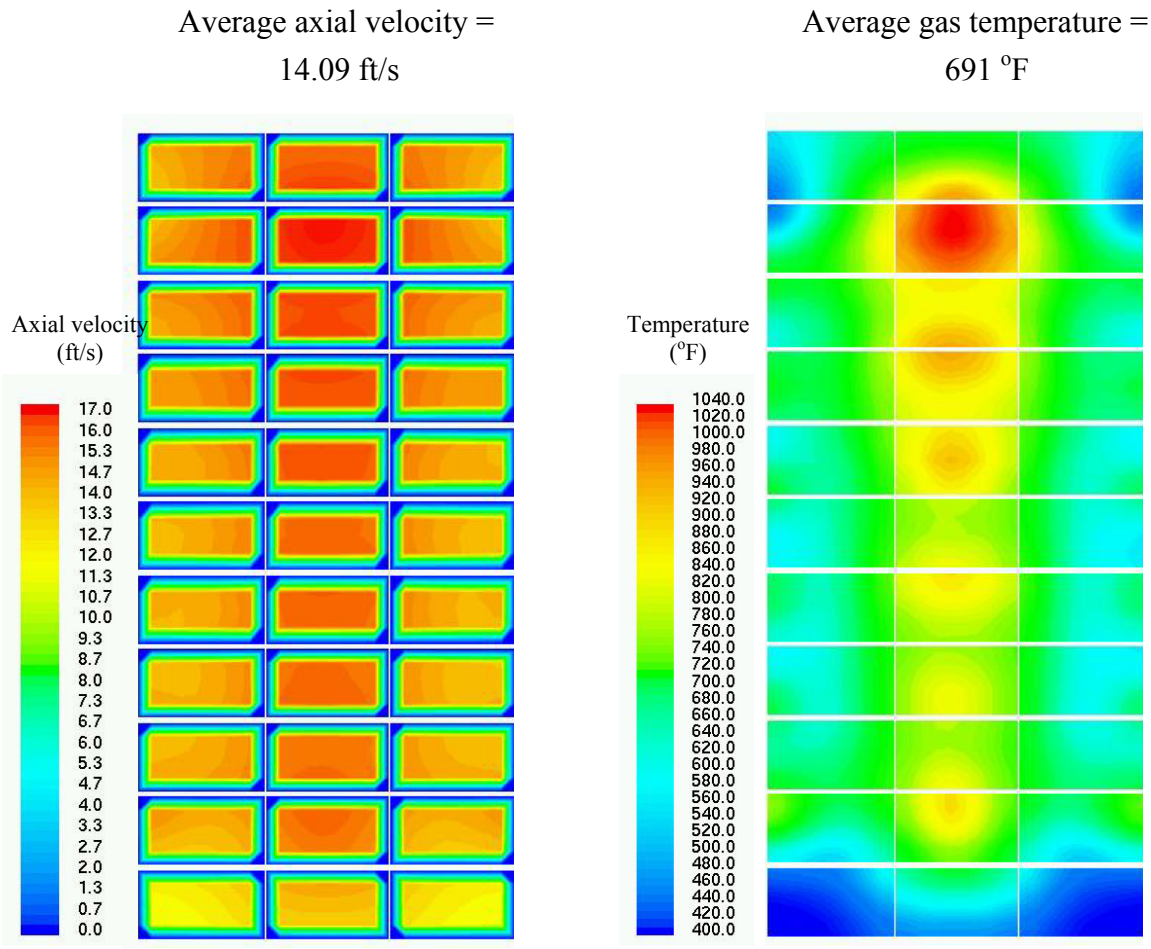

Figure 7-31: Contours of gas axial velocity component (ft/s) and gas temperature (°F) entering SCR catalyst, modified burner geometry, fired case

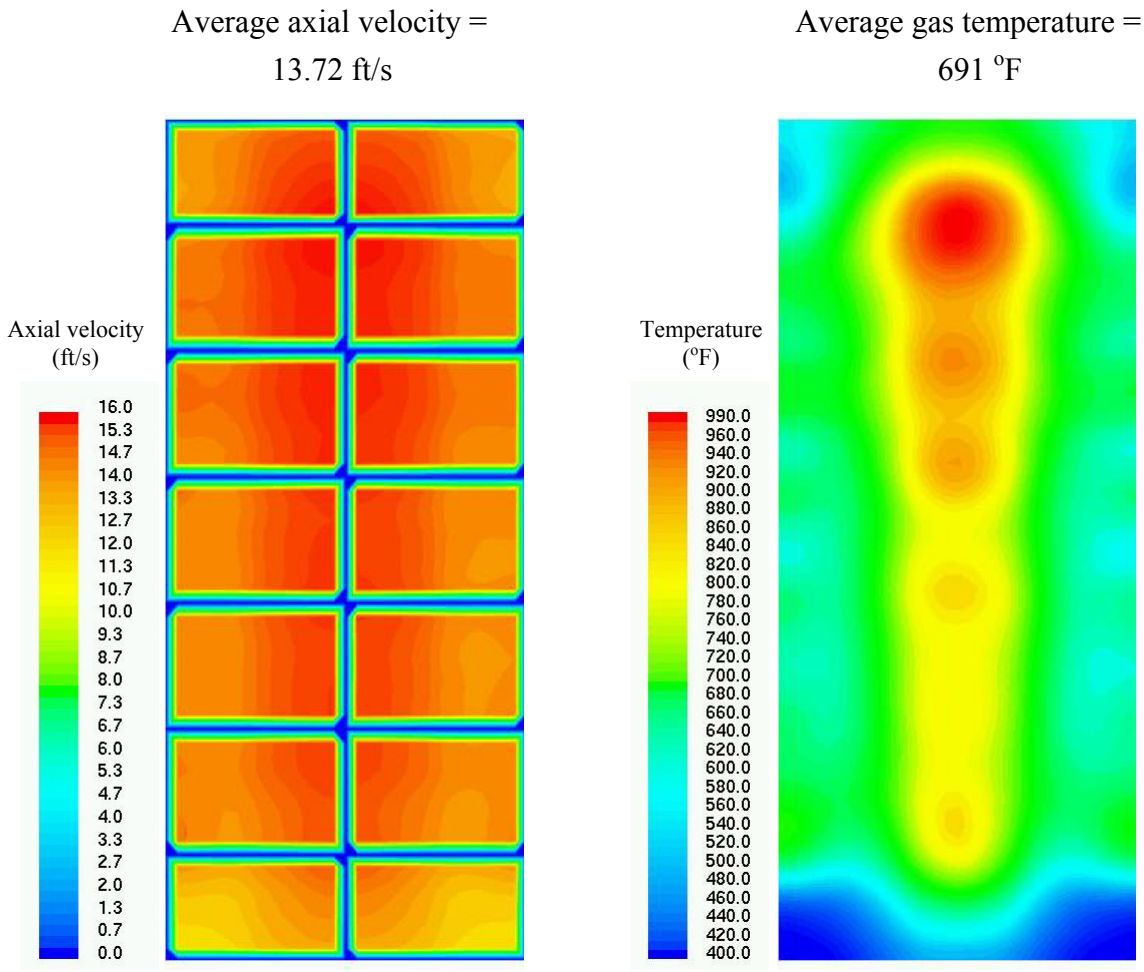

Figure 7-32: Contours of gas axial velocity component (ft/s) and gas temperature (°F) entering IPSH1 (Box 3), modified burner geometry, fired case

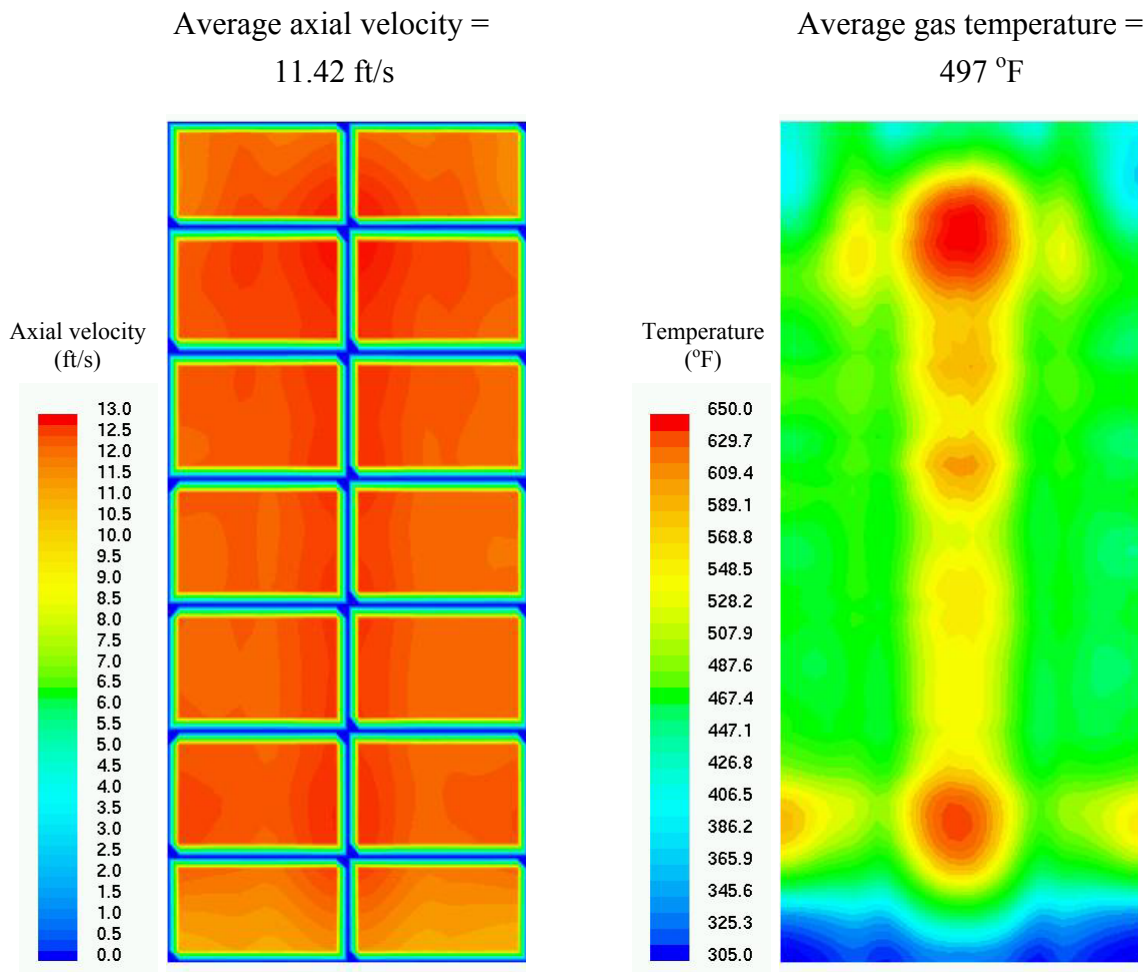

Figure 7-33: Contours of gas axial velocity component (ft/s) and gas temperature (°F) entering HPEC3 (Box 4), modified burner geometry, fired case

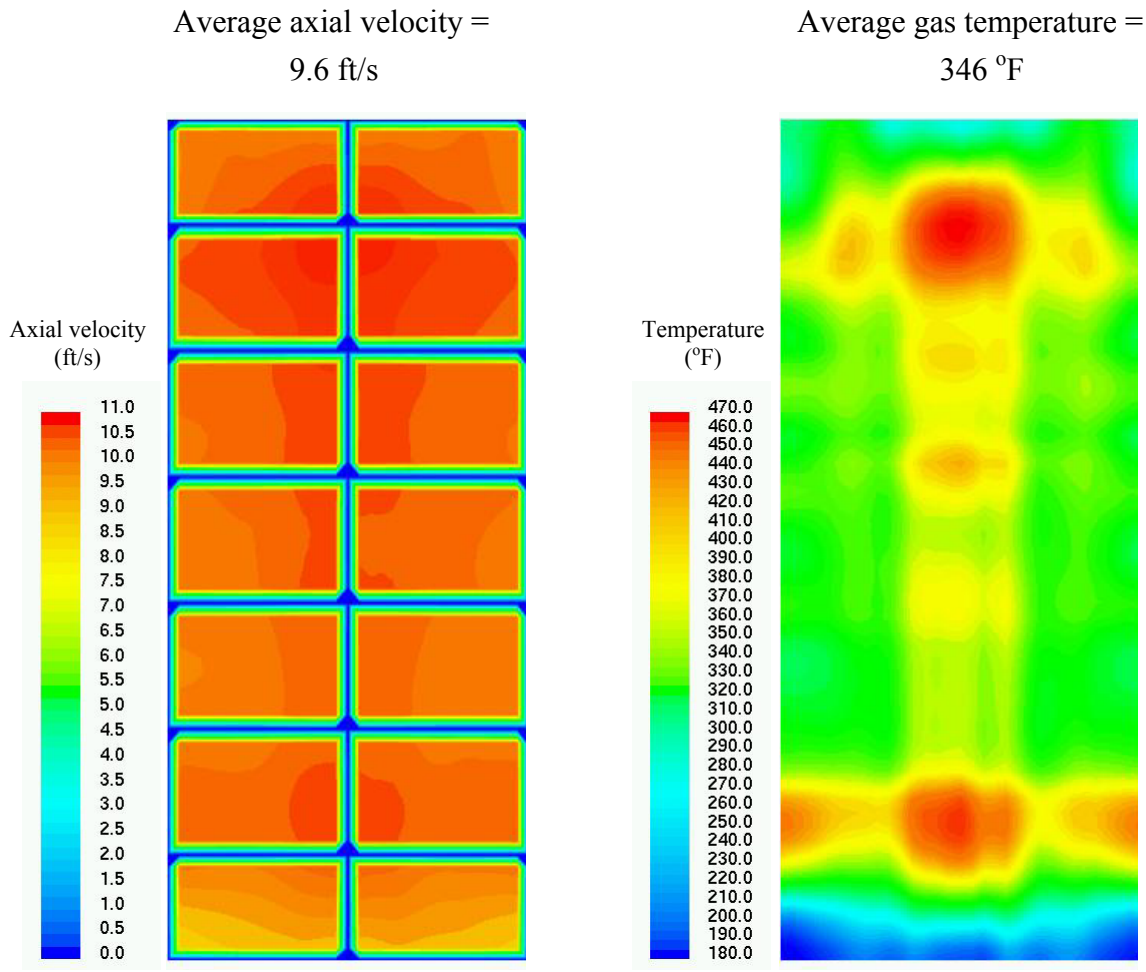

Figure 7-34: Contours of gas axial velocity component (ft/s) and gas temperature (°F) entering LPEV3 (Box 5), modified burner geometry, fired case

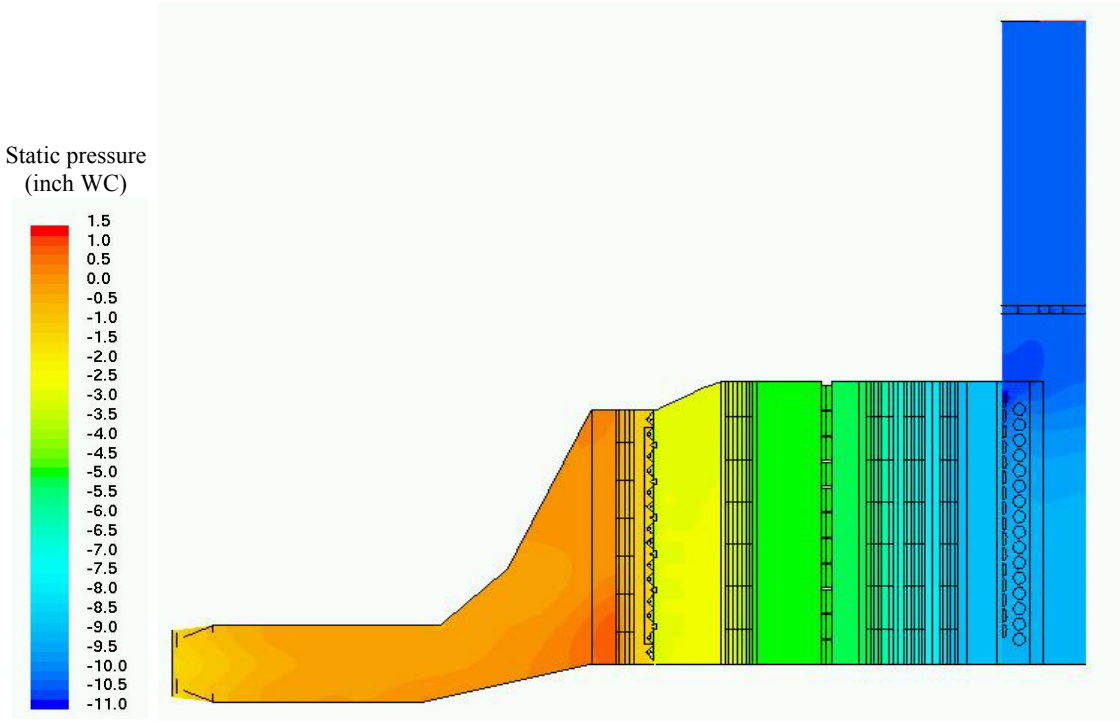

a) Boiler z-mid plane

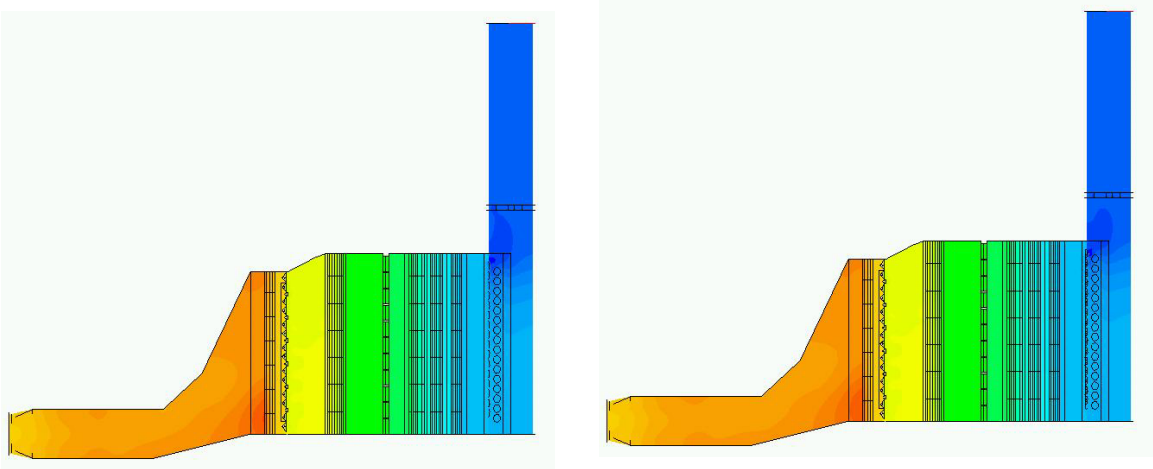

c) b) left -40 inches offset, right +40 inches offset

Figure 7-35: Static pressure contour along mid section of model (inch WC), modified burner geometry, fired case

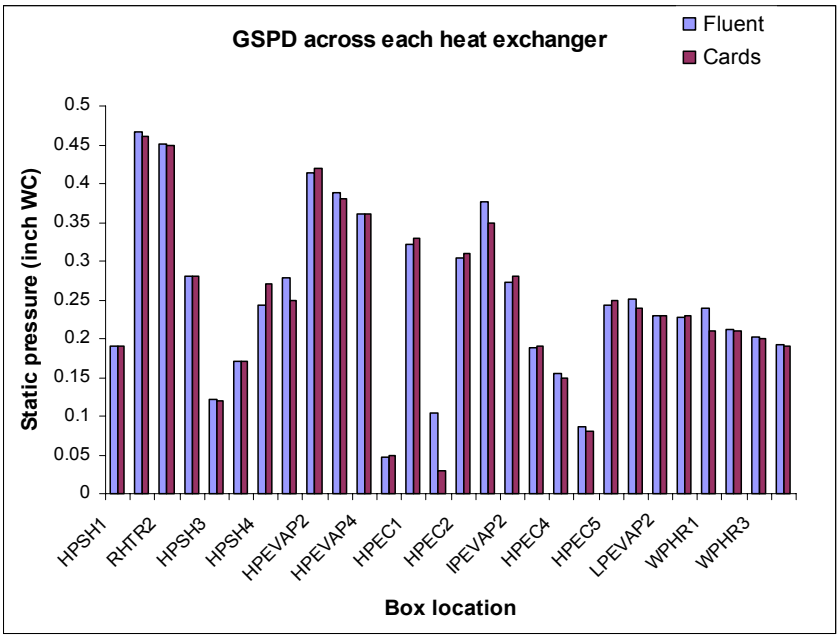

a) Comparison of module GSPD (Fluent Vs CARDS)

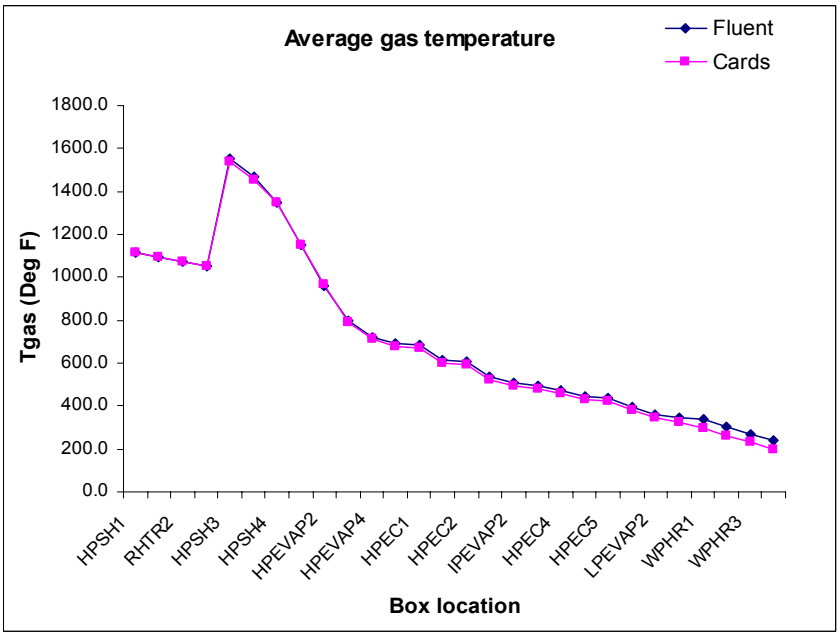

b) Comparison of average gas temperature (Fluent Vs CARDS)

Figure 7-36: Comparison of gas side pressure drop and gas temperature (^{o}F) at different heat exchangers with CARDS, modified burner geometry, fired case

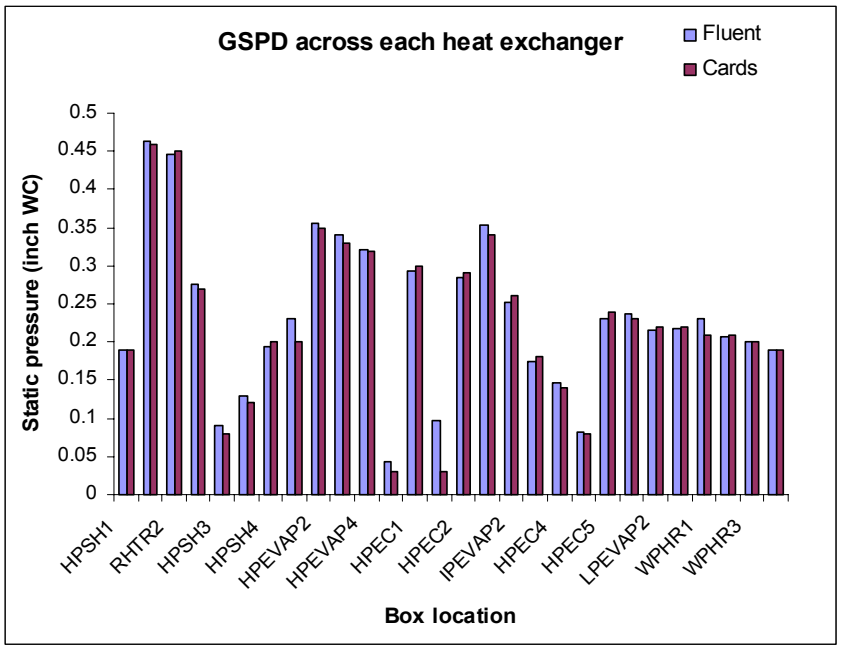

a) Comparison of module GSPD (Fluent Vs CARDS)

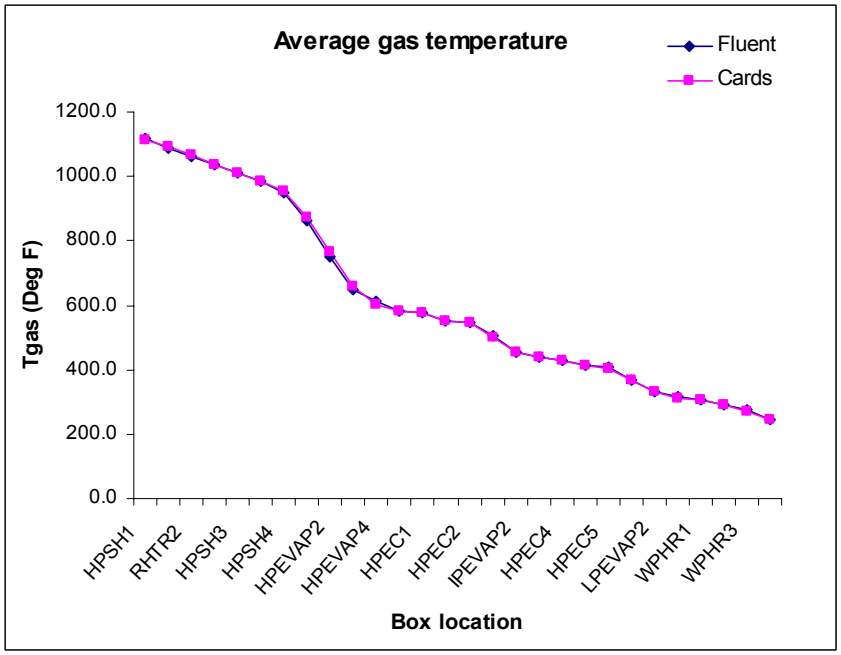

b) Comparison of average gas temperature (Fluent Vs CARDS)

Figure 7-37: Comparison of gas side pressure drop and gas temperature (^{o}F) at different heat exchangers with CARDS, modified burner geometry, unfired case

Chapter 8

Conclusions

Flow modeling of the complete gas path for two heat recovery steam generator designs has been completed successfully. The two HRSGs used for the flow modeling are the Beatrice HRSG, designed to operate on a side-exhaust gas turbine and the Current Creek HRSG, designed to operate with an axial exhaust gas turbine. Both of the selected models are fired-type heat recovery steam generators and include duct burners to provide supplementary firing when ever necessary. Flow modeling results are used to evaluate the existing design based upon the gas-side flow and temperature distributions within the inner gas path of the heat recovery steam generator.

The following conclusions have been drawn from the CFD analysis of the Beatrice HRSG:

- The inlet duct design is not adequate for this HRSG, and considering the design limitations, the suggestion made to make the gas-side flow better is to change the existing distribution grid for one that offers more resistance and induces high gas-side pressure drop.

- The velocity distribution into the top burner is observed to be insufficient for the ideal performance of the burner, which suggests the use only one burner (i.e. the bottom burner), to add heat energy into the system.
- The supporting structure provided to support the CO catalyst resulted in uneven distribution of flow near the bottom wall at the AIG location. It is suggested to block the area near the floor between the CO catalyst and SCR catalyst to facilitate smooth flow into the AIG and SCR catalyst.
- The overall flow modeling predictions are observed to be in good agreement with the CARDS predictions.

The following conclusions have been drawn from the CFD analysis of the Current Creek HRSG:

- The inlet duct design results in satisfactory gas velocity distribution into the heat exchanger surfaces, with gas flow uniformly distributed at the heat exchanger surfaces and good side-side symmetry for the performance cases modeled
- The gas flow distribution into the burner array is evaluated and is found to meet the flow requirements for the burner. The initial burner design is found to be inadequate, resulting in high temperature peaks at the heat exchanger section downstream of the burner.
- A revised burner configuration is suggested and modeled and is found to perform well. The new burner configuration reduces the temperature peaks without changing the heat addition capacity of the burner.
- Flow distribution into the SCR catalyst and the AIG location are found to be uniform.

- The effect of the blockage because of supporting structures for the SCR catalyst is studied. It is observed that the flow is not affected by the supporting structures.
- The overall flow modeling predictions are observed to be in good agreement with the CARDS predictions.

Overall, it can be concluded that the flow modeling analysis of the HRSG helps improve the design and helps facilitate the smooth operation of HRSG. It can be concluded that CFD analysis of HRSGs can be included in the design process of HRSG as a part of the design evaluation tool, which can help to validate the performance of the HRSG based upon the gas-side flow and can even help improve the design just like in the above two HRSG designs.

References

1) *A. ongiro, V. I. Ugursal, A. M. Al Taweel and J. D. Walker*, "Modeling of Heat Recovery Steam Generator Performance", Applied Thermal Engineering Vol. 17. No 5. pp 427-446, 1997

2) *Alessandro Franco, Alessandro Russo,* "Combined Cycle plant efficiency increase based on the optimization of heat recovery steam generator operating parameters", International Journal of Thermal Sciences, 41 (2002) 843-859.

3) *B. V. Reddy, G. Ramkiran, K. Ashok Kumar, P. K. Nag*, "Second Law analysis of a waste heat recovery steam generator", International Journal of Heat and Mass Transfer 45 (2002) 1807-1814.

4) *C. Casarosa, A. Franco*, "Thermodynamic optimization of operative parameters for heat recovery in combined plants", International Journal of applied Thermodynamics, 4 (2001).

5) *Keith C. Kaufman,* "VPI Flow modeling Report for Pacificorp/Stone & Webster Current Creek Project".

6) *M. Lisizka, G. Manfrida, A. Ziebik*, "Parametric study of HRSG in case of repowered industrial CHP plant", Energy Conversion and Management 44(2003) 995-1012.

7) *Manuel Valdes and Jose L Rapun*, "Optimization of heat recovery steam generators for combined cycle gas turbine power plants", Applied thermal Engineering, Vol. 21, Issue 11, Aug. 2001, 1149-1159.

8) *Marie-Noëlle Dumont∗, Georges Heyen*, "Mathematical Modeling and design of an advanced once through heat recovery steam generator", Computers and Chemical Engineering 28 (2004) 651-660.

9) *Nvrss Subhramanam, S. Rajaram and N. Kamalnathan*, "HRSGs for combined cycle power plants", Heat Recovery systems & CHP, Vol. 15, Issue 2, Febraury 1995, 155-161.

10) *S. Knudsen, G. L. Morrison, M. Behnia and S. Furbo*, "Analysis of the flow structure and heat transfer in a vertical mantle heat exchanger", Solar energy 2004.

11) *FLUENT 6.1 Documentation*

Appendix:

A-1 Heat exchanger input parameters for fixed heat rejection approach

The following text commands show the input specifications to set the heat exchanger duty for HPSH1 (fired case, Beatrice HRSG). The similar method is followed to setup the heat exchanger parameters for the remaining heat exchangers.

/define/user-defined/heat-exchanger/heat-exchanger
Enable heat exchanger model [no] yes
We need to enable the heat exchanger model only once.

/define/user-defined/heat-exchanger/heat-exchanger/heat-exchanger-zone
(hpsh1,hpsh2,hpsh3,hpevap1,hpevap2,hpevap3,hpec1,hpec2,lpsh,hpec3,hpec4,
hpec5,lpevap1,lpevap2,lpevap3,wphr1,wphr2,wphr3,wphr4,wphr5,wphr6)

Fluid Zone [hpsh1] hpsh1
Number of Passes [2] 1
Number of Rows/Pass [5] 5
Number of Cols/Pass [1] 1
Coolant Inlet Direction-x [1] 0
Coolant Inlet Direction-y [0] 1
Coolant Inlet Direction-z [0] 0
Pass-to-Pass Direction-x [0] 0
Pass-to-Pass Direction-y [1] 0
Pass-to-Pass Direction-z [0] 1

Simple-Effectiveness-Model or NTU-Model

Model Option [“ntu-model”]

Constant Specific-Heat or User-Defined-Enthalpy

Coolant-Properties Method [“constant-specific-heat”]
Specific Heat (j/kg-k) [4000] 2592

1. Fixed Heat Rejection? Or
2. Fixed Inlet Temperature?

Choose one of the two available options [2] 1
Heat Rejection (w) [8000] 3883575
Coolant Flow Rate (kg/s) [0.6] 34.84
Coolant Temperature (k) 766

Heat Exchanger Core Model [“default-model’]
Set HPSH1 to Heat Exchanger Zone

A-2 Heat exchanger input parameters for fixed inlet temperature

The following text commands show the input specifications to set the heat exchanger parameters using the fixed inlet temperature for HPSH1 (fired case, Beatrice HRSG). The similar method is followed to setup the heat exchanger parameters for the remaining heat exchangers. In this method the heat exchanger model has to be set so that we can define the effectiveness separately for each of the heat exchangers. The input parameters for setting the heat exchanger model are given first before setting the heat exchanger input parameters.

/define/user-defined/heat-exchanger/heat-exchanger
Enable heat exchanger model [no] yes
We need to enable the heat exchanger model only once.

/define/user-defined/heat-exchanger/heat-exchanger-model
Model [default model] "hpsh1'
** *Inputs for pressure drop*
Min Flow to Face Area [0.8]
Entrance loss Coefficient [0.3]
Exit loss coefficient [0.08]
Air side Surface Area (m2) [6]
Min Cross Section Flow Area (m2) [0.2]
Core Friction Coefficient [8]
Core Friction Exponent [0.5]
** *Inputs for effectiveness*
Number of points [1]
Mass flow rate (kg/s) [1]
NTU [1]

/define/user-defined/heat-exchanger/heat-exchanger-zone
(hpsh1,hpsh2,hpsh3,hpevap1,hpevap2,hpevap3,hpec1,hpec2,lpsh,hpec3,hpec4,
hpec5,lpevap1,lpevap2,lpevap3,wphr1,wphr2,wphr3,wphr4,wphr5,wphr6)

Fluid Zone [hpsh1] hpsh1
Number of Passes [2] 1
Number of Rows/Pass [5] 5
Number of Cols/Pass [1] 1
Coolant Inlet Direction-x [1] 0
Coolant Inlet Direction-y [0] 1
Coolant Inlet Direction-z [0] 0
Pass-to-Pass Direction-x [0] 0
Pass-to-Pass Direction-y [1] 0
Pass-to-Pass Direction-z [0] 1

Simple-Effectiveness-Model or NTU-Model

Model Option [“ntu-model”]

Constant Specific-Heat or User-Defined-Enthalpy

Coolant-Properties Method [“constant-specific-heat”]
Specific Heat (j/kg-k) [4000] 2592

1. Fixed Heat Rejection? Or
2. Fixed Inlet Temperature?

Choose one of the two available options [2] 2

Coolant Flow Rate (kg/s) [0.6] 34.84
Coolant Temperature (k) 766

Heat Exchanger Core Model [“default-model’] “hpsh1”
Set HPSH1 to Heat Exchanger Zone

A-3 Setting the boundary condition for porous media (pressure drop parameters)

The following text commands show the input details to achieve the given heat exchanger pressure drop using the porous media inertial resistance parameters. This section shows the text commands to set the inertial resistance parameter for one of the heat exchangers. Similar method is followed to setup the porous media pressure drop parameters for the remaining heat exchangers.

/define/boundary-conditions/fluid
Zone id/name [fluid] hpsh1
Specify source terms? [no]
Specify fixed values? [no]
Motion Type: Stationary {yes]
X-Origin of Rotation-Axis (m) [0]
Y-Origin of Rotation-Axis (m) [0]
Z-Origin of Rotation-Axis (m) [0]
X-Component of Rotation-Axis [0]
Y-Component of Rotation-Axis [0]
Z-Component of Rotation-Axis [0]
Deactivated Thread [no]
Laminar zone? [no]
Porous zone? [yes]
Conical porous zone? [no]
X-Component of Direction-1 Vector [0]
Y-Component of Direction-1 Vector [0]
Z-Component of Direction-1 Vector [1]
X-Component of Direction-2 Vector [0]
Y-Component of Direction-2 Vector [1]
Z-Component of Direction-2 Vector [0]
Use profile for Direction-1 Viscous Resistance? [no]
Direction-1 Viscous Resistance (1/m2) [0]
Use profile for Direction-2 Viscous Resistance? [no]
Direction-2 Viscous Resistance (1/m2) [0]
Use profile for Direction-3 Viscous Resistance? [no]
Direction-3 Viscous Resistance (1/m2) [0]
Use profile for Direction-1 Inertial Resistance? [no]
Direction-1 Viscous Resistance (1/m) [0] 1000
Use profile for Direction-1 Inertial Resistance? [no]
Direction-2 Viscous Resistance (1/m) [0] 1000
Use profile for Direction-1 Inertial Resistance? [no]
Direction-3 Viscous Resistance (1/m) [0] 40

Leave the remaining inputs as default values.

A-4 procedure to check the heat exchanger duty

The feature in the heat exchanger report feature provided in fluent is used to check the duty of heat exchanger. This can be verified by using the text commands in fluent.

This example shows the report verified for fixed inlet temperature Beatrice fired case.
Define/user-defined/heat-exchanger/heat-exchanger-report
Heat Exchanger Zone [] hpsh1

Fluid Zone = hpsh1
Heat Exchanger Model = hpsh1

Coolant Flow Rate =3.484ooe+01 kg/s
Coolant Specific Heat = 2.592e03 J/Kg-K
Fixed Inlet temperature = 766 K
Macro 0 T_inlet = 7.66e02 Q_rej = -1.10653e06 Eff_ave = 2.2057e-01
Macro 1 T_inlet = 7.78e02 Q_rej = -8.40778e05 Eff_ave = 2.5337e-01
Macro 2 T_inlet = 7.87e02 Q_rej = -7.20851e05 Eff_ave = 2.5840e-01
Macro 3 T_inlet = 7.95e02 Q_rej = -5.01378e05 Eff_ave = 2.5506e-01
Macro 4 T_inlet = 8.01e02 Q_rej = -4.56610e05 Eff_ave = 2.4771e-01
Total Heat Rejected = -3.62615e06 w
Outlet Temperature = 806.15 K

Vita

Veera Venkata Sunil Kumar Vytla was born on September 24th 1978, in Andhra Pradesh, India. He received his Diploma in Mechanical Engineering in 1997 from Andhra University, and Bachelors in Engineering in Mechanical Engineering in 2002 from Osmania University. He is currently pursuing his Ph.D degree at Uniersity of Kentucky.